Swansea University
Prifysgol Abertawe

Deposition and Characterisation of Silicon Oxynitride Dielectric Films for Waveguide Applications

Parisa Rahbari

[redacted]

2019

DECLARATION

This work has not previously been accepted in substance for any degree and is not being concurrently submitted in candidature for any degree.

Signed .....  .... (candidate)

Date .....18-01-2021.....

STATEMENT 1

This thesis is the result of my own investigations, except where otherwise stated. Where correction services have been used, the extent and nature of the correction is clearly marked in a footnote(s).

Other sources are acknowledged by footnotes giving explicit references. A bibliography is appended.

Signed .....  .... (candidate)

Date .....18-01-2021.....

STATEMENT 2

I hereby give consent for my thesis, if accepted, to be available for photocopying and for inter-library loan, and for the title and summary to be made available to outside organisations.

Signed .....  ..... (candidate)

Date .....18-01-2021.....

NB: *Candidates on whose behalf a bar on access has been approved by the University (see Note 7), should use the following version of Statement 2:*

I hereby give consent for my thesis, if accepted, to be available for photocopying and for inter-library loans **after expiry of a bar on access approved by the Swansea University.**

Signed .....  ..... (candidate)

Date .....18-01-2021.....

ACKNOWLEDGMENT

At this moment of accomplishment, I would like to thank my hero, my dear father, Sohrab Rahbari. I am greatly indebted to you Dad, for all your inspiration, encouragement and the belief you always had in me. You taught me the importance of knowledge and education and how this leads to clarity and enlightenment in life. Your soul and love will always stay with me until I meet you again.

I would like to express my sincere gratitude to my supervisors at Swansea University Department of Engineering, Dr. Matt Elwin and Dr. Richard Cobley, for their continuous support, guidance, patience and motivation throughout my studies. Their knowledge and advice have been invaluable throughout the entire process. Their guidance helped me throughout my research and writing of this thesis.

Thanks, should also be extended to my industrial sponsor Dr. William Ring from BB-Photonics Ltd, for his inspiration on this project and in the securing of funds for the research to proceed. Without his precious support it would not have been possible to conduct this research. I also would like to thank the European Social Fund and KESSII team for providing funds and their incredible support in giving me this fantastic opportunity to do this master's degree.

I would like to thank all other research groups and CNH colleagues, especially the Dr. Gareth Blaney, Dr. Jonathon Evans, Dr. Barbara Gomes and Dr. Dominic Fung for their help and support throughout my study. I also greatly appreciate the support of my colleagues Prof. Gill Alexandrowicz and Helen Chadwick for their encouragement, kind support and understanding while I was writing this thesis.

I would like to thank the most special person in my life, my beloved husband, my true love, Mostafa. Words cannot express my love and appreciation to you my darling. Thank you for all your emotional support, continued and unfailing love and understanding during my pursuit of MSc degree. The presence of you in my life and the love and happiness you brought, gave me strength through my life and especially during my studies. I love you with all my heart and soul. I also appreciate my lovely children Emma and Idin, you always gave me love and hope during my life I am truly proud and consider myself a very lucky person to have a wonderful, loving and caring children as you.

I would like to acknowledge the people who mean so much to me. My wonderful and kindest mother, Mina and my dear family, Ali, Yasha, Raha, Owen, Aysan, Sahar and my lovely nieces and nephew Aynaz and Arsham and my best friends Shafagh and Ima. I salute you all for your unconditional love, care and sacrifice you made, which shaped my life. You gave me strength and patience to work hard through all these years.

This thesis is dedicated to my wonderful parents, Sohrab and Mina,
and my beloved husband Mostafa

ABSTRACT

Within the last decade, chemical vapor deposition (CVD)-grown silicon oxynitride (SiOxNy) thin films have become increasingly important for applications in low cost, compact, integrated optical devices. The major advantage of SiOxNy is the tunability of its refractive index over a wide range (n = 1.45– 2), resulting in a large degree of freedom for integrated optics design.

The plasma-enhanced chemical vapor deposition (PECVD) technique is attractive because of the possibility of working with relatively high deposition rates and at low deposition temperatures (300 – 400 ^{0}C), so that it is compatible with well-established microelectronic processing . Furthermore, the CVD technique permits control of the structural, mechanical and optical properties of the deposited films by adjusting the deposition parameters of the CVD process. Silicon oxynitride films (SiOxNy) grown using PECVD have been studied for many applications in the microelectronics and optoelectronics industry, i.e. as passivation coatings, thin gate dielectrics, as well as membranes and optical waveguides for micromechanical systems (MEMS). Controlling the gas flow of the precursor reactant gases permits deposition of SiOxNy films with different silicon, oxygen and nitrogen concentration ratios. The tuneable film composition allows properties such as refractive index, mechanical stress , dielectric constant and optical gap to be varied in a controlled manner.

SiOxNy is a highly appropriate material for the combination of waveguides with silicon micromachining technology, since the ability to tune the refractive index is very important for the development of optical applications. These applications involve the integration of planar optical waveguides with micromechanical components on silicon substrates for applications including integrated sensors and optical communication devices. The SiOxNy films also provide advantages in terms of low mechanical stress, high deposition rates and high resistance to chemical corrosion, a very important characteristic for MEMS applications.

Knowledge of the bond structure, elemental composition and stoichiometry of different silicon oxynitride (SiON) layers is useful in order to understand the optical behaviour and properties of the fabricated material thin films, since these physical and chemical properties strongly influence the material quality, and subsequently the material's optical loss. A high concentration of Si-H and Si-Si bonds is well known to be responsible for the formation of undesired grains, pores and columnar microstructures that can cause scattering and absorption losses. Thus, reduction of these bonds is desirable in order to improve material quality.

NH_3 has been the precursor gas of choice (as opposed to N_2) when deposition SiOxNy films, because the energies of N–H bonds are almost three times smaller than those of N ≡ N bonds (391 kJ/mol versus 941 kJ/mol), and therefore require less energy to break. In practice, this allows lower energy or lower temperature deposition processes. However, the use of NH_3 gas in the deposition process has been reported to lead to unwanted N–H bonds in the deposited films.[1] The use of N_2O - bond energies N-O (201 KJ/mol); N=O (607 KJ/mol) - instead of NH_3 during the deposition process can reduce the overall amount of hydrogen in the deposition processes gas chemistry and hence reduces the overall presence of N−H and Si-H bonds, which act as absorption centres. The use of N2O reduces the overall Hydrogen content of the deposited films, even though some hydrogen is present, pertaining to the use of SiH_4 as the silicon precursor.

In this work, films with different nitrogen, silicon and oxygen composition ratios were obtained in PECVD deposited SiOxNy films, by varying the N_2O, and SiH_4 gas flows while maintaining constant all other deposition conditions.

Spectroscopic ellipsometry was employed to obtain the refractive index and the thickness of the SiOxNy films at a variety of points across the surface of a 100 mm wafer. These measurements were performed at in order to determine the standard deviation of the refractive index and the thickness uniformity across the wafer. The RI and film thickness have been monitored at three different wavelengths (636 nm, 1310 nm and 1550 nm).

Extensive characterisation has been performed on these films, including Energy Dispersive X-ray Spectroscopy (EDX), X-ray Photoelectron Spectroscopy (XPS), and Fourier Transform Infra-Red (FTIR) spectroscopy.

Optical losses were measured using a prism coupler (Metricon), in order to assess the optical performance of the SiOxNy thin films.

The application of these films is in optical waveguides for data communications. Reducing the hydrogen content of the films minimises optical losses through reduced absorption and reduced scattering. Deposition of high refractive index SiOxNy films also allows a high index contrast (the difference in refractive index between the core and cladding layers in an optical waveguide device). A high index contrast permits a higher radius of curvature of a waveguide bend – allowing a more tightly packed curved waveguide structure to be fabricated – thus reducing the waveguide footprint and consequently reducing the ultimate device cost.

CONTENTS

TABLE OF FIGURES

TABLE OF TABLES

1 INTRODUCTION

Over recent years, much attention has been paid to silicon-based dielectrics such as silicon oxides, silicon nitrides, and silicon oxynitrides as suitable materials for integrated optics [2]. This interest has been inspired primarily by their encouraging optical properties such as low absorption losses in the visible and near infrared. In particular, silicon oxynitrides can be tuned to have a range of refractive indices of anything between pure SiO_2 (RI of 1.46) to S_3N_4 (RI of 2.0), which makes them very suitable for waveguide applications. Even higher RI films can be obtained by forming silicon rich nitrides. These films have RI values up to 3.1 – moving towards the 3.7 RI of amorphous silicon.

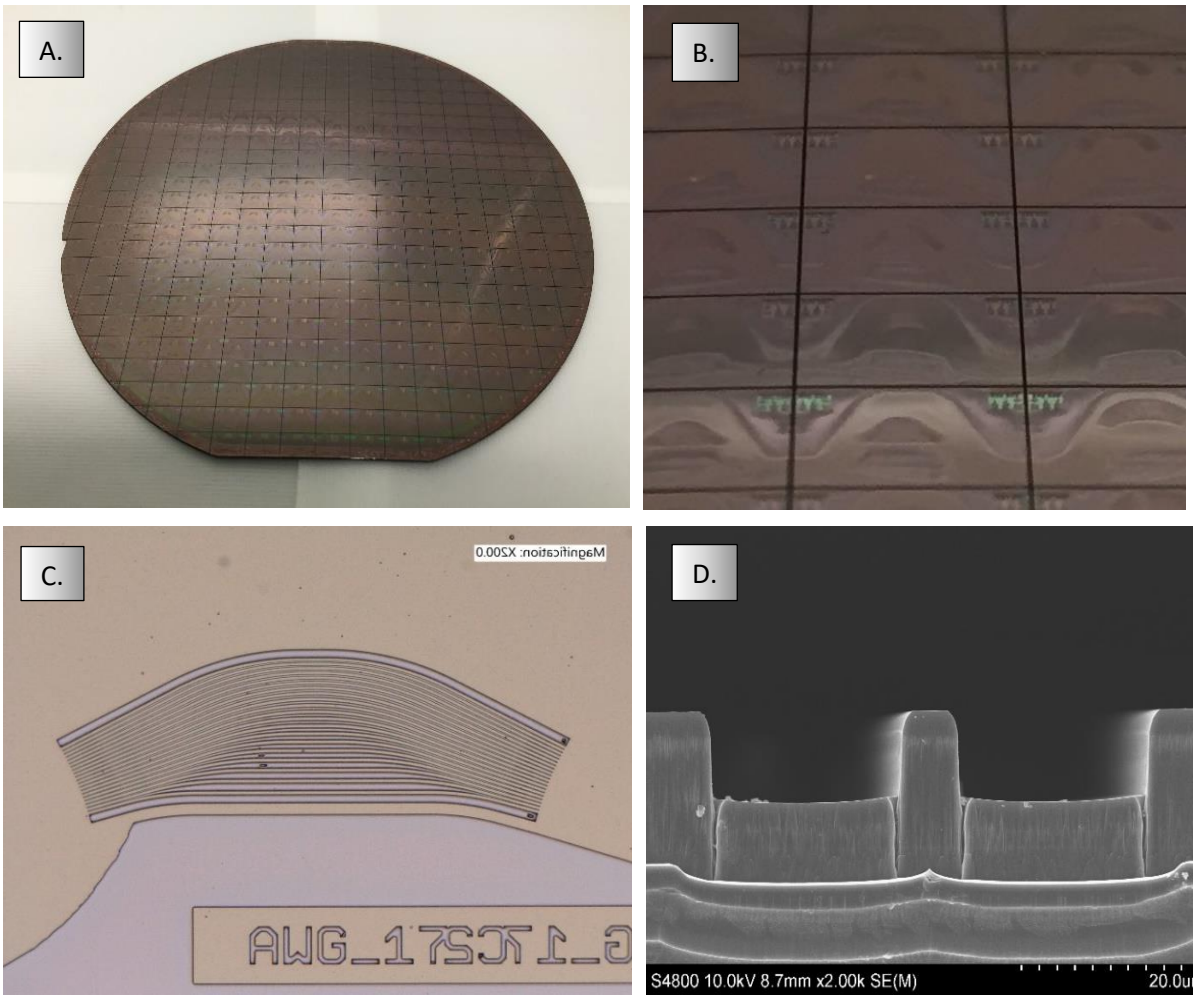

Figure 1-1. (A) Optical WDM waveguide chips fabricated on a silicon wafer substrate. (B) Higher magnification image of these small WDM waveguide chips. (C) Angled SEM image of cross section of a WDM waveguide. (D) Cross section of a WDM waveguide taken by SEM spectroscopy.

A typical optical waveguide device is illustrated in Figure 1-1. The structure consists of a silicon oxynitride core, patterned on top of a silicon dioxide on silicon substrate and surrounded by a silicon dioxide cladding layer. Light is confined in 2 dimensions in the silicon oxynitride core layer by the surrounding SiO_2. The difference in RI between the core layer and the cladding is termed the index contrast. The higher this value, the higher the radius of curvature can be used in the waveguide device.

In optical waveguide structures the ideal refractive index value for the silicon oxynitride is around 1.7. This allows a sufficiently high index contrast between the silicon oxynitride waveguide core material and the surrounding silicon oxynitride cladding layer with 1.55 refractive index. The index contrast used in this work was typically 0.15– substantially higher than previously reported devices.

In addition, oxynitrides with an RI of 1.7 have relatively low absorption in the visible region at wavelengths between 370 nm and 636 nm. Higher RI films, though yielding a higher index contrast, also have higher absorption and scattering. There is thus a trade-off between optical contrast and absorption / scattering. The combination of absorption and scattering constitutes the "optical loss". At the wavelengths used in optical communication devices (636 nm, 1310 nm and 1550 nm), there are local minima in the optical loss. The lowest loss is seen at 1550 nm – which is now the most commonly used wavelength in communications devices.

This thesis presents development of highly uniform silicon oxynitride films with target RI values of 1.55 and 1.7 on 100 mm diameter silicon dioxide / silicon wafers for application in waveguide devices. Extensive characterisation work has been performed in order to obtain the optimal performance oxynitride layer and to understand the mechanisms behind the optical losses of oxynitride films deposited using different PECVD process conditions.

Before considering these films in more detail, it is important to provide some background information on the materials, processes and devices used for optical waveguides and to understand the device parameters and operating constraints of such devices. These topics are reviewed in the following sections, culminating in a review of optical waveguide devices and their applications

2 LITERATURE REVIEW

2.1 Light-Matter interaction

This thesis discusses the development and optimisation of dielectric materials (silicon oxynitrides) for application in waveguide devices. In order to understand the performance of dielectric materials in terms of their potential performance in waveguide devices, one must first have a knowledge of light-matter interactions. These interactions are reviewed in the following section.

There are two values to describe the optical properties which determine the interaction of light with a material. They are generally represented as a complex number with real and imaginary parts. The complex refractive index (ñ) consists of the real part which is the index (n), describing the ratio of phase velocity (v) within a material to the speed of light in vacuum, plus the imaginary part – comprising the extinction coefficient (k), which indicates the amount of attenuation when the electromagnetic wave propagates through the material ($k \geq 0$) . Thus, these two components are associated with refraction and absorption of light, respectively and they can be considered as the fingerprint of each material.

$$\tilde{n} = n + i\,k \qquad (1)$$

The optical properties can be also be represented as the complex dielectric function:

$$\tilde{\varepsilon} = \varepsilon_1 + i\,\varepsilon_2 \qquad (2)$$

Where $\tilde{\varepsilon}$ is the dielectric constant or relative permittivity, ε_1 is the volume polarizability and ε_2 is the volume absorption. The relationship between $\tilde{\varepsilon}$ and $\tilde{n}$ is:

$$\tilde{\varepsilon} = \tilde{n}^2 \qquad (3)$$

We must now consider the interaction of an electromagnetic field with an atom when the electromagnetic wave travels through a medium. In an atom, which consists of the nucleus and the electron cloud around it, they slightly separate and the nucleus move in opposite directions of the electrons. This momentary alignment of the atoms creates its own electric field, which can oppose the externally applied electric field (the electromagnetic wave). This opposing electric field causes a reduction of the net electric field

and the concept of relative permittivity ($\tilde{\varepsilon}$) comes from this behaviour. Materials that experience a large decrease in the net electric field are said to have large relative permittivity. A schematic of this process has been illustrated in Figure 2-1.

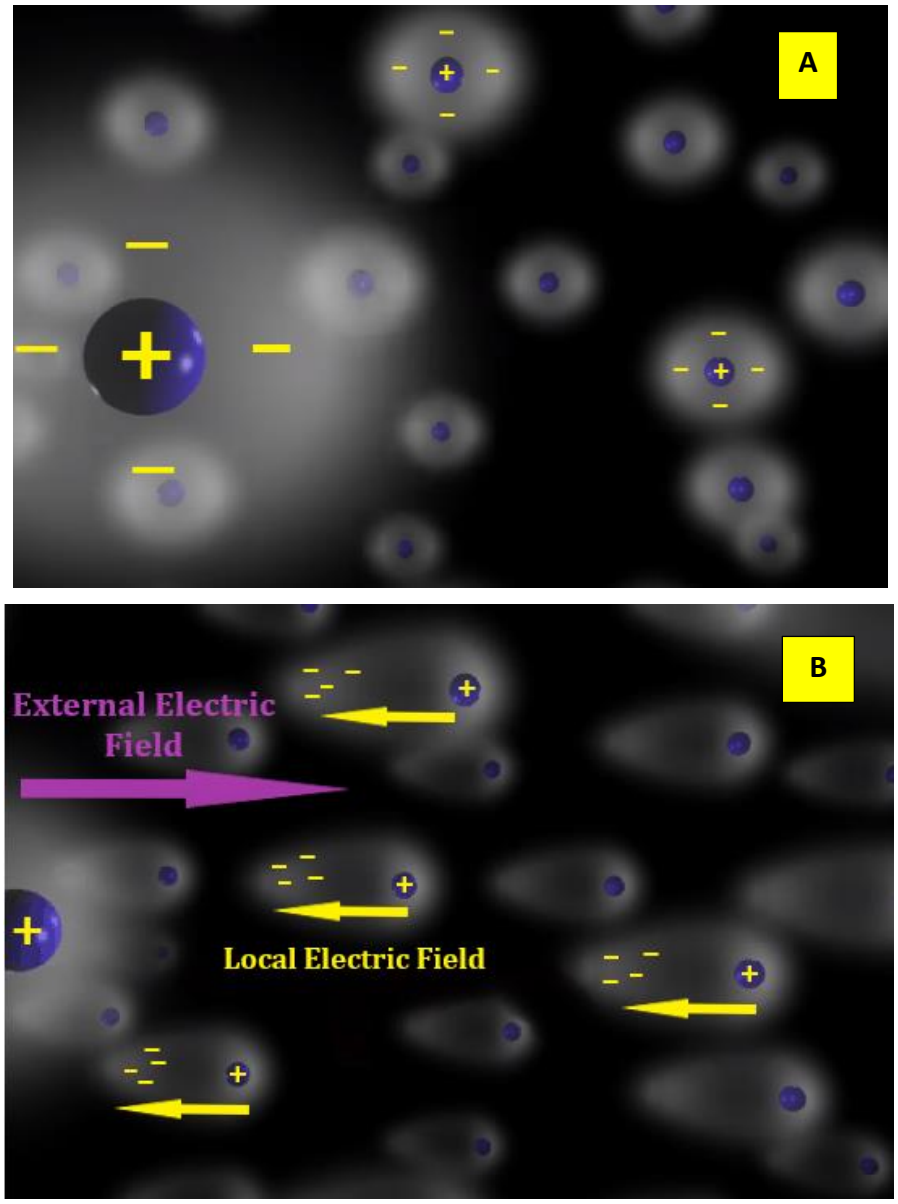

Figure 2-1 (A) nucleus (positive charges) and electrons (negative charges) in the absence of the external electric field and (B) Alignment of positive and negative charges in the present of an external electric field.

For polar molecules (molecules with permanent dipole moment, such as H_2O) in the absence of external electric field their electric dipoles are oriented randomly, and hence cancel each

other out, resulting in a zero-net polarisation. However, when applying an electric field which exerts torque on the molecules, they rotate in order to align their dipole moments with the external field. This induces a large polarisation, Figure 2-2 (A).

In non-polar molecules (molecules with no permanent dipole moment), such as CO_2 or N_2O, because of the rectilinear shape of the molecule, there is a zero net dipole moment. In this case also, as in neutral atoms, the molecule can become instantaneously polarized, Figure 2-2 (B).

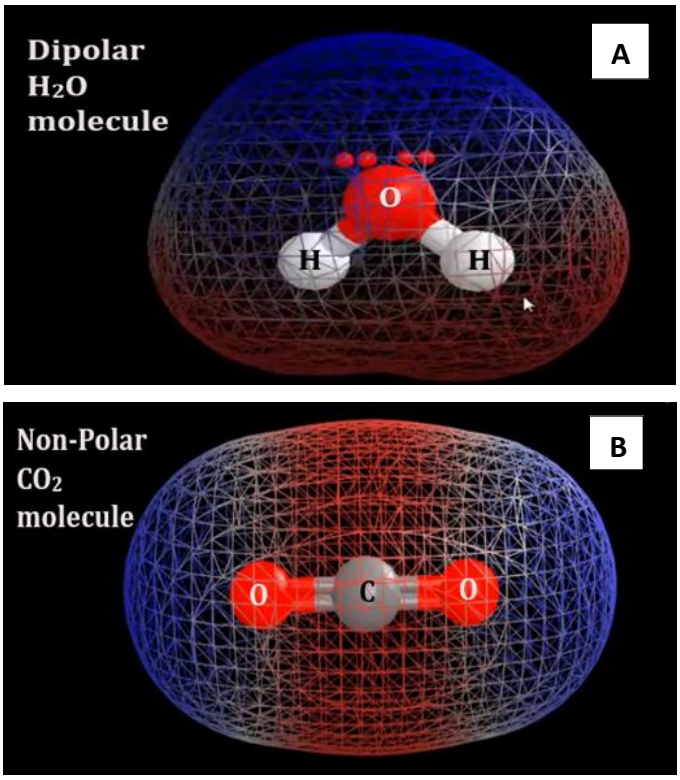

Figure 2-2 Illustration of polarisation in polar (H_2O) (A) and non-polar (CO_2) (B) molecules.

The dipole moment thus depends on the geometrical arrangement of the charges, and by measuring the moment one can therefore gain information concerning the polarizability of the molecule.

The polarization (P) with (Coulombs/m^2) unit, is defined as the dipole moment (p) per unit volume (where N refers to the number of charge dipoles per unit volume in the material):

$$P = Np \qquad (4)$$

Also, the polarization of a material is proportional to the strength of the applied electric field by the material's electric susceptibility (χ_e) and also the electric displacement (D), according to the Maxwell question:

$$\vec{P} \propto \vec{E} \qquad (5)$$

$$\vec{P} = \varepsilon_0 \chi_e \vec{E} \qquad (6)$$

$$\tilde{\varepsilon} = \frac{\varepsilon}{\varepsilon_0} = 1 + \chi_e \qquad (7)$$

$$\tilde{\varepsilon} = \frac{\mathrm{P}}{\varepsilon_0 \mathrm{E}} + 1 \qquad (8)$$

$$\vec{D} = \varepsilon_0 \vec{E} + \vec{P} \qquad (9)$$

where χ_e is a positive, dimensionless constant is a measure of how easily it polarizes in response to an electric field, ε_0 is the electric permittivity of vacuum, ε is the electric permittivity of the medium, $\tilde{\varepsilon}$ is the relative permittivity and $\vec{E}$ is an applied electric field.

A material doesn't polarise instantaneously in response to an applied field as the susceptibility (or equivalently the permittivity) is frequency dependent. The change of susceptibility with respect to frequency characterizes the dispersion properties of the material.

The more electrically susceptible the material, the larger the displacement (polarizability) or the greater the number of dipoles present.

When considering the behaviour of light in a dispersive medium, we can use the Lorentz oscillator model. It is a similar model to the polarization model i.e. the displacement of bound charges under the effect of an external field but assumes that charges (electrons) do not respond instantaneously to an applied time–varying field. This classical model, though relatively crude compared to quantum models that are sophisticated enough to describe atomic–scale phenomena, it can successfully be used to describe many experimental results.

When an external oscillating electromagnetic field is applied to an atom, it causes the electrons in that atom to oscillate. The induced electric field caused by these oscillating particles has a natural frequency which is not necessarily the same as the frequency of the incident light. When the frequency of incident light approximates to the particles' natural frequency (resonance

condition), the electrons can oscillate more strongly, and a larger opposing electric field is created. This larger opposing electric field translates into a larger relative permittivity and, therefore, a larger index of refraction.

Figure 2-3 shows the polarisation mechanisms described above, can be thought of as some displacement of a charged particle from some equilibrium position.

The definition of Polarizability can be written as:

$$\vec{p} = \alpha \vec{E} \qquad (10)$$

Where α is the Lorentz polarizability of a single atom:

$$\alpha = -\frac{q^2}{m}\frac{1}{\omega_0^2 - \omega^2 + i\omega\Gamma} \qquad (11)$$

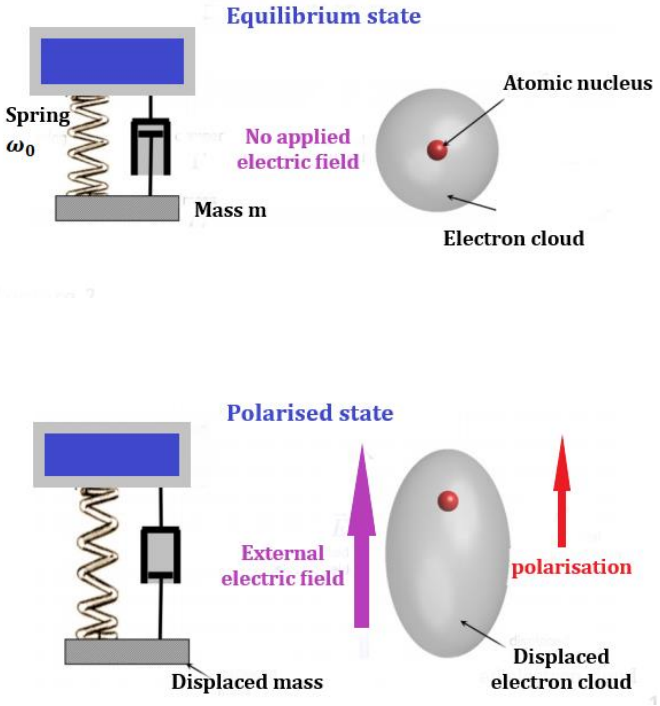

Figure 2-3 Application of an external oscillating electromagnetic field to an atom, causing the electrons in that atom to oscillate.

A medium through which a wave can propagate without dispersion is said to be transparent for that wave. When an electromagnetic wave travels through a medium with a high refractive index, it slows down. For example, in silicon nitride (RI = 2) an electromagnetic wave travels more slowly than through silicon dioxide (RI = 1.45).

According to Beer's Law (R), the light intensity decreases as it travels through an absorbing material. This absorption (k>0) occurs in both UV and IR due to different mechanisms that take energy from the light wave. IR absorption is commonly caused by molecular vibration, i.e. phonons, while UV absorption is generally due to electronic transitions, where light provides energy to excite an electron to an excited state. The decrease in the light intensity per length z (where $z \neq 1$) can be described as:

$$I(z) = I_0^{-i\alpha z} \qquad (12)$$

Where, I_0 is the light intensity before it enters the medium, α is the absorption coefficient and I (z) is the intensity at distance z. Figure 2-4 shows a schematic of the light attenuation during propagation in a medium. The relation of extinction coefficient with absorption coefficient is described as:

$$\alpha = \frac{4\pi k}{\lambda} \qquad (13)$$

Where λ is the wavelength, k is the extinction coefficient (which indicates the amount of attenuation when the electromagnetic wave propagates through the material ($k \geq 0$)) and α represents the absorption coefficient.

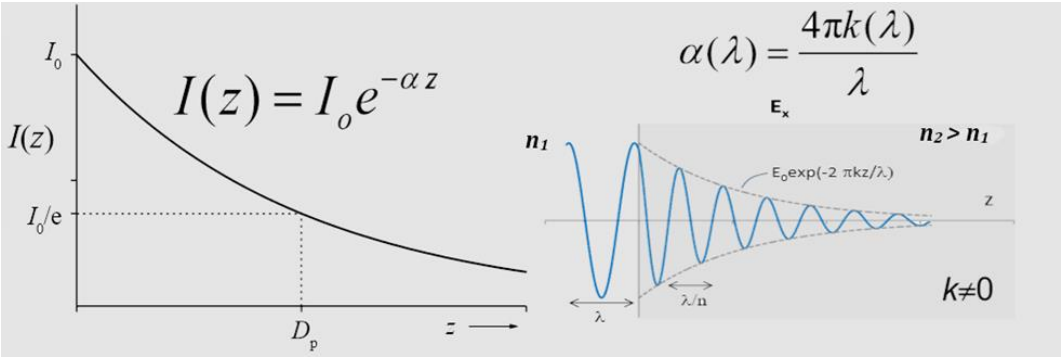

Figure 2-4. Decreasing the light intensity during propagation in a medium. (Picture has taken from J.A.Woollam, Introduction to Ellipsometry).

2.2 Semiconductor

In the last several decades, semiconductor physics has been one of the most advancing and exciting areas of physics. Semiconductors and their related materials play an incredible role in new technology, with almost all current electronic devices reliant on semiconductor-based devices. Because of their useful properties, such as, conducting electric current run in one direction only, having variable resistance and increased electrical conductivity with increasing temperature, semiconductor-based devices are now extensively used in many applications such as, communications, computers, cars and automotive, mobile phones, and healthcare.

Semiconductor materials have an electrical conductivity between conductors (generally metals) and non-conductors or insulators. They are consisting of closely grouped crystalline atoms which arranged in a highly ordered pattern, called “lattice”. Compared to the conducting materials (metals), semiconductors have very few free electrons which are able to flow and generate electrical current under ambient conditions – as there a few thermally generated carriers in the undoped “intrinsic” semiconductor material. Figure 2-5 shows a schematic of conductor, semiconductor and insulator materials, in terms of the energy levels of their quantum states for the electrons.

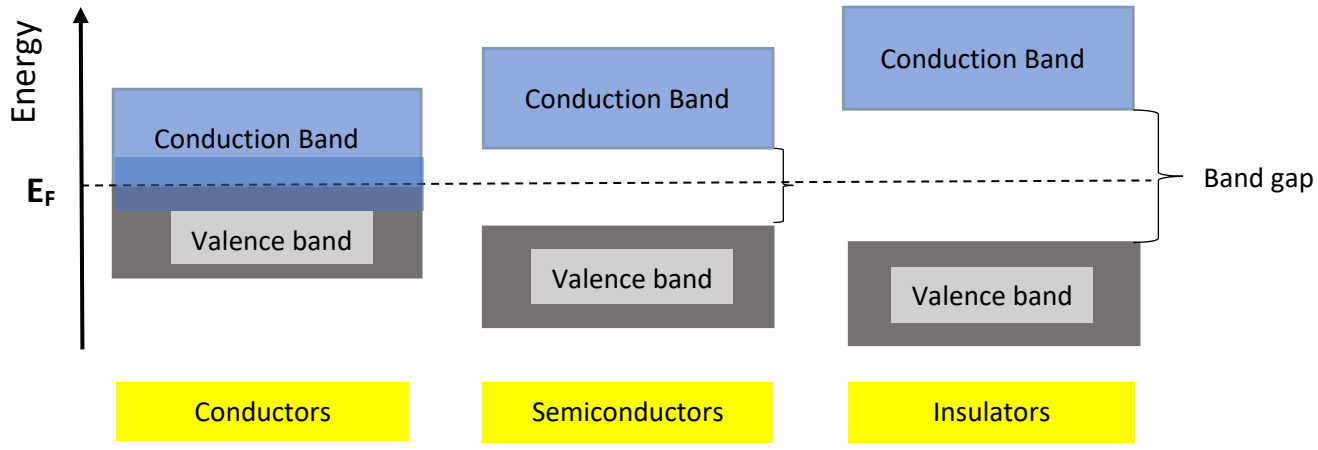

Figure 2-5 Schematic of the band structure of conductor, semiconductor and insulator materials.

The Fermi energy level (the energy level corresponding to highest occupied energy state at temperature zero Kelvin). In conductors, the valence and conduction bands overlap, and the Fermi level can lie within this region. In conductors like metals, there is a "sea" of free

electrons. As the valence band and the conduction band are overlapped, with no band gap, as soon as an electric field is applied, these electrons can move as a group under the influence of the applied electric field - yielding high electrical conductivity, even at low temperatures.

In semiconductor and insulator materials, the electrons in the valence band are separated by an energy gap, which is called the “band gap”. Therefore, in these materials, the Fermi energy level position is within the band gap.

In semiconductor materials at 0 K, the states in the conduction band are empty whilst the valence band is full of electrons. A complete filled or empty band cannot contribute to current transport; therefore, semiconductors are insulators at 0 K. The conduction and the valence band are separated by a band gap where there are no allowed states for electrons.

At T > 0 K, electrons are thermally excited, and they contribute to the electrical conduction by excitation from the valence to the conduction band. In semiconductors, the band gap energy value, is in in the range of $Eg \leq 3$ eV which allows bands close to the Fermi level to be thermally populated with electrons or holes. However, in insulators there is a large band gap ($E_g \gtrsim 3$ eV) and there is little probability of thermal or photonic excitation contributing to electrical conduction in these materials.

There are a large number of elements and compounds with semiconducting properties e.g. silicon, germanium, as well as compound semiconductors like silicon carbide or gallium arsenide. In Figure 2-6 A, the electronic structure of silicon, the most well-known and commonly used semiconductor material, is illustrated. Silicon is a Group IV semiconductor, which is in the same group of the periodic table as Carbon.

If carbon is the main building brick of life, silicon by virtue of is non-toxic nature, high temperature conductivity and low cost, is the main building brick of integrated electronic circuits and technology. Fortunately, both carbon and silicon hare highly abundant elements on earth.

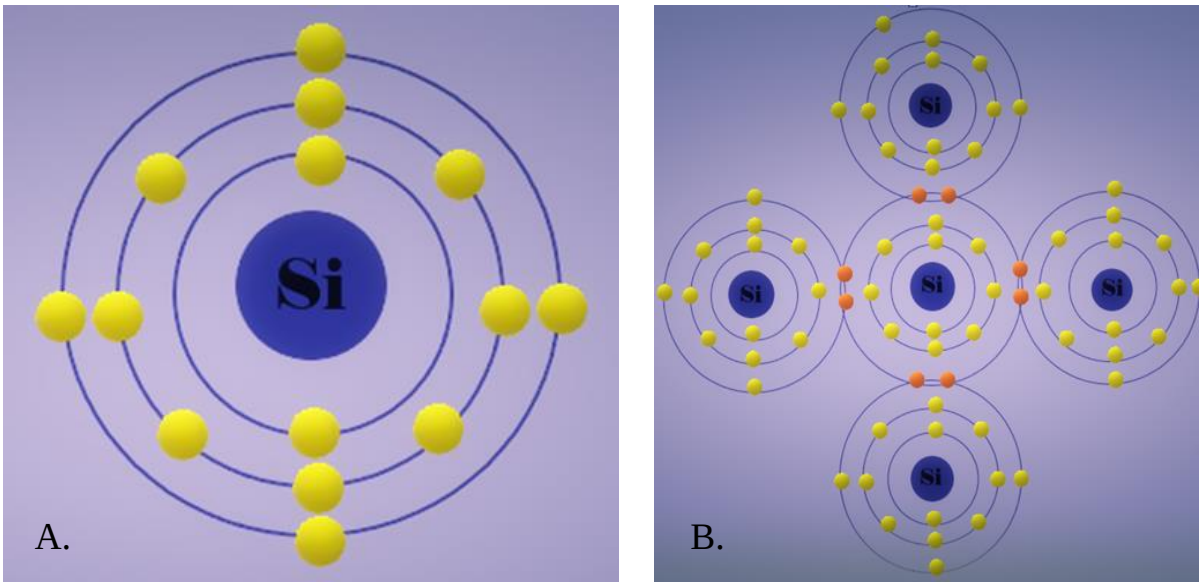

Figure 2-6 A. Schematic of the silicon atomic structure with a total of 14 electrons of 4 of them are in the valence band, the outer shell energy level. B. Schematic of a silicon crystal lattice. Silicon has four valence electrons in its outermost shell which it shares with its neighbouring silicon atoms to form full orbitals with eight electrons.

Pure silicon is an intrinsic semiconductor. Each silicon atom has four valence electrons in its outermost shell which gives it the equal potential to gain or lose electrons. Silicon by covalent bonding, is able to share its electrons with its neighbouring silicon atoms, resulting in the formation of a full orbital of eight electrons at absolute zero temperature Figure 2-6 B. At non-zero temperatures, due to the thermal excitation of electrons, the conduction band would be occupied by the electron charge carriers and the same number of holes would be left behind in the valence band, in pure silicon. However, the bond structure between two silicon atoms is such that each atom shares one electron with its neighbour making the bond very stable. Therefore, this type of bond structure limits the number of free electrons available for any electrical conduction.

Consider a free (isolated) silicon atom with quantized energy levels and 14 electrons where the probability of finding an electron occupying any particular state is based on the Schrödinger equation. If some of these identical silicon atoms are built into a crystal lattice, the electron wavefunction of neighbouring atoms begins to overlap because of the corelative interaction between the atoms. This leads to splitting of the energy levels, based on Pauli's exclusion principle. Due to this principle, the discrete energy levels of any individual atoms are split into bands relating to a pair instead of to each individual atom. (see Figure 2-7)

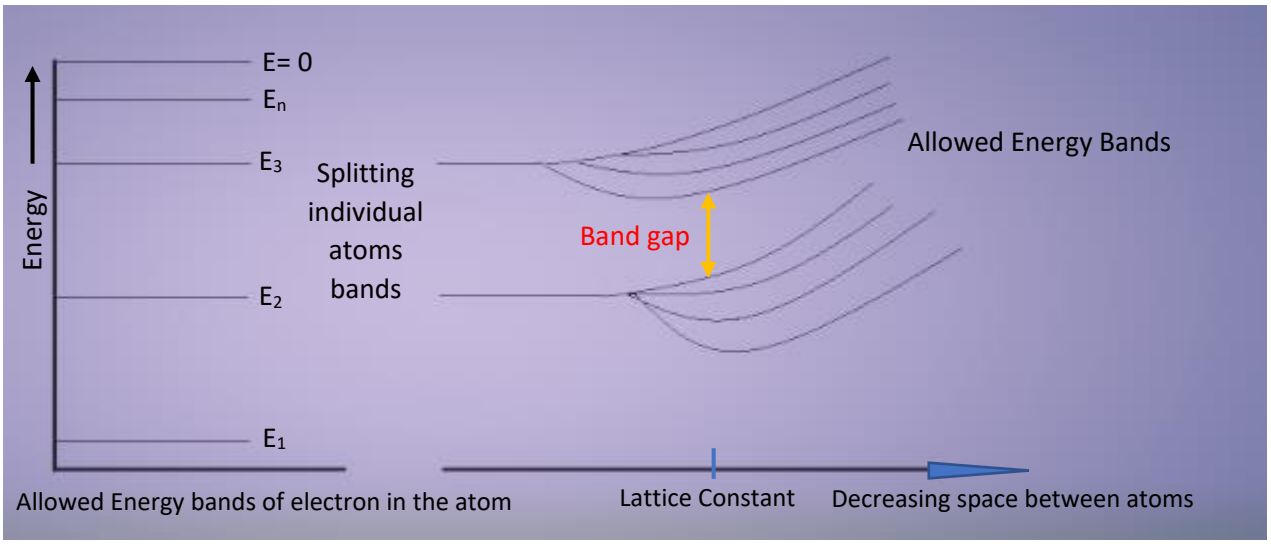

Figure 2-7. Individual allowed energy levels of an electron in the atom (left). Splitting of the individual energy levels by decreasing atomic spacing (right).

The band gap energy decreases from top to bottom of groups in the periodic table. For example, the band gap energy of C (Diamond), Si, Ge and Sn are 5.5 eV, 1.1 eV, 0.7 eV, and 0.1 eV, respectively. This is because as the atomic number increases, the number of electrons and shells increase, which results in increases in the equilibrium bond lengths. It is therefore easier to promote the outermost electrons in the valence band to the conduction band. For instance, the silicon band gap with its $3p^2$ valence orbital, is larger than Germanium with a $4s^2$ orbital.

2.3 N-Type and P-Type Semiconductors

As described in the previous section, conductivity of pure silicon is very low, but by adding a small percentage of another donor or acceptor element (with excess electrons or holes) to the silicon crystalline structure, more free electrons or holes can be created. The densities of respective carriers will increase and this result in a dramatic change of the silicon conductivity enabling it to be used as a material for electronic devices (see Figure 2-8). This process is called "doping" which leads to form the two types of the extrinsic semiconductors, N-type and P-type.

Figure 2-8 Introducing a small portion impurity atom to a lattice site, dramatically changes the electronic properties of the semiconductor structure. (Picture taken from https://www.pinterest.co.uk/pin/656751558144017354/)

N-type semiconductors form, by adding donor elements with excess electrons such as; Phosphorus (P), Arsenic (As) and Antimony (Sb) from Group V, and P-type semiconductors forms by adding acceptor elements with a deficit of an electron from Group III such as Born (B), Gallium (Ga) and Indium (In).

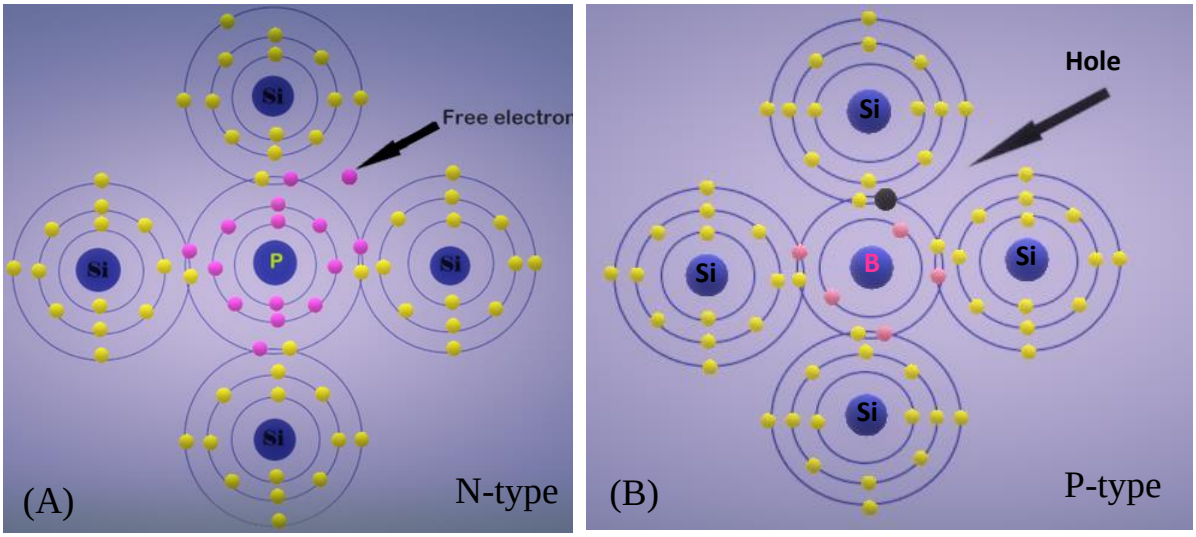

Figure 2-9 (A) N-Type doping by adding Phosphorus (P) donor atoms to the crystalline silicon structure which leads to free electrons in the semiconductor structure and an increase the conductivity of the crystal lattice. Figure (B) P-type doping by adding Boron (B) acceptor atoms to the silicon crystalline structure and increasing the conductivity of the silicon semiconductor by producing holes in the structure.

Figure 2-9 (A) shows a schematic of N-type doping by addition of Phosphorus (P) donor atoms into the silicon crystalline structure. Phosphorus atoms have five electrons to share with neighbouring silicon atoms. Four of these orbital electrons make the covalent bands with surrounding silicon atoms and that leaves one electron which is loosely bound and therefore behaves as a free mobile electron. When an external electric voltage is applied, this makes electron flow – electrical current.

In N-type semiconductors, the energy levels of the donor atoms (the red line in Figure 2-10 lies just slightly below the conduction band in the forbidden gap. The existence of these additional electrons, which may be easily excited and hop into the conduction band, contributes to current flow. Therefore, electrons are the majority charge carriers in N-type semiconductors.

Figure 2-9 (B) illustrates a schematic of P-type doping by adding Boron (B), one of the most commonly used doping agents, as an impurity acceptor atom to the silicon lattice structure. Boron, having only three valence electrons in its outer orbital, cannot make a complete bond with one of the neighbouring silicon atoms, as one electron is missing. Therefore, these Boron atoms, form positively charge carriers, which are known as “holes” in the silicon semiconductor structure.

The hole in this doped silicon lattice structure, attracts a neighbouring electron to fill itself. However, when this neighbouring electron leaves its position to fill an aforementioned hole, it creates a new hole which then needs to be occupied and filled by attracting another neighbouring liberated electron. In this process, it seems that the holes are moving as a positive charge through the crystal lattice structure, (holes effectively move in the opposite direction of the free electrons) which results in deficiency of electrons and infers a positive charge on the crystal.

In P-type semiconductors, the energy levels of the acceptor atoms, (electron-accepting levels), lie just above the top of the valence band in the forbidden gap and allow more holes to be introduced into the valence band. Electrons from the valence band can then easily hop into the acceptor atom holes, even at low temperature. In this type of semiconductor, positive holes are the majority charge carriers.

Therefore, both electrons and holes contribute to current flow. A schematic representation of the N-type and P-type concept is shown in Figure 2-10.

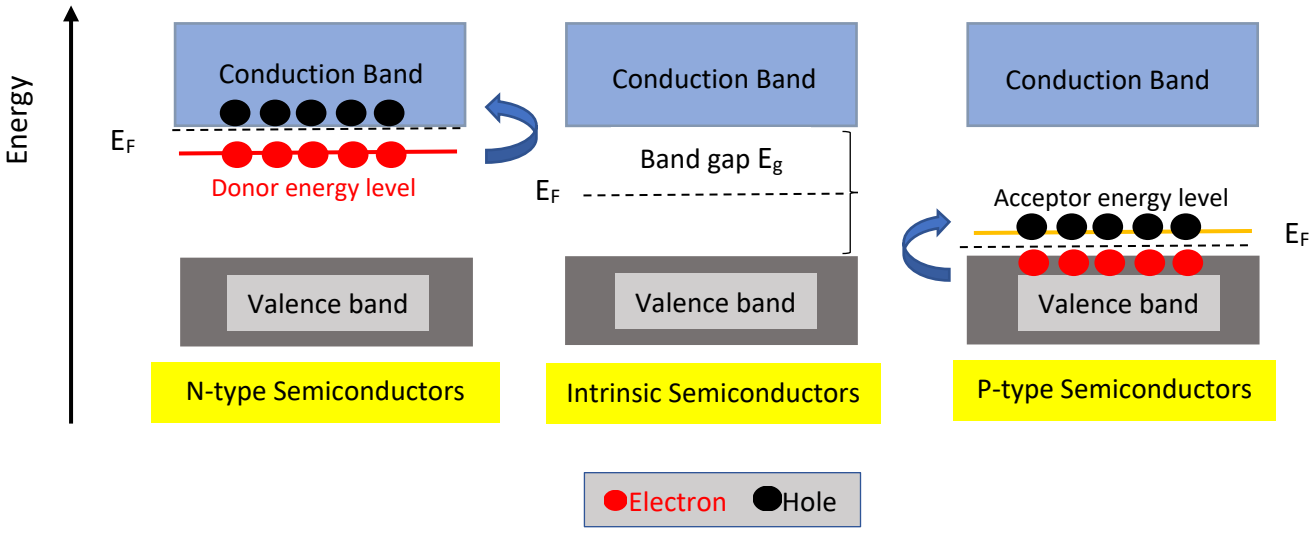

Figure 2-10 Schematic of N and P type doping. In intrinsic (pure) semiconductors, the fermi level is halfway between the valence and conduction bands. In N-type semiconductors, adding donor impurities to the crystalline lattice structure leads to an increase the number of free mobile electrons, presenting additional allowed energy levels close to the conduction band and shifting the fermi energy level close to the conduction band which makes it easy to for these electrons to hop to the conduction band and contribute to current flow.

2.4 Direct and Indirect Band Gap semiconductors

Input of sufficient enough energy in the form of photon or heat, causes electrons excitation from their initial state in the valence band to higher energy states in the conduction band. Excitation of an electron leaves behind a hole with net positive charge. The electrons in the conduction band are known as mobile negative charge carriers, whilst the holes in the valence band are positive charge carriers.

According to the Planck–Einstein relation, the excitation energy required is equal to:

$$E = h\upsilon = h\frac{C}{\lambda} \qquad (1)$$

Where, E is the required energy, υ is the frequency, *h* is the plank constant (6.626×10^{-34} J.s) and *C* is the speed of light in vacuum.

Electrons are not able to stay in a higher energy level for an unlimited time. Therefore, according to conservation of energy, the electron relaxes back to its initial lower energy state, E_V, by releasing the excess energy $h\upsilon$ in a process known as recombination. This recombination energy may be emitted as a photon or given away to the lattice as phonons or heat. The routes for excitation and recombination give two types of semiconductors (direct or indirect bandgap).

When a free electron or a hole moves, it carries a quantum momentum which has a parabolic relation with its energy:

$$\hbar = \frac{h}{2\pi} \qquad (2)$$

$$P = \hbar k = \frac{E}{C} \qquad (3)$$

$$E = \frac{P^2}{2m} = \frac{\hbar^2 k^2}{2m} \qquad (4)$$

$$E = a\,k^2 \qquad (5)$$

where P ($\hbar k$) is the momentum, h is the plank constant (6.626×10^{-34} J.s), $\hbar$ is the reduced Planck constant, k is the wavevector, E is the electron energy, C is the speed of light in vacuum.

By plotting allowed values of energy as a function of momentum, the minimum and the maximum states of the valence and conduction bands are characterized by a certain value in the Energy-Momentum (E-k) diagram. The excitation and recombination processes in E-k space, require the electron and the hole's momentum to be the same in order for these processes to take place. But these values are not always equal. Therefore, there are two possibilities which determine the two type of semiconductor materials.

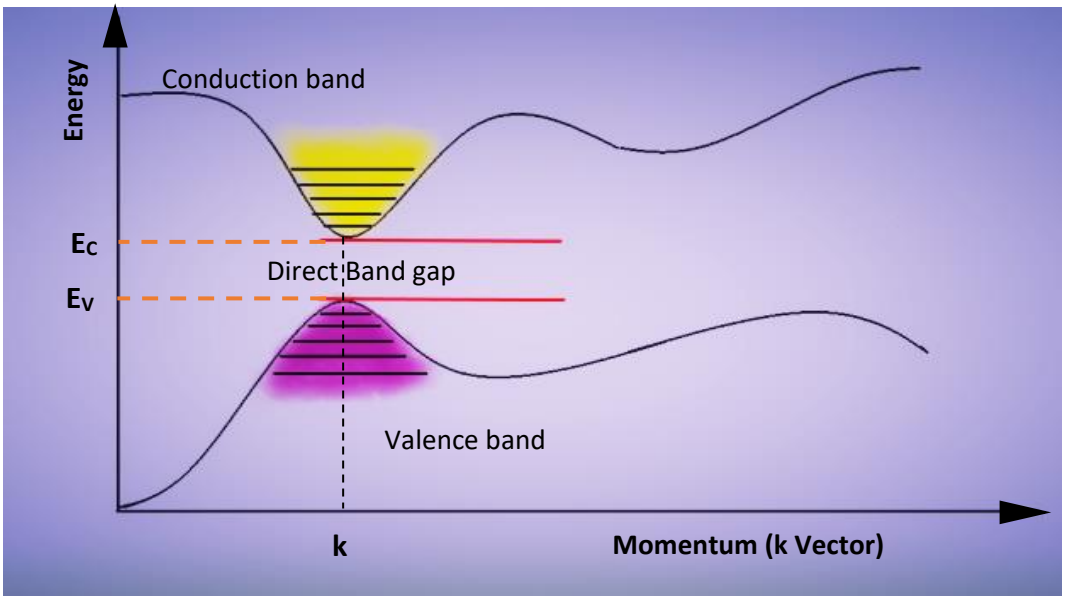

Figure 2-11. Illustration of direct band gap semiconductor energy / momentum plot.

In, a direct band gap semiconductor (Figure 2-11), the momentum of electrons and holes in both the conduction and the valence band have the same value of k vector. Therefore, an electron makes a simple transition to the conduction band by absorbing a photon with energy equal to the band gap, without a change in momentum. The electron relaxes back to the valence band in a recombination process and is annihilated be recombination with a hole. This releases a small amount of energy as direct emission of a photon. The momentum similarity of the valence and conduction band results in a high probability for radiative processes in these types of semiconductor materials.

In indirect gap semiconductors such as Si, Ge or GaP, the picture is more complicated, as the valence band has a maximum at a value of k1, which is different from the minimum k value of the conduction band. Therefore, energy transitions between the valence and conduction bands

for an electron also require a change in momentum. A photon cannot carry the necessary momentum in order to comply with conservation rules. Hence a phonon which carries little energy and large momentum is simultaneously needed. Since this electron-hole pair - photon – phonon process has a low probability of occurring, in practise indirect gap semiconductors are very poor light emitters.

In indirect bandgap semiconductors (Figure 2-12), an electron transfers the excess momentum to the crystal lattice by making a transition through an intermediate defect trap state and emission of a phonon. This transitional state is placed within the band gap and is known as a trap state. Trap states are related to the presence of structural defects or foreign atoms (impurities or dopants) in the crystal lattice. The trapped electron in this state, makes its second transition as soon as an empty state appears in the valence band. Recombination of an electron and a hole results in annihilation of them both. Therefore, in indirect band gap semiconductors, nonradiative processes dominate and these materials are not suitable to be used in light emitting devices.

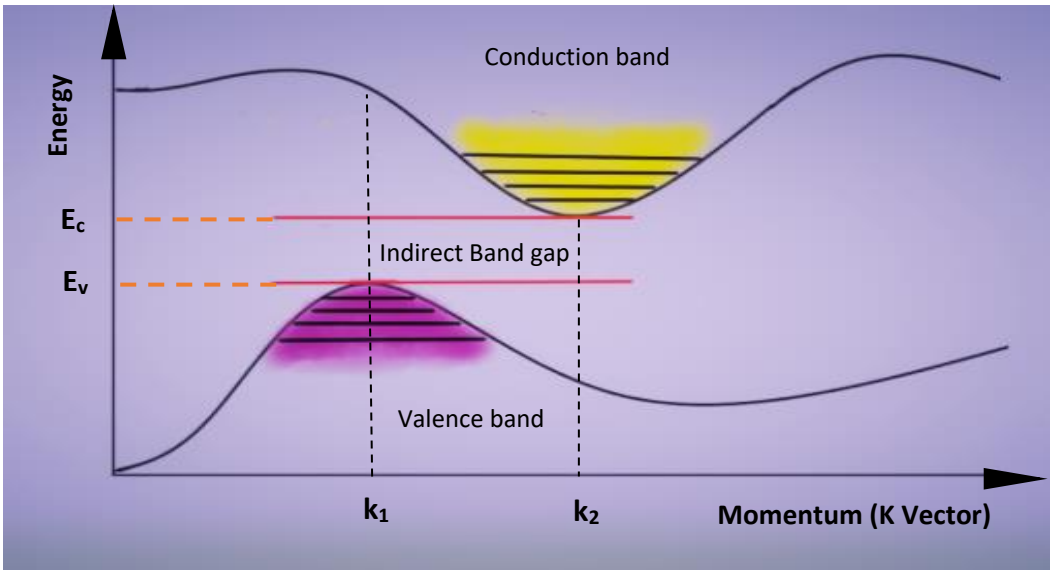

Figure 2-12. Illustration of Indirect bandgap semiconductor.

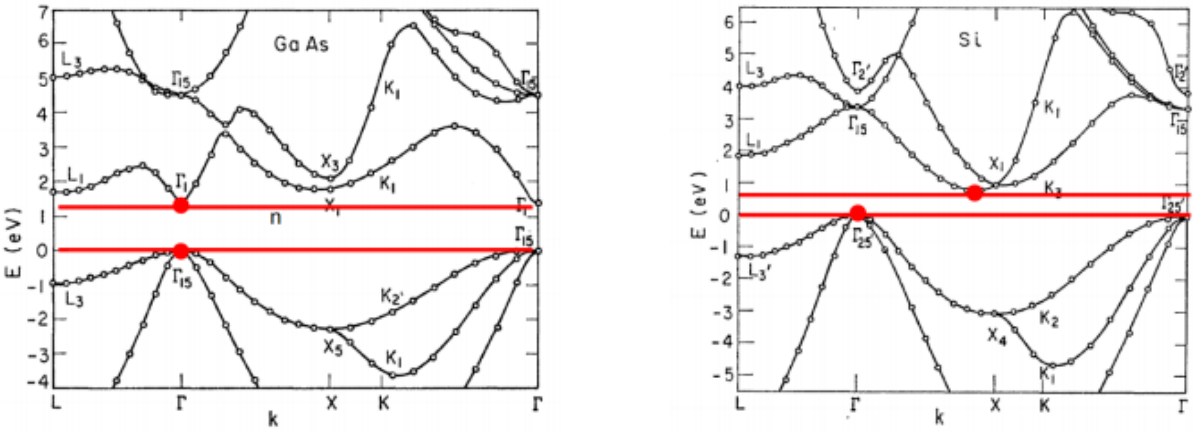

Figure 2-13. Band structures of GaAs and Si. Taken by T.K. Bergstrasser and M. L. Cohen [taken from Physical Review B 141, 798, (1966)]

Figure 2-13 illustrates the energy-momentum curves for a GaAs (a direct bandgap semiconductor) and Si (an indirect bandgap semiconductor). The figure shows that in GaAs the top of the valence band and the bottom of the conduction band have the same k value at Γ.

In photonic and optoelectronic devices, semiconductor materials are used in combination with dielectric materials. The semiconductor material in photonic devices can often function as the active part of the device, whilst the dielectric materials function as the passive component.

For example, in silicon photonic devices the silicon can be used as a core waveguide whilst the dielectric silicon dioxide layer is used as a cladding or passivating material confining light to the core.

2.5 Silicon Photonics

Silicon is also widely used in photonic devices, particularly in waveguide and optical communications devices. Silicon photonics is a versatile photonic integration platform that leverages the infrastructure and fabrication processes known from standard CMOS technology. Silicon's transparency for wavelengths greater than 1.1 μm makes this technology very attractive for a wide range of applications in the datacom and telecom industries, which operate in the wavelength windows around 1.3 and 1.55 μm, respectively.

The main application is in silicon photonics-based transmitters and receivers for optical interconnects, but there is great potential for broadening the scope to such applications as sensing. Other examples of silicon photonic devices will be presented next:

2.5.1 Waveguide

Optical waveguide is a most important part of every photonic circuit. In 1980s, the first type of waveguides, silicon on doped silicon [3][4] silicon on sapphire [5], silicon germanium [5], and Silicon on Insulator (SOI) [6] were produced. In optical communications applications, the dielectric layers patterned and etched as the channels on SOI or silicon substrate to form the silicon photonic waveguides which are able to transmit the light without significant optical losses. Recently, Using waveguide devices in sensing applications is one of the most important achievements in this field [7].

Waveguides have historically been based on optical fibres, made of glass (silicon dioxide), used for transmission of photonic signals in optical communications systems. These fibres can be used to transport signals in short, medium and long-haul optical communications applications.

Optical fibres are most commonly made from silicon dioxide. However other glass materials may also be used, and plastic optical fibre can be used for short-distance applications.

The optical fibre has a cylindrical core of a dielectric waveguide material, usually silicon dioxide, surrounded by another dielectric material with a lower refractive index. The different refractive indices can be achieved by doping the different silicon dioxide layers or blending

silica with other oxides such as Germanium Oxide. The refractive index of the silica layers can be increased by varying the amount of Germania added to increase the fibre's RI.

Optical fibres with a silicon core and a silicon dioxide cladding layer (thus yielding a high RI contrast) have also been researched [8]. Issues with these type of fibres include high loss in the amorphous or polycrystalline silicon medium [9].

More recently, alternative waveguide designs such as planar (or slab), strip or rib waveguides have been developed.

A silicon waveguide consists of a silicon core with a high refractive index of around 3.5 at wavelengths from 1260 nm to 1675 nm – used for communications. The silicon bandgap of 1.12eV equates to 1100 nm and hence silicon has negligible absorption at the telecommunication wavelengths [10].

As mentioned above silicon dioxide (oxide) also has minimal absorption at these wavelengths.

In the waveguide devices, silicon oxide is used as a cladding material for silicon waveguides, where the oxide confines light to the silicon core through total internal reflection [11]

The communications bands at 1310 nm and 1550 nm are used in these applications. Figure 2-14 and Figure 2-15 show the structures of some common waveguide formats.

Figure 2-14 shows the structure of an asymmetric slab waveguide, consisting of three different dielectric layers each with a thickness t_n and refractive index n_n. The order of the refractive indices is $n_1 > n_2$ and $n_1 > n_3$, so that total internal reflection can occur at each interface.

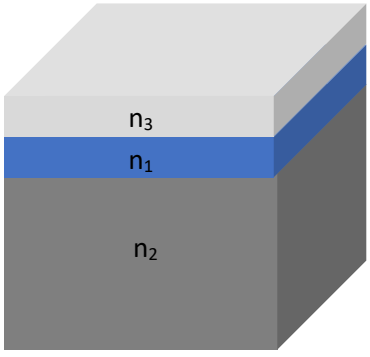

Figure 2-14. Slab waveguide structure.

The n_1 layer is often referred to as the core or guiding layer and has a high RI, whilst n_2 is the substrate and n_3 is the cladding layer, both with lower RI.

For silicon waveguides, n1 is typically silicon with n2 being buried oxide layer and n3 also an oxide layer.

In the slab waveguide, optical confinement is only in one transverse direction, the core is sandwiched between cladding layers in only one direction. They are primarily used for high-power waveguide lasers and amplifiers [12].

2.5.1.1 Strip waveguide

The strip waveguide is another simple structure which has a rectangular cross section core, made of a high RI material such as silicon or silicon nitride, clad with a lower RI material (silicon dioxide). Roughness of the side walls of the strip waveguide is critical and a reduced RI contrast can lessen the impact of interface roughness – the major source of optical loss in such structures.

2.5.1.2 Rib waveguide

A rib or ridge type waveguide is similar to the strip waveguide but achieved via a partial etch of the silicon layer of an SOI wafer (see Figure 2-15).

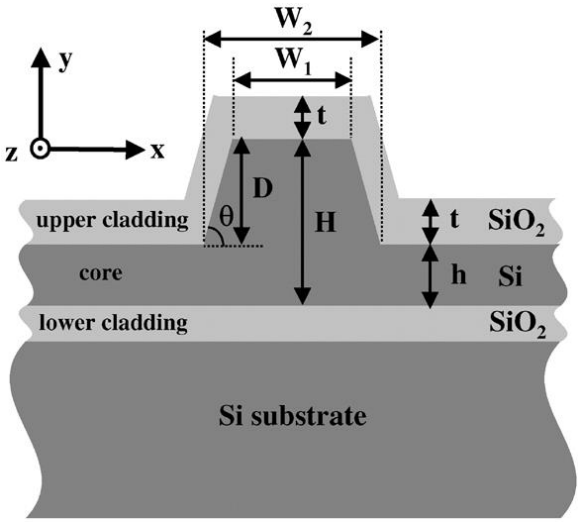

Figure 2-15. Schematic of a Rib waveguide (reproduced from [JOURNAL OF LIGHTWAVE TECHNOLOGY, VOL. 23, NO. 3, MARCH 2005])

A difficulty of the structure is the control required for the etch depth of the rib or ridge feature, as unlike the strip waveguide, the rib does not provide a chemically different etch stop like the BOX.

There are several other possible waveguide configurations which have advantages and disadvantages in terms of optical performance and fabrication complexity.

2.5.1.3 Silicon nitride Waveguide

The high linear and nonlinear losses in silicon optical waveguides can be avoided by using silicon nitride Si3N4 as the core material. Silicon nitride is an electrical insulator and is transparent at visible and IR wavelengths, but has some shortcomings relative to silicon-based photonics, for example, the RI is lower - around 2.0 for communication wavelengths. The lower RI of silicon nitride in comparison to silicon means that its waveguide performance is affected by less dense integration and a lower nonlinear Kerr effect.

A more in-depth discussion of materials used for waveguides is presented in the following sections.

2.6 Dielectric

The term dielectric was first coined by Faraday to suggest a structure which is analogous to current flow through a capacitor, where during the charging process a current introduced at one plate (usually a metal) flows through the insulator to charge another plate (also usually a metal). [13]. The dielectric material fulfils the insulator material function in this case.

More recently, dielectrics have been used not only as electrical insulators, but also as photonic materials – capable of transporting light, without significant optical losses.

Several dielectric materials have been developed for photonic applications, but the most common are silicon dioxide (oxide) and silicon nitride. These materials, in addition to the hybrid silicon oxynitride materials, are reviewed in the following sections.

2.6.1 Silicon dioxide and silicon nitride

Silicon dioxide (SiO_2) is an electrical insulator and is commonly used in electronics devices as such. SiO_2 is also widely used in photonic devices such as waveguides. In waveguides SiO_2 is used as the low RI layer of the waveguide device.

Silicon nitride is a well-known material in the CMOS industry where it has been used for many years as an insulator and implant masking material. Silicon nitride is increasingly being used as a material for waveguides, where it can be used as the high index core.

A material with intermediate stoichiometry and intermediate properties between silicon dioxide and silicon nitride is silicon oxynitride, discussed in the following section.

2.6.2 Silicon oxynitride

Silicon oxynitride (SiNxOy) is an important dielectric material in new semiconductor and optoelectronic technology which has been extensively studied because of its attractive properties and significant electronic and mechanical performance. Some of these properties are included of low thermal expansion coefficient and low thermal conductivity [14][15], outstanding oxidation resistance up to 1600 C^o, and high temperature strength without degradation up to 1400 C^o [16].

The other excellent properties of silicon oxynitride is a low dielectric constant of this material [17] which is attractive as ceramic insulators. Dielectric constant (k), or relative permittivity ($\tilde{\varepsilon}$), is the ratio of permittivity of a substance to the permittivity of free space. In other words, dielectric constant is the ratio of the amount of electrical energy stored in a material by an applied voltage, relative to that stored in a vacuum. As the dielectric constant increases, the electric flux density which is the total amount of electrical charge per area, increases as well. Therefore, materials with larger dielectric constant are able to hold large quantities of charge for long periods of time.

In electronic devices, dielectric materials usually operate as an insulator. In the latest devices, silicon dioxide is being replaced by alternative dielectric materials, in some cases. One of the methods to reduce the size of the microelectronic devices is using a high dielectric constant (high- k) material in their fabrication. In digital circuits, insulating dielectrics separate the conducting parts like wire interconnects and transistors, from one another. When scaling down the components in size, the conductive parts of the device will be closer together and the insulating dielectric will thus be thinner to the point where charges will be built up and unwanted transfer of signals between them affect the performance of the device. Therefore, using a high dielectric constant material enables the thinner later to maintain its insulating properties in these reduced scale devices.

SiN_xO_y is a material with an intermediate phase between silicon dioxide (SiO_2) and silicon nitride (Si_3N_4) [18], which has the ability to withstand at high temperature [19][14].

The refractive index of silicon oxynitride can be anywhere in between two extremes from silicon oxide with 1.45 to silicon nitride with refractive index of 2. Therefore, the large range of refractive index of silicon oxynitride, gives the greater options for different designs in optoelectronic devices which makes it an interesting material in this field .

Because of all these unique performances, SiN_xO_y has great potential for being used in microelectronic fabrication [20], micro electromechanical systems (MEMS), optoelectronic devices and integrated circuits such as waveguides or thin-film transistors optical, gate dielectric materials, sensors for optical telecommunication and sensing device applications.

2.6.3 Precursor gases used in silicon oxynitride PECVD deposition

There are three different precursor gases which combination of them results to produce the silicon oxynitride dielectric material film. These gases are including of silane (SiH_4), nitrous oxide (N_2O) and nitrogen gas (N_2) using high frequency or instead of nitrogen gas, using ammonia (NH_3) with low frequency PECVD technique, which they provide the silicon, oxygen and nitrogen respectively to the film composition. Nitrous oxide (N_2O) is used as the source of the oxygen, instead of oxygen gas (O_2) because the chemical bonds in N_2O break more easily than O_2 bonds.

The advantage of using NH_3 precursor gas instead of N_2 in silicon oxynitride deposition is that the energies of N-H bonds are almost three times smaller than those of N ≡ N bonds (391 kJ/mol versus 941 kJ/mol), and therefore requires less energy or temperature to break. However, it is reported that using NH_3 gas in the deposition process, leads to undesired N-H bonds in the deposited films [21][22][23][24]. The N-H bonds can absorb energy and this lead to unwanted optical losses [25][26].

Changing the gas flow ratio of these reactant gases during the deposition process, results to change the film composition which leads to achieve the desired refractive index of the film.

2.7 Silicon nitride, oxide and oxynitride waveguides

2.7.1 Silicon nitride / silicon oxide waveguide design

Significant effort has been expended on achieving reduced size and footprint of waveguide devices to enable higher levels of integration in planar light wave circuits (PLCs). Waveguide bends and splitters are critical elements of the waveguide design which ultimately determine the footprint of the waveguide device.

The design of an ideal low loss waveguide device is not a straightforward work. As mentioned above, one of the main parameters which determines the characteristics of light propagation and the scale of integration of a photonic device is the refractive index contrast of a waveguide. The contrast is the difference between the core and the cladding refractive index. It has a footprint on determining some properties such as the fabrication processes, repeatability, waveguide dimensions, waveguide losses and bending radius. The contrast itself, is determined by choosing different dielectric materials or different compositions as the core and cladding layers in the waveguide device. Therefore, the material selection plays a crucial role in the operation of a fabricated device. Every optical technology has its own rule, advantage and limitations which determine the material selection.

Low refractive index contrast waveguides in low index materials such as silica typically have a minimum bend radius of multiple millimetres to several centimetres, which creates an ultimate limit to device size reduction. Waveguides with a low refractive index contrast between the core and the cladding may also have issues with light leakage from the core to the cladding.

Therefore, a logical approach to reducing the size of waveguide is to use waveguides with high refractive index contrast. A high index contrast allows a smaller minimum bend radius. In addition, the higher the contrast, the higher the degree of bending that can be designed into the waveguide. For example, at the communications wavelengths of 1.3 μm and 1.5 μm wavelength core materials with a large refractive index contrast - such as Si or poly-Si embedded in a low index cladding of SiO_2 may be used. The high index contrast permits total

internal reflection (TIR) to confine light to the waveguide, even when the bend radius is reduced to the order of a few microns.

One of the issues which must be considered in designing a waveguide is optical waveguide leakage. This occurs when a low refractive index waveguide is deposited on top of a high index substrate such as silicon. This problem could be solved either by increasing the thickness of the buffer layer, which is the layer between substrate and the core or by changing the core to the higher refractive index material such as silicon nitride [27] .

In addition to the dielectric materials used in waveguide designs such as the rib or ridge waveguide, the device fabrication can also have an impact. In the ridge waveguide, the core material is etched into a mesa structure. The etch process, if not performed well, can lead to sidewall roughness (emanating from the etch process used to define the waveguide structure). It has been reported that using silicon nitride as the core dielectric material in a waveguide device allows a greater better tolerance sidewall roughness than for a silicon core. Another beneficial aspect of using a silicon nitride core is that its relative refractive index difference can increase to 0.62 – the index difference between Silicon nitride and silicon dioxide. This large difference allows for a tight bending radius, which in turn enables improved device integration. However, disadvantages of using Si_3N_4 include low fracture toughness and poor electrical insulator properties. This has limited the application of silicon nitride in waveguides.

An alternative to silicon nitride is to use silicon dioxide in waveguide devices. As already mentioned, silicon dioxide is widely used in microelectronics [28][29][30] – as an electrically insulating layer - but is also commonly used in optical waveguides [31], due to its low dielectric constant, low defect density, and low residual stress. However, oxygen, sodium, and boron can all diffuse within the SiO_2 film and therefore modify the optical properties of the film. For this reason silicon dioxide is not an optimal material for encapsulation layers [32]. This is in contrast to Si_3N_4, where the diffusion is less of an issue.

A more flexible material, with some of the best properties of both silicon dioxide and silicon nitride is silicon oxynitride, SiNxOy, which is a promising candidate for optical devices. SiNxOy has tunable optical and electrical performance – depending on the stoichiometry or chemical composition of the SiNxOy film. This can be tuned during the deposition process, and in so doing, its refractive index and dielectric constant can also be tuned [33]. In summary the SiNxOy is a highly attractive material for many applications including integrated circuits (IC) [34], barrier layers [35], optical waveguides [36].

2.8 Optical loss

The most important concern in designing a waveguide is losing the light energy during propagating inside the waveguide. loss in a system can be expressed as [37]:

$$\text{Loss}_{\text{dB}} = 10 \log \frac{P_{out}}{P_{in}}$$

where P_{in} is the input power to the optical device (such as fiber) and P_{out} is the power available at the output of the fiber. Optical loss is typically expressed in terms of decibels (dB) and can be calculated using:

2.9 The infrared band used in telecommunications

FTIR absorption is important when considering the attenuation of light in silica type optical devices such as fiber optics, as the silica may absorb strongly in the infrared region, typically around 850, 1300 and 1550 nm (Figure 2-16). When designing materials for optical device applications, minimised IR absorption is highly desirable. The optical signal attenuates during Transmission along the optical fiber. This attenuation depends on the wavelength of the light beam.

The attenuation of glass optical fiber is caused by two factors, absorption and scattering. Scattering is caused by light bouncing off atoms or molecules in the glass. It is strongly a function of wavelength, with longer wavelengths having much lower scattering. This is the reason of appearing the sky, blue.

Absorption occurs at several specific wavelengths, which for silica are predominantly at wavelengths in the Infra-Red.

Infrared radiation is emitted or absorbed by molecules when they change their rotational-vibrational movements. It excites vibrational modes in a molecule through a change in the dipole moment. Bonds have specific bending or stretching modes which absorb IR radiation at specific frequencies. For example, in a silicon nitride film, there may be absorptions due to Si-

H stretching or bending modes, and asymmetric or symmetric Si-N stretching modes. All these stretching or bending modes will absorb at different IR frequencies.

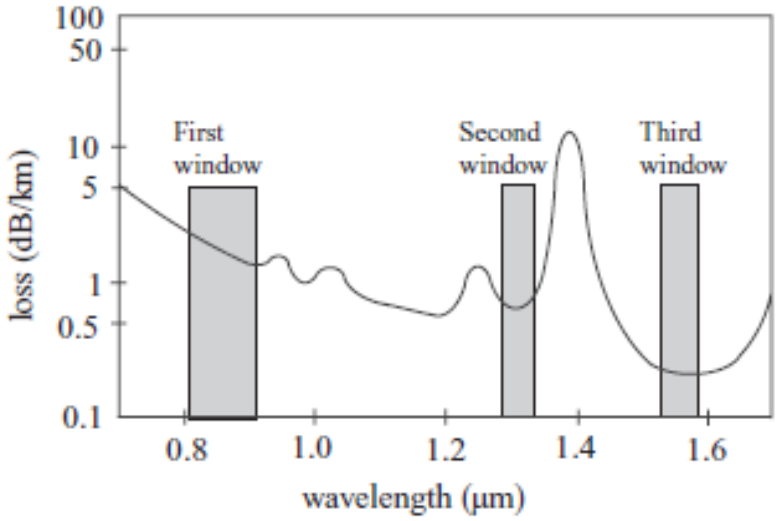

Figure 2-16. Three different three optical communications windows The Attenuation-Wavelength Curve and the Transmission Windows of an Optical Fiber.(Image is taken from Marek Wartak's Computational Photonics book).

Selecting regions of the infrared spectrum where there is little absorbance infers suitability for photonic components. Limitations of using longer infrared wavelengths relate to light absorption producing significant heating effects. At longer wavelengths, ambient temperature becomes important as it contributes background noise, making signals difficult to interpret.

The International Telecommunications Union (ITU) has published some standards for optical communications. According to this standard, the part of the infrared spectrum that is used is divided into seven bands based on availability of light sources, transmitting/absorbing materials (fibers) and detectors. Thus, different manufacturers are able to develop their components which are compatible with the standards for optical communication. The six-transmission bands which are specified by ITU are listed in Table 1.

Table 1. The six-transmission bands are specified by ITU.

Band	Descriptor	Wavelength (nm)
O	Original	1260-1360
E	Extended	1360-1460
S	Short wavelength	1460-1530
C	Conventional	1530-1565
L	Long wavelength	1565-1625
U	Ultralong wavelength	1625-1675

Bandwidth is the portion of the spectrum that a given telecommunications system can use. A system that operates with frequencies between 150 and 200 MHz has a bandwidth of 50 megahertz. An important distinction in spectrum technology is the difference between narrowband and broadband. Narrowband signals have a smaller bandwidth (kilohertz) and are used for limited services such as paging and low-speed data transmission. Broadband signals have a large bandwidth (megahertz) and can support many advanced telecommunications services such as high-speed data and video transmission. The precise dividing line between broadband and narrowband is not always clear, and changes as technology evolves.

Between all these telecommunication bands, the C band shows the lowest optical loss and therefore, it is commonly used in many optical applications such as Wavelength-Division Multiplexing (WDM) technology. WDM is one of the most widely used devices in optical communication technology. The C band corresponds to the region of the FTIR spectrum with lowest optical loss – sometimes referred to as the “Third window” (Figure 2-16). The Third window transmission region is predominantly used in optical communications today. Previously, the first and second windows were used, as they also represent regions of low optical loss. The first window region is also known to have minimal optical scattering as well as low absorption. The second window has lower absorption than the first window. The third window has the lowest optical absorption and this the lowest losses. All three windows are important in optical communications and thus experimental investigations often use light sources at 636 nm, 1310 nm and 1550 nm wavelengths to characterise the IR absorbance by

materials at these wavelengths. Indeed, these three wavelengths have been used to assess the optical absorbance properties of silicon oxynitride films in this thesis.

Figure 2-17 schematically shows a typical WDM transmission system. At the transmitter side, multiple optical transmitters – each emitting at a different wavelength – individually send signals to the multiplexer (MUX), where the signals are multiplexed. The multiplexed signals are then transmitted over one main transmission line (optical fiber cable). At the receiver side, the signals are de-multiplexed by a wavelength de-multiplexer (DEMUX) and sent to multiple receivers.

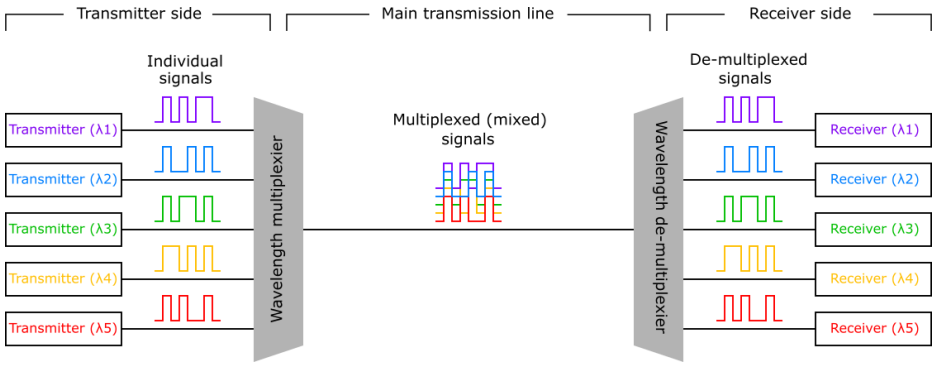

Figure 2-17. Schematic of Transmitter input into multiplexer (MUX) for signal mixing and then subsequent de-multiplexing.(Picture taken from wikipedia/Wavelength-division_multiplexing)

One primary advantage of using WDM technology is in reducing the number of fibers used in the main transmission line. The distance of an optical transmission line sometimes exceeds 1,000 km, and the cost of fiber cable manufacturing/deployment would become a serious issue if installation of a high-fiber-count cable over a very long distance was required. Using WDM technology, (1) the number of fibers in an optical cable is reduced, and (2) the number of wavelength multiplexer/de-multiplexers basically remains the same no matter how long the transmission distance is. For that reason, WDM generally becomes advantageous as the transmission distance becomes longer.

The optical loss of the silicon oxynitride films in the wavelength range of visible light is very low (about 0.2 or 0.5 dB/cm). However, in the near infrared region, the vibrational overtones of hydrogen bonds increase the absorption which leads to optical loss in this region. In the third optical communication window, this loss is due to the third and second harmonic overtones of the Si-H and N-H bonds, respectively. The absorption peaks of these overtones are in the wavelength range of 1480 to 1520 nm.

2.10 Photonic devices

Semiconductor devices have traditionally been based on silicon. More recently, compound semiconductor materials, in particular III-V semiconductors have been used in device applications – particularly for optoelectronics and photonic devices. The advantages of III-V materials relate to the wide variety of materials and layered structures that can be created by varying the elemental ratio of the material; the ease with which these materials can be grown on top of one another; and the direct bandgap of many of these materials – which makes them highly suitable for optoelectronic and photonic devices.

III-V materials are thus extensively used in optoelectronic and photonic devices. Examples of III-V photonic devices include: VCSELs (Vertical Cavity Surface Emitting Lasers), which are used in 3D facial recognition, LIDAR and other 3D scanning systems.

2.11 Light emitting diode

The light-emitting diode (LED) is one of the basic but common optoelectrical devices which are extremely used in life and technology since the invention on 1962 [38]. LED's are semiconductor light sources containing which work based on electron-hole recombination process. LED's emit light when current flows through this device which is contain of p and n type semiconductor materials with direct band gap energy such as Gallium phosphorus arsenide (GaPAs). Electrons in the semiconductor recombine with holes, releasing energy in the form of spontaneous photon emission therefore, LED diodes emit in the form of incoherent, diverted beam of lights. The magnitude of energy needed for an electron to cross the band gap of the semiconductor material used in this device, determines the frequency of the emitted photons which results in different light colour in LED's and the intensity of the light would be determined by the number of electrons undergoing this process which is dependent on the applied voltage and the level of doping. (see Figure 2-18).

Figure 2-18. Schematic of the three different colour LEDs

2.11.1 Light amplification by the stimulated emission (Laser)

Light Amplification by the Stimulated Emission of Radiation (LASER) is a source of coherent light. The first laser operation was demonstrated in 1960. The operation of a laser is very similar to an electrical oscillator, where the gain is provided by the active medium which can be a gas, a solid, a liquid or a semiconductor, while the feedback is obtained with mirrors, one of them being semi-transparent in order to couple light out of the cavity. Light amplification is obtained by exciting or pumping the medium so that more atoms are in the upper energy level than in the lower level.

This operation is called “population inversion”, while pumping can be achieved electrically (DC or RF) or optically (flashlamp or laser).

The first semiconductor (SC) laser was demonstrated in 1962 nearly simultaneously by IBM, GE and MIT Lincoln Lab. For semiconductor lasers, the active medium is a direct band gap semiconductor material such as gallium arsenide (GaAs) and the “lasing transition” energy is related to the bandgap energy.

2.11.2 Laser diode

A laser diode also known as an injection laser, is a type of semiconductor source device, which is similar to a light-emitting diode, but converting electrical energy into a high intensity monochromatic, coherent radiation. In a laser diode a laser beam is produced at the diode’s junction which is a boundary between two types of semiconductor materials, P-type and N-

type, inside a single crystal of semiconductor. Therefore, in a laser diode, the P-N junction of the semiconductor diode acts as the laser medium or active medium.

When electrical energy applies to a laser diode device, electron will be injected into the diode. The free electron moves from N - type to the P- type material. In this process, some of the electrons interact with the valence band electrons and excites them to the higher energy level, conduction band, and the other recombine with the holes in the P-type material and release a light. This part of the process is called spontaneous emission.

The photons which are generated by spontaneous emission, will go through the P-N junction region and stimulate the excited electrons there. This result to release more photons at this stage which is called stimulated emission. The two ends of the laser diode structure are optically reflective. One end reflects the light completely, but the other end is partially reflective. The generated light in the P-N junction will bounce back and forth between the two reflective surfaces which results to produce an extensive optical gain. The light generated due to the stimulated emission finally escapes through the partially reflective end of the laser diode to produce a narrow coherence beam laser light. (see Figure 2-19)

One of the semiconductor materials used in producing a laser diode is doped gallium arsenide with selenium, aluminium, and silicon doping agents to make a P and N type of the layers.

Laser diodes are used in optical fiber systems, compact disc (CD) players, laser printers, remote-control devices, and intrusion detection systems.

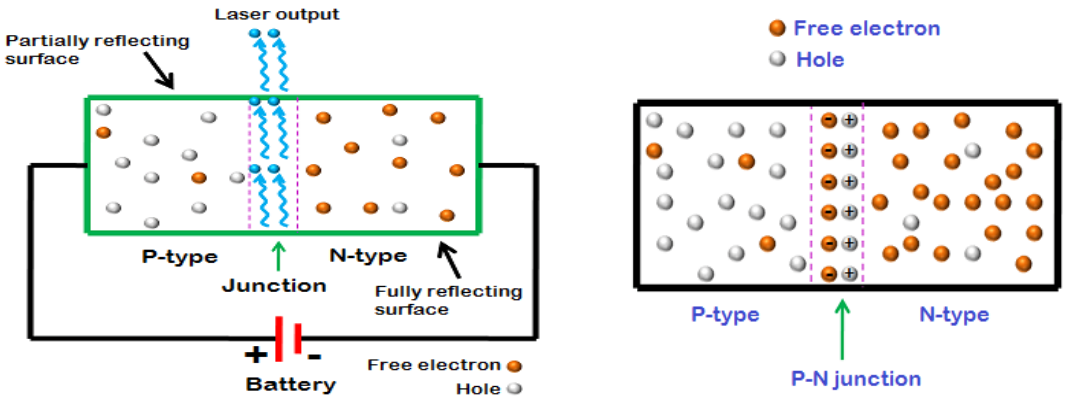

Figure 2-19. Laser diode device(Taken from physics-and-radio-electronics.com/electronic-devices-and-circuits/semiconductor-diodes/laserdiode)

2.11.3 Displays

A display device is an output device for presentation of information in visual or tactile form. Common applications for electronic visual displays are television sets or computer monitors. When the input information that is supplied has an electrical signal the display is called an electronic display. Some of the technologies used to create the various displays include ELDs, LEDs including OLED (Organic LEDs), Q-Dot displays.

2.11.4 Electroluminescent (ELD) display

Electroluminescent Displays (ELDs) are a type of Flat panel display created by placing a layer of semiconductor material such as GaAs between two layers of conductors. When electric current passes through an EL device, is causes excitation of the atoms and results in emission of different colour of light - based on the material used.

2.11.5 LED displays

A LED display is a flat panel display that uses light-emitting diodes as pixels for a video display. Their brightness allows them to be used outdoors where they are visible in the sun for store signs and billboards, destination signs on public transport vehicles, as well as variable-message signs on highways.

2.11.6 Quantum dot displays

A quantum dot display is a display device that uses quantum dots (QD), nanocrystal with semiconductor properties, available to glow by receiving energy. Depending on the dot's size it glows at a specific wavelength of light by producing pure monochromatic red, green, and blue light. which enhances brightness and colour performance of the display.

2.11.7 Optical amplifiers

An optical amplifier is a device to amplify optical signals directly without conversion into electrical signals. An optical amplifier is basically a laser without feedback. They play an important role in enabling technology for optical communication networks.

Before the commercialization of optical amplifiers, the optical signals needed to be electronically regenerate which was include of receiving, cleaning from the noises and amplifying electronically every 80-100 km to be able to transmit them over the long distance to the next communication centre.

Using optical amplifier with wavelength-division multiplexing (WDM) technology together, results to transmission of multiple channels over the same fiber.

Transmitting many terabits of data over kilometres distances and providing the data capacity required for communication networks, all relies on optical amplifiers.

One of the basic properties of an optical amplifier is its operating gain, which is the amount by which the input optical signal is amplified. The gain is typically measured in dB.

Semiconductor Optical amplifiers (SOA) are similar to laser diodes. The difference is an optical amplifier does not have end mirrors, having fiber attached to both the ends instead. They amplify an optical signal that comes from either fiber end transmit an amplified version of the signal out of the other fiber end. SOAs work for 1310 nm and 1550 nm systems. A weak signal is sent through the active region of the semiconductor which then via stimulated emission, results in a stronger signal emitted from the semiconductor.

2.11.8 Microwave photonic

Microwave photonics can be generally defined as the study of high-speed photonic devices operating at microwave or millimetre wave frequencies and their use in microwave or photonic systems. The term of microwave photonics was introduced in 1991 and used to describe novel optoelectronic components based upon the interaction of traveling optical and microwaves [39].

Very wide-bandwidth microwave photonic components are essential components because they are now needed in optical fiber communication systems.

Microwave photonics is an emerging field in which high frequency electronic signals are generated, distributed, processed and analysed using the strength of photonic techniques.

3 METHODS

3.1 Energy-dispersive X-Ray Spectroscopy (EDX)

Energy-Dispersive X-Ray Spectroscopy (EDX) has been used in this work to determine the chemical composition of deposited oxynitride films.

Energy Dispersive X-Ray Analysis (EDX), sometimes referred to as EDS or EDAX, is an X-ray technique used to identify the elemental composition of materials with atomic number (Z)>3. The EDX system is an extra capability that is integrated with the Hitachi S4800 Scanning Electron Microscopy (SEM) used in this work. Imaging using the SEM identifies the site of interest on the sample material which can simultaneously be chemically mapped using EDX. This technique is non-destructive; therefore, the sample can be analysed many times over. The other advantage of this technique is that the specimens of interest can be analysed with little or no sample preparation.

In EDX characterisation, the electron interaction with the sample generates X-rays which can then be recorded as characteristic spectra for each sample analysed, with spectral peaks related to the elements making up the composition of the sample.

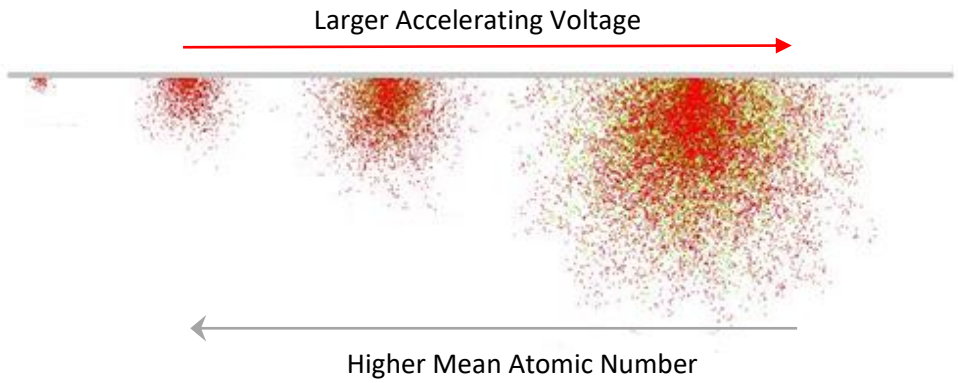

Figure 3-1. Illustration of electron beam interaction with sample, creating an interaction volume.

In the EDX technique, an electron beam is focussed on the sample, penetrating into the sample and dispersing within the sample to form an interaction volume with the atoms inside that sample volume (Figure 3-1). The size of the interaction volume depends on the mean atomic number or density of the sample and the accelerating voltage of the incoming electron beam. For larger accelerating voltages, the interaction volume will be larger, while for samples with higher mean atomic number, the interaction volume is smaller.

There are two types of X-rays which can result from these interactions: Continuum (Bremsstrahlung) X-rays, and Characteristic X-rays.

In continuum X-Rays, an electron from the incoming electron beam with energy E_0, interacts with the electrical field of the nucleus in the atom and results in a slowing down or changing of the direction of the electron, but without ionization taking place (Figure 3-2). During this inelastic scattering interaction, the electron loses energy in the form of X-rays, with energy less than the energy of the incoming electron ($\leq E_0$).

As a lot of the low energy X-rays produced in this way, will be absorbed by the sample or the detector, the continuum X-ray contributes a whale shape background (Figure 3-3) upon which characteristic elemental lines are superimposed, in the EDX spectrum (Figure 3-3).

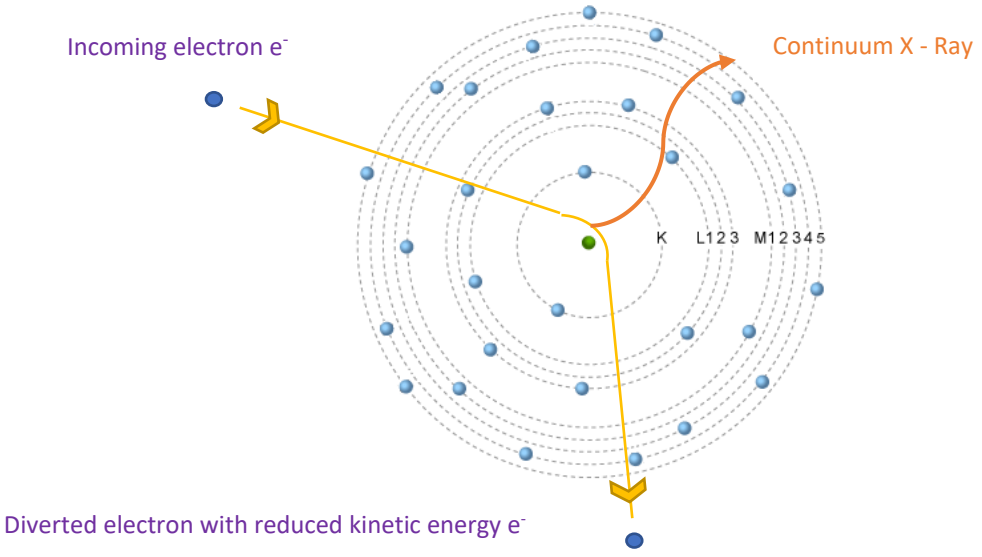

Figure 3-2 . Illustration of electron interaction with an atom yielding a Continuum X-ray.

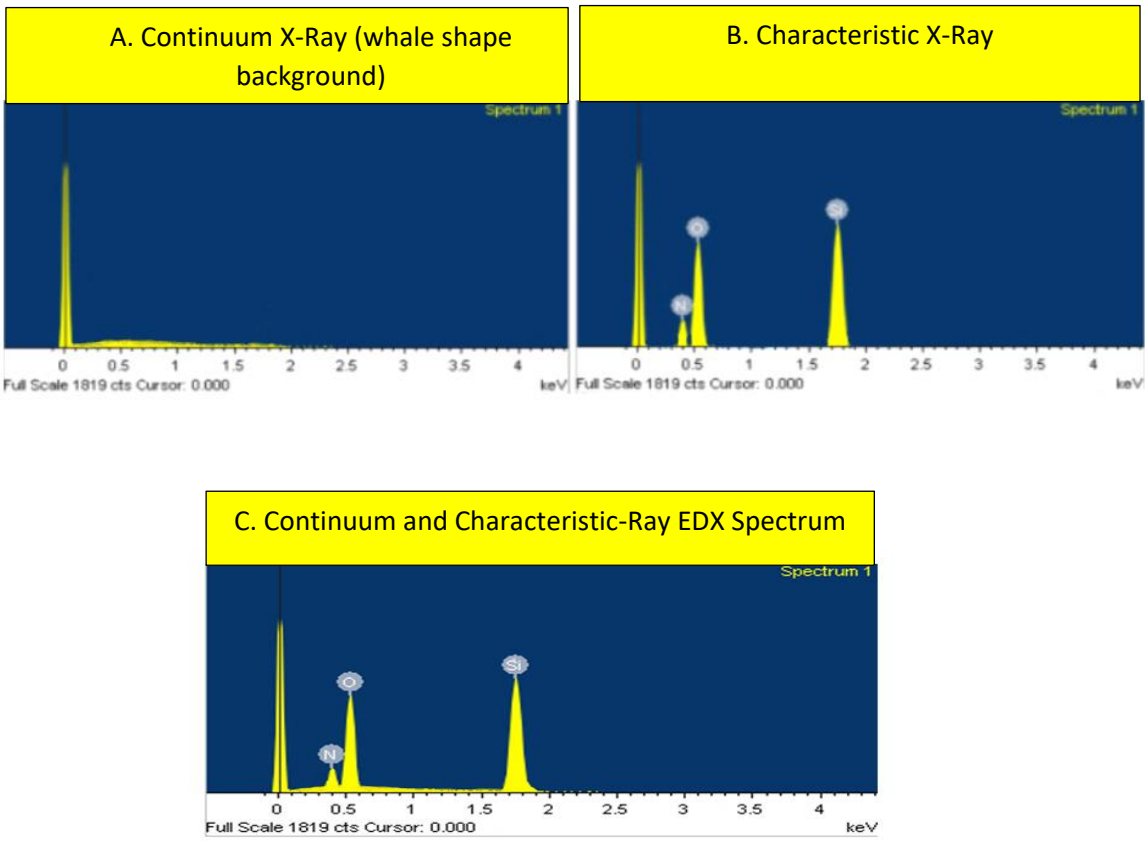

Figure 3-3. Illustration of Continuum and Characteristic X-ray spectra produced using EDX.

3.1.1 Characteristic X-Rays

In characteristic X-ray production, the incoming electron must transfer a minimum amount of energy which is proportional to the binding energy of a particular inner shell electron. Each electron in the atom has its own specific, characteristic energy. By receiving the desired amount of energy from the incoming electron beam, an electron is ejected from one of the inner shells of the atom (Figure 3-4Figure 3-4). The atom is thus ionized but exists in an unstable state (as it has a missing inner electron). The atom can regain stability if an electron from an outer shell fills the inner shell vacancy. This electron relaxation process produces an X-ray photon as a by-product. The energy of the emitted X-ray is equal to the difference between the ionization energies of the outer and inner electrons involved in the transition.

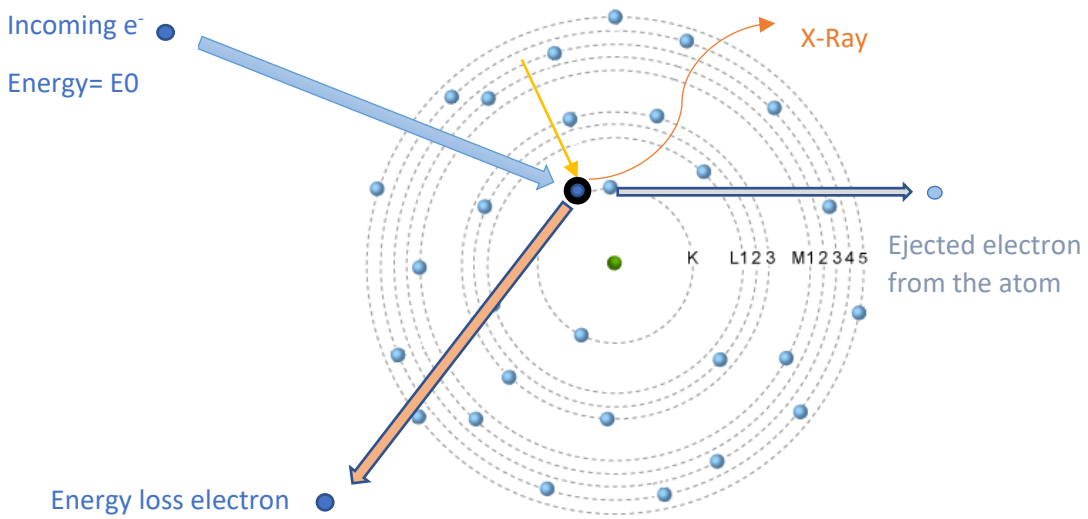

Figure 3-4. Illustration of electron ejection and subsequent electronic relaxation, resulting in production of a characteristic X-ray.

X-ray lines are identified by a capital Roman letter which indicate the atomic shell containing the inner vacancy (K, L or M) and a Greek letter (α, β, etc) defining the degree of separation between the core level and the outer shell, belonging to an electron which drops to fill that vacancy (Figure 3-5) . For example, Si Kα indicates a silicon atom that had its K shell ionised and subsequently filled by an electron in the L shell (α = 1).

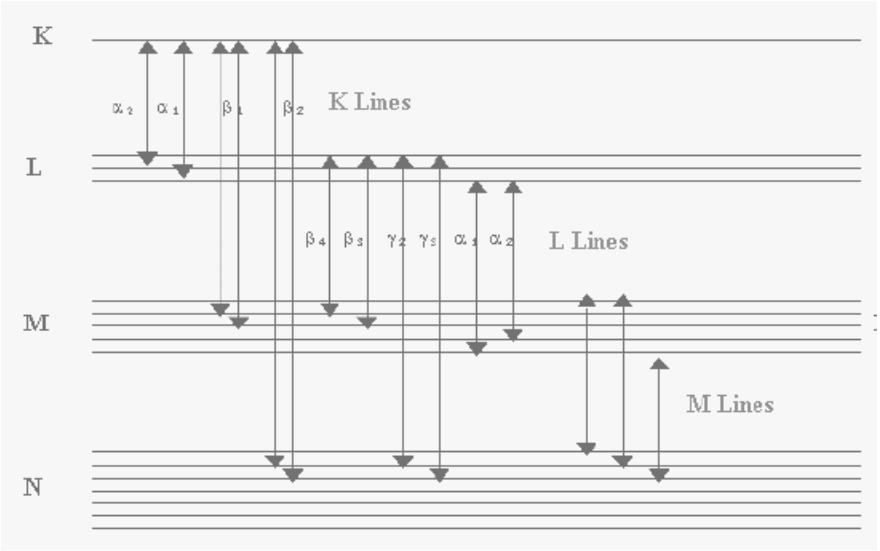

Figure 3-5. KLMN electronic energy levels in an atom [Reproduced from X-Ray Fluorescence Analytical Technique, Moussa Bounakhla& Mounia Tahri]

The closer to the nucleus, the stronger and more tightly bound the electrons are. For example, the binding energy for a K-shell electron is greater than that of an L-shell electron, since the K-shell electron is closer to the nucleus. Therefore, more energy is required to ionize the K shell, and it follows that the energies of the K series X-ray lines for each element are greater than those of the L series, which are greater than those of the M. That is, for every element: $E_K > E_L > E_M$

The X-rays produced are detected by an Energy Dispersive detector which displays the signal as a spectrum, or histogram, of intensity (number of X-rays or X-ray count rate) versus X-ray energy. The energies of the Characteristic X-rays allow the elements making up the sample to be identified, while the intensities of the Characteristic X-ray peaks allow the concentrations of the elements to be quantified.

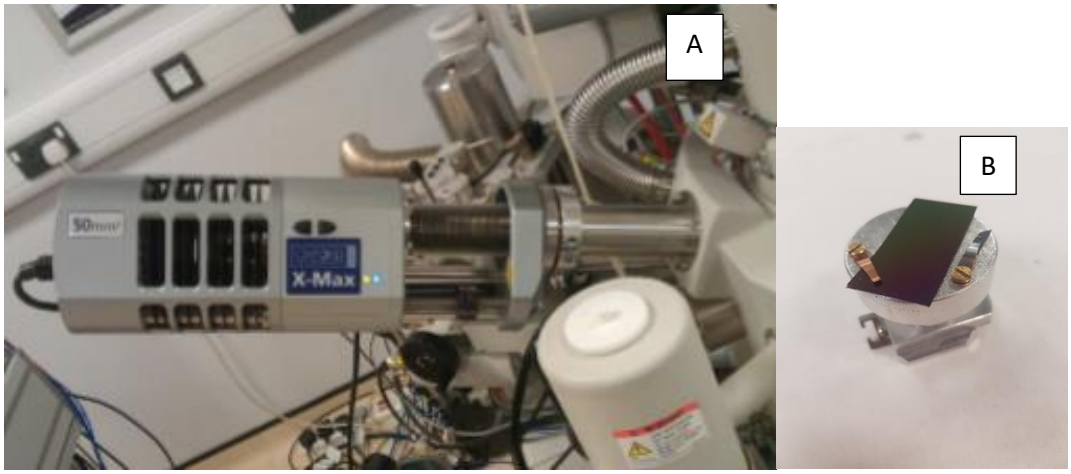

Figure 3-6. (A) Oxford Instruments X-Max silicon drift detector and sample on stub. (B) sample.

In this project, an Oxford Instruments X-Max silicon drift detector integrated into the Hitachi S-4800 SEM (Figure 3-6) has been used as an EDX detector. Acceleration voltages of between 5–20 kV was used in order to observe the higher order transitions that support the identification of the elemental composition of the samples. To maximise the count rate, the filament current was set to the upper limit of 20 mA.

EDX spectra recorded the Characteristic peaks which identify the related elements present in the silicon oxynitride films and the atomic percentage of these elements, (which is very important in order to understand the effects of these ratios on the optical properties of the films).

The continuum X-ray is present as a background under the characteristic peaks. The primary electron beam may interact with an electron in the sample, resulting in ejection it with some amount of kinetic energy. If the ejected electron was weakly bound, it typically emerges with only a few eVs of energy and is called a secondary electron. Therefore, as well as the continuum X-ray emission in the background, a large peak also appears in the low energy region of the spectra which is due to secondary electron emission. They are inelastically scattered by electrons within an atom and have low energy and can only escape the sample if they are generated near its surface.

3.2 X-Ray Photoelectron Spectroscopy (XPS)

Figure 3-7. XPS AXIS Supra instrument from Kratos Analytical running the ESCApe software (taken from Kratos Axis Supra.ltd)

X-ray Photoelectron Spectroscopy (XPS) is a surface analysis technique which uses X-ray energy, usually Aluminium K_α X-rays with energy E_{photon} = 1486.7 eV, to irradiate a material under a high vacuum condition, (P~10^{-8} millibar) or ultra-high vacuum (UHV;P<10^{-9} millibar), while measuring the Kinetic energies and the number of the electrons which escape from the top 10 nm of the sample surface of the analysed sample. (see Figure 3-7)

In this technique, the high energy X-ray can ionise an electron from the core shell (inner 1s or 2s electrons) of the surface atoms resulting in electron emission from the atomic orbitals of the chemical species present in the sample. The ejected electron has a kinetic energy specific to a particular surface atom. According to the base work of Rutherford and the theoretical Einstein formula, by measuring the ejected electron's kinetic energies (using XPS instrument) and taking the known, X-ray energy (E_{photon} = 1486.7eV) into account, information is yielded on the binding energies of each element present in the material.

$$E_{Binding} = E_{Photon} - (E_{Kinetic} + \varphi)$$

where $E_{Kinetic}$ is the kinetic energy of the emitted photoelectron which is measured, $E_{Binding}$ is the energy of the electron in the initial state, φ is the work function and E_{Photon} is the photon (X-ray) energy.

These binding energies are characteristic of particular atoms e.g. C, N, O, Si etc. but can also yield more detailed information on the atomic environment of a particular atom.

For example, if a carbon is bonded to hydrogen atoms, it has a different bonding condition to a carbon atom bonded to Oxygen. These different bonding conditions result in the ionised core electrons having slightly different binding energies. The difference in binding energy caused by neighbouring bonded atoms is the "chemical shift".

An Al Kα X-ray source used to irradiate the samples (Figure 3-8) with an energy of 1486.7eV. Survey scan acquisition was carried out to collect the data in the binding energy range to 0 – 1200 eV in 0.3 eV steps, at a pass energy of 40 eV. The pass energy was chosen to avoid broadening of the peaks, therefore providing the highest absolute peak resolution within a reasonable scan time. Core level spectra were typically scanned in 0.1 eV steps at a pass energy of 20 eV. All data (including the survey scans) were averaged over 3 passes.

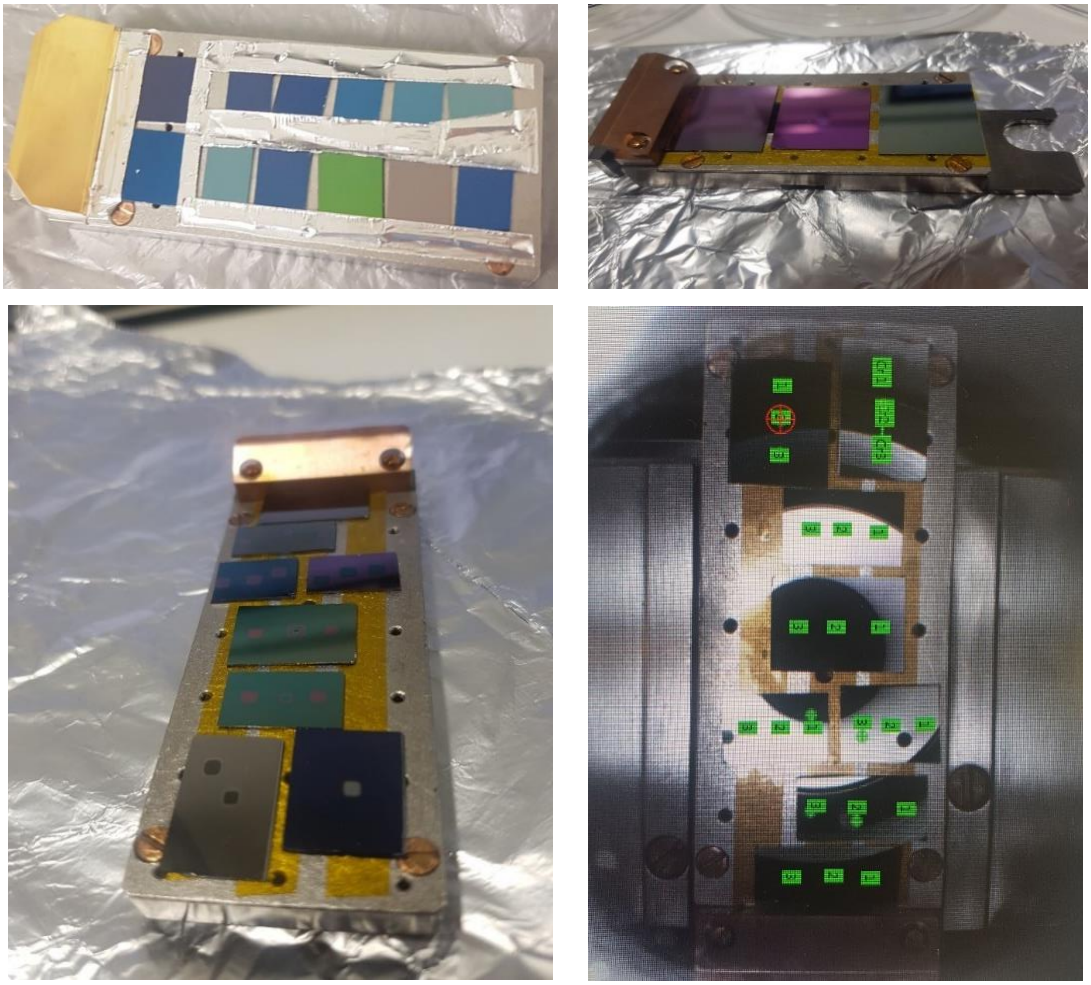

Figure 3-8. Samples for XPS

Data analysis and fitting was performed using CasaXPS software and the peaks were fitted with Gaussian/Lorentzian curve with respect to the background noise.

3.3 Plasma Enhanced Chemical Vapor Deposition (PECVD)

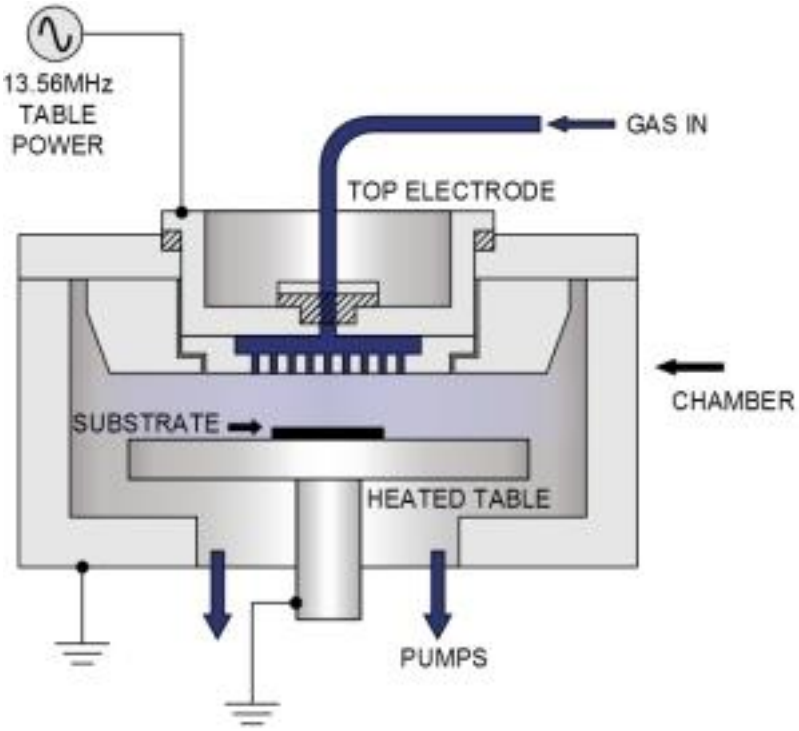

Figure 3-9. Schematic of PECVD chamber, showing top showerhead electrode, heated bottom electrode and gas inlet and extraction (Taken from plasma.oxinst.com/technology).

Plasma Enhanced Chemical Deposition (PECVD) (Figure 3-9) uses a plasma rather than a temperature as the source of activation energy in order to breakdown precursor gases and deposit thin films. The plasma process means there is no need for high temperature and thus it is possible to use low temperature deposition processes on temperature sensitive substrates. Plasma is an energetic ionised gas which consists of approximately equal numbers of positively charged ions and negatively electrons. In the PECVD system, a mixture of gases is used to form the plasma to deposit thin films onto a substrate.

In a plasma, electrons lose their energy inefficiently by collision - due to the huge mass difference in the two-body collision with an atom, therefore temperature equilibration happens very slowly. Electrons are very hot, with energies from 1 to 10 eV which is equivalent to 10^3 to 10^4 Kelvin, while the envelope of the plasma remains at a much lower temperature, usually between room temperature and 400°C. Because the electrons have a high energy, various

chemical reactions that could otherwise have only taken place at that high temperature, can take place in the comparatively cooler plasma.

This becomes particularly useful when there is a restriction over the temperature, in terms of the safe temperature for devices. For example, after fabrication some devices such as transistors, integrated circuit etc. may degrade at temperatures above 200℃. Devices may also need to include a surface passivation layer (often silicon nitride) to avoid any corruption during use or handling. Sodium contamination, from human handling can be prevented using a passivation layer on the device, preventing the performance of the device from being degraded. Metal components in the transistors or ICs are often Aluminium, which has a low melting point. Thus, low temperature PECVD process are required to deposit passivation layers.

PECVD is often used to deposit Silicon dioxide, silicon nitride and silicon oxynitride thin film dielectric insulating materials - which are very commonly used in nano and micro technology devices and systems.

Table 2 lists some of the basic chemical reactions, that can be used to deposit SiO_2, with different techniques. These are compared in terms of the different temperatures required for deposition. Thermal CVD of silicon dioxide is performed at 900°C. By using PECVD deposition of silicon dioxide, it is possible to reduce the deposition temperature to 200°C.

Table 2. Comparison of silicon dioxide deposition parameters using thermal CVD and PECVD.

Technique	Reactants	Products	Temperature needed C^0
Plasma	SiH_4 + 4 N_2O	SiO_2 + 2 H_2O + 4 N_2	~ 200
No Plasma	SiH_4 + O_2	SiO_2 + 2 H_2	~ 450
No Plasma	$SiCl_2H_2$ + N_2O	SiO_2 + N_2 + HCl	~ 900

In this work, an SPTS PECVD tool was used to deposit silicon oxynitride dielectric layers. The PECVD instrument consists of (i) a Load lock (where the wafer is loaded into the instrument); a chamber (where the chemical processes occur); a shower head (the perforated upper electrode, connected to the Cathode which allows precursor gases into the chamber); a platen (the lower electrode connected to the anode, on which the substrate is placed); an RF power

source (used to generate the plasma); and a gas mixture input (mixes the all gases and allows them to flow into the chamber through the shower head).

The substrate is placed on the lower platen electrode, which is permanently grounded. The platen is often heated during deposition processes usually at around 300^0C. Heating the sample assists in the material deposition process. However, as mentioned above, this temperature is much lower than a non-plasma CVD system processes.

The upper electrode is called the shower head, due to its perforations, and is designed to help the uniformity of deposition across the substrate. This electrode is connected to high voltage radio frequency power, (RF electrical connection), which provides the power needed to generate a plasma inside the chamber.

Stainless-steel tubes carry the different reactant gases to the gas mixer and then to the deposition chamber through the shower head (see

Figure 3-10). These gases are typically N_2, SiH_4, N_2O, C_4F_6, O_2 and CF_4 – depending on the material to be deposited. Computer-controlled valves of the Mass Flow Controllers (MFCs) control the exact flow of these gases. Each material uses specific gases and controlled flow rates / pressures, which are specified in the deposition recipes for each material.

Different gases can be used to deposit the different materials such as silicon dioxide, silicon nitride or silicon oxynitride. The pressure of the gases is allowed to stabilise and can be varied from a milli Torr up to a few Torr. This stabilisation typically takes less than one minute, then high voltage is applied to the chamber electrode to ionise the gas molecules. This ionisation of SiH_4, N_2O and N_2 gas molecules, generates chemically reactive creates radicals such as (SiH_m ,O, NO, N), neutrals, ions (SiH_m^+, O^+ ,NO^+), and reactive species, the combination of which subsequently form thin layers of the dielectric material on the substrate.

Electron impact ionization, dissociation of silane and nitrous oxide reactions are demonstrated in Table 3.

Table 3. Possible basic reactions in active plasma environments.

Reaction	General equation	Example
Ionization	$e + A \rightarrow A^+ + 2e$	$e + N_2 \rightarrow N_2^+ + 2e$ $e + N_2O \rightarrow N_2 + O^+ + e + e$
Excitation	$e + A \rightarrow A^* + e$	$e + O_2 \rightarrow O_2^* + e$
Dissociation	$e + AB \rightarrow e + A + B$	$e + SiH_4 \rightarrow e + SiH_3 + H$ $e + N_2O \rightarrow NO + N + e + e$

Significant research has been performed in order to identify the correct source gases and process conditions required to depositing various dielectric films. The grow rate of the film is constant, so a desired thickness film could be achieved by running the process for certain amount of time.

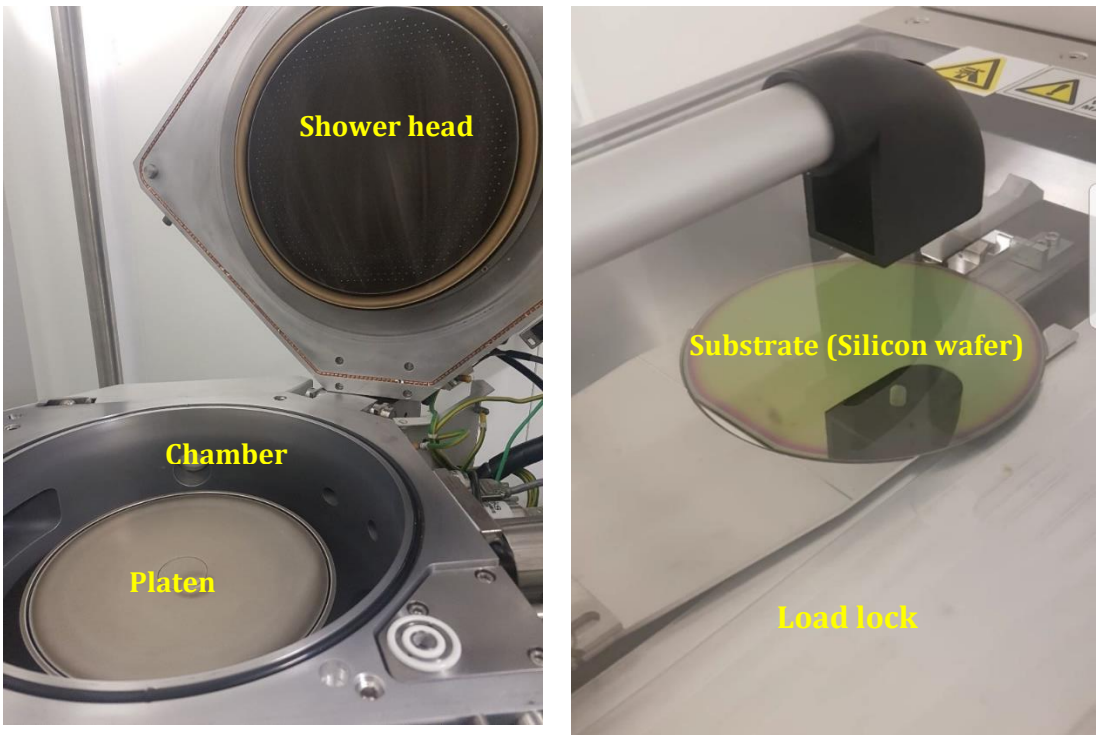

Figure 3-10. A picture taken from a PECVD used in this project. It shows a load lock for placing a silicon substrate and the internal chamber consist of a platen and shower head.

To terminate the film deposition process, the RF voltage and gas flows must be turned off. When the thin film deposition is completed, and the sample is removed from the chamber, the chamber needs to be cleaned by a process “Etch back” to remove and pump out all the species stuck to the chamber components. After etching back and depositing a 1 micron of silicon oxide in the empty chamber, the PECVD tool is ready to be used for the next deposition process.

In this project, a constant chamber pressure of 2000 mil Torr, 150W RF power, 300°C^0 platen temperature and 250°C^0 shower head temperature was used. The gap between the live shower head and the earthed platen is 20mm.

To achieve the desired low bombardment energy, the RF power, which is the source of the power to generate a plasma, is applied to the upper electrode (Cathode) and the substrate is placed on the lower electrode (Anode) which is permanently grounded. This results in less ions being attracted to the substrate - useful for devices which are sensitive to Ion Damage.

3.4 Ellipsometry

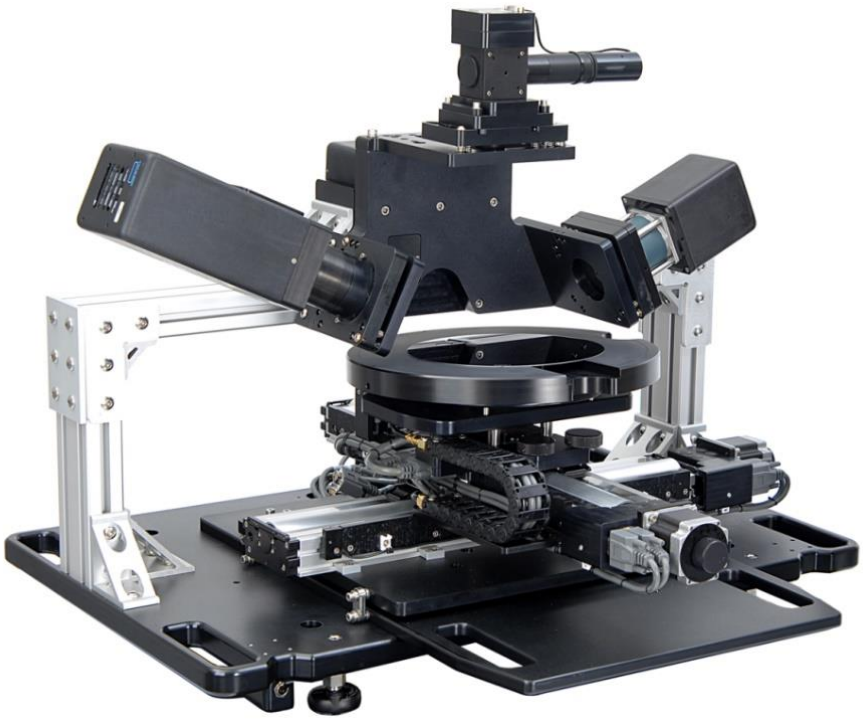

Figure 3-11 Picture of ellipsometer (Taken from https://www.jawoollam.com/products/m-2000-ellipsometer).

Ellipsometry (see ellipsometer in Figure 3-11) is generally a non-destructive, non-invasive, convenient and accurate characterisation technique to measure the transmission and reflection properties of thin films, using reflected incident light. This optical analysis technique requires no sample preparation or special measurement environment. The non-destructive technique can be used to analyse samples of almost any size and shape. The non-contact nature of the technique lends itself to measuring materials like semiconductor wafers and layers deposited on them.

Ellipsometry is based on light undergoing changes in polarization when it is reflected from or transmitted through a sample. These changes are characteristic of the surface structure of the sample. Thus, by analysing the reflected light beam it is possible to obtain information about the sample material such as film thickness and refractive index.

To understand the way ellipsometer works, one needs to understand the polarisation phenomenon.

In 1860, James Clerk Maxwell described light as a propagating oscillating wave of perpendicular electric and magnetic fields - electromagnetic radiation traveling at the speed of light **c**.

As well as the oscillations of the electric and magnetic fields being perpendicular to each other, they are also perpendicular to the direction of wave propagation, forming a transverse wave. They are in–phase with each other, reaching minima and maxima together. (see Figure 3-12)

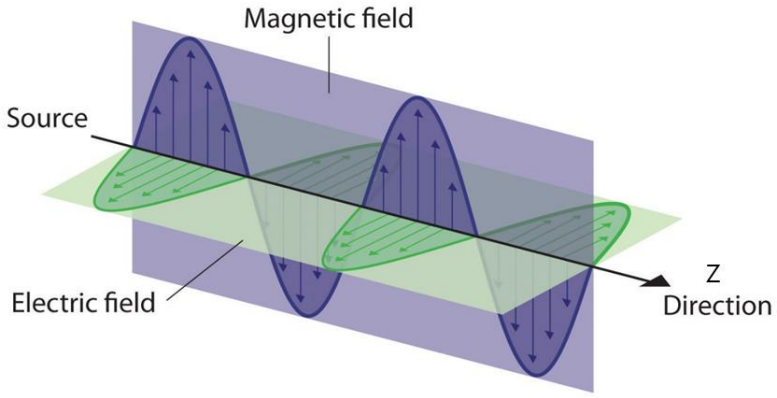

Figure 3-12. Illustration of an electromagnetic wave (taken from, Microwave Spectroscopy Applied Chemistry).

.

The electromagnetic wave function shows the relation between different parameters of the wave when it is propagating in space . Both electric (1) and magnetic (2) equations have the form of the general wave equation for a wave travelling in the Z direction:

$$\frac{\partial^2 E}{\partial Z^2} = \mu_0 \varepsilon_0 \frac{\partial E^2}{\partial^2 t} \qquad (1)$$

$$\frac{\partial^2 B}{\partial Z^2} = \mu_0 \varepsilon_0 \frac{\partial B^2}{\partial^2 t} \qquad (2)$$

Where; μ_0 is the permeability of free space, ε_0 is the permittivity of free space.

The simplest solutions to the differential equations (1) and (2) are sinusoidal wave functions, which can be written as, (3) for the electric and (4) for the magnetic fields:

$$E(z, t) = E_{max} \cos(k z - \omega t) \qquad (3)$$

$$B(z, t) = B_{max} \cos(k z - \omega t) \qquad (4)$$

Where, k ($k = 2\pi/\lambda$) is the wavenumber, ω ($\omega = 2\pi f$) is the angular frequency, and $\omega/k = \lambda f = c$

The speed of electric and magnetic waves (electromagnetic wave), are equal and can be calculated by:

$$c = \frac{1}{\sqrt{\mu_0 \varepsilon_0}} = 2.997 \times 10^8 \frac{m}{s} \qquad (5)$$

The most important component of light wave is its electric–field component. When a light ray propagates in the z direction, the electric field vector E is confined to vibrate in an x y plane, perpendicular to the z axis and has two components: parallel (p-Polarised) and perpendicular (s-Polarised, from the German ”Senkrecht”) to the plane of incidence (Figure 3-13).

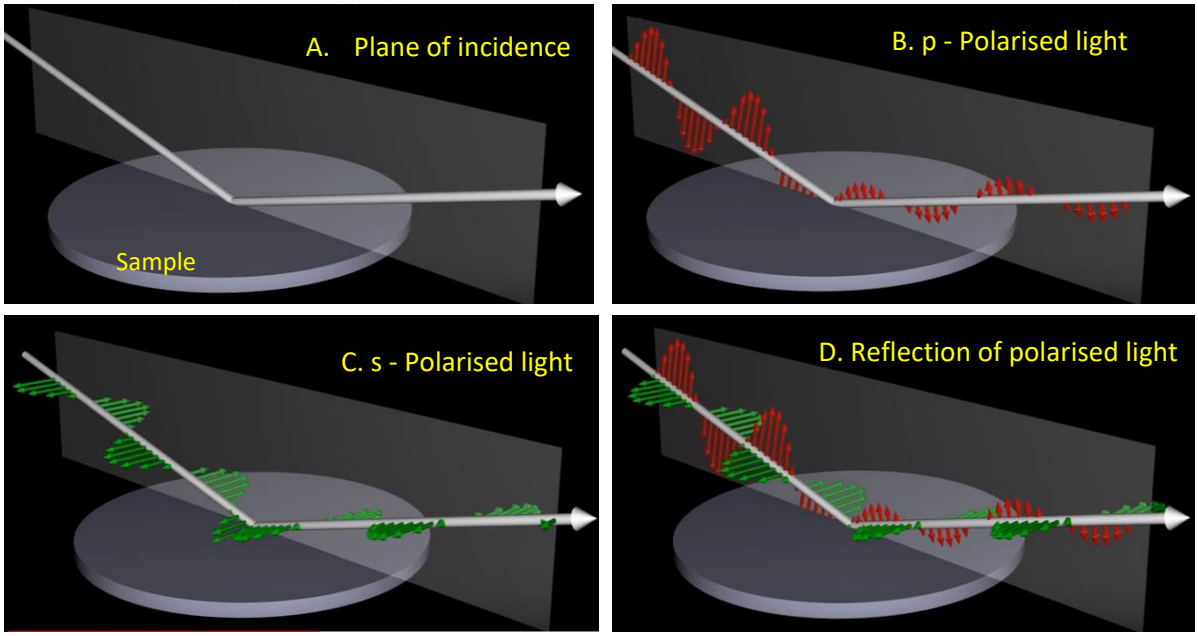

Figure 3-13 Interaction of polarised light with a thin film (Taken from Introduction to Ellipsometry and Polarized Light).

If the z-axis is defined as the direction of propagation then, the E-field can be described as a linear combination of x and y components:

$$E(z, t) = E_x \hat{x} + E_y \hat{y} \qquad (6)$$

where:

$$E_x(z, t) = E_{0x} \cos(\omega t - k z + \varphi_x) = E_{0x}\, e^{i(\omega t + \varphi_x)} = E_{0x}\, e^{i\varphi_x}\, e^{i\omega t} \quad (7)$$

$$E_y(z, t) = E_{0y} \cos(\omega t - k z + \varphi_y) = E_{0y}\, e^{i(\omega t + \varphi_y)} = E_{0y}\, e^{i\varphi_y}\, e^{i\omega t} \quad (8)$$

Where, E_x and E_y represent the electric components in the x and y axis respectively, E_{0x} and E_{0y} are the two relative electric field amplitudes and φ_x and φ_y are relative phases.

This two-dimensional component should not be confused with the two components of an electromagnetic wave. Each of the electric and the magnetic fields, presents two-dimensional transverse wave behaviours.

Following an understanding of the polarisation concept, it is possible to divide polarisation into three different polarisation states, which include linear, circular and elliptically polarisation. In elliptical polarisation, the electric field resulting from the orthogonal linear components, which are out of phase (except $\varphi = \frac{\pi}{2}$) and/or with different amount of amplitudes, rotates in an elliptical trajectory around the direction of propagation of light and describes the elliptical polarisation. This is where the name "ellipsometry" originates from.

The general form of light can then be stated using as:

$$E_x = E_{0x} \cos(\omega t - k z) \quad (11)$$

$$E_y = E_{0y} \cos(\omega t - k z + \varphi) \quad (12)$$

Which can be written as:

$$\left(\frac{E_y}{E_{0y}}\right)^2 + \left(\frac{E_x}{E_{0x}}\right)^2 - 2\,\frac{E_y}{E_{0y}}\frac{E_y}{E_{0y}}\cos(\varphi) + cos^2(\varphi) = 1 \quad (13)$$

Therefore, equation (13) defines an ellipse in the x y - plane.

Every Ellipsometer contains the same basic components in their two arms. A light source, which covers a certain spectral range in the infrared, visible or ultraviolet spectral region and a polarisation generator in the source arm, a polarisation analyser and detector, in the detector arm. The electromagnetic radiation is emitted by a light source and linearly polarized by a polariser. This polarised light then strikes the sample. After reflection, the radiation passes a second polarizer, which is called the analyser, and then reaches the detector. The angle of incidence can be adjusted using these source and detector arms. (See Figure 3-14).

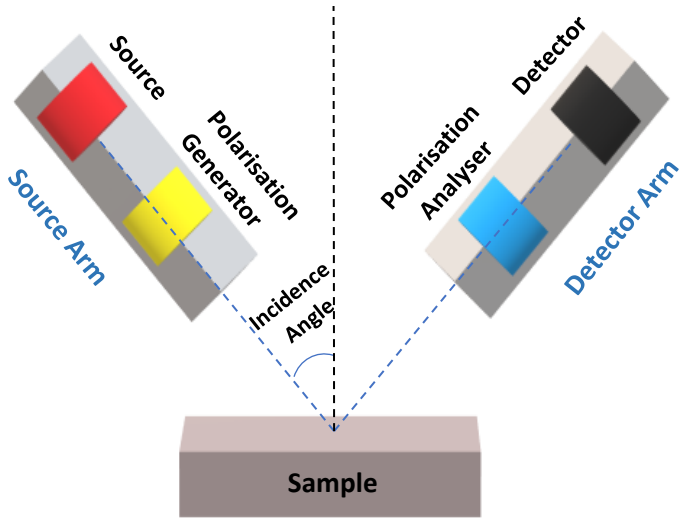

Figure 3-14. An ellipsometer is contain of some basic components of, a light source, a polarisation generator, a polarisation analyser and a detector.

The Ellipsometer is not able to directly measure the refractive index and the thickness of a film. In order to measure these parameters, the ellipsometer generates a referenced linear polarised beam. As this beam reflects off the sample, the s and p polarisation components, undergo amplitude and phase changes. To determine these changes, the detector converts the received reflected elliptically polarised light into an electronic signal. This information is compared to the known referenced input polarization and measures the change in phase which is characterized by the angle Δ, and the amplitude change which is characterized by ψ. (see Figure 3-15). Both Δ and ψ are functions of wavelength (λ) or energy and are used in the fundamental equation governing ellipsometry.

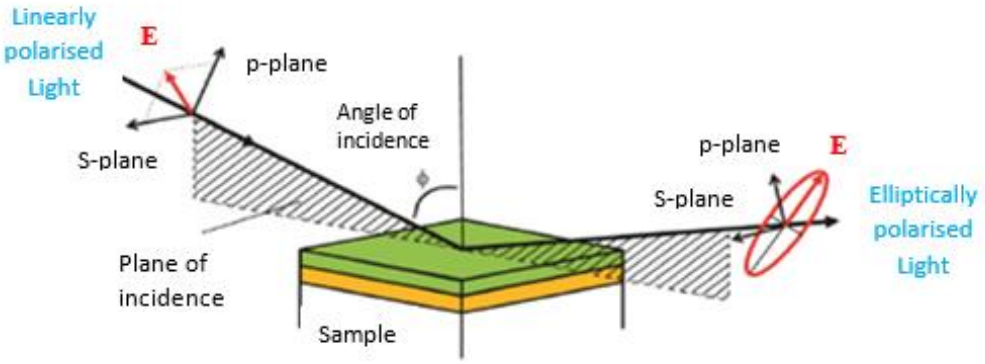

Figure 3-15 A simple ellipsometry measurement. The incident light is linear with both p- and s- components. The reflected light has undergone amplitude and phase changes for both p- and s- polarized light, and ellipsometry measures their changes. (taken from J.A.Woollam)

The amplitudes of the s and p components, after reflection and normalization to their initial values, are denoted by r_s and r_p, respectively which are the complex Fresnel reflection coefficients of the light whose, electric fields are perpendicular and parallel to the plane of incidence, respectively. Ellipsometry measures the complex reflectance of a system, ρ, which is the ratio of r_s and r_p and parametrized by the amplitude component Ψ and the phase difference (shift) between the p-polarised and s-polarised light, Δ, such that:

$$\tan(\psi) = \frac{|r_p|}{|r_s|} \qquad (14)$$

$$\Delta = \delta_{Outgoing} - \delta_{Incoming} \qquad (15)$$

$$\rho = \frac{r_p}{r_s} = \tan(\psi)\, e^{i\Delta} \qquad (16)$$

Ellipsometry parameters (Ψ, Δ) have unique characteristics at the Brewster angle. In particular, Ψ reaches a minimum at the Brewster angle for p-polarized light. The angle of incidence is chosen close to the Brewster angle of the sample to ensure a maximum difference in r_s and r_p.

The measured Ψ and Δ cannot be converted directly into the optical constants of the sample. Normally, a model analysis must be performed with ellipsometry. After a sample is measured, a model is constructed to describe the sample. The model is used to calculate the predicted response from Fresnel's equations, which describes the reflection and transmission of light when incident on an interface between different optical media and describe each material with thickness and optical constants. The best match between the model and the experiment data is

then found. An estimator, like the Mean Squared Error (MSE), is used to quantify the difference between the experimental and the model curves and the best fit corresponds to the lowest MSE. The procedure used to deduce material properties from ellipsometry measurements follows the flow chart in Figure 3-16.

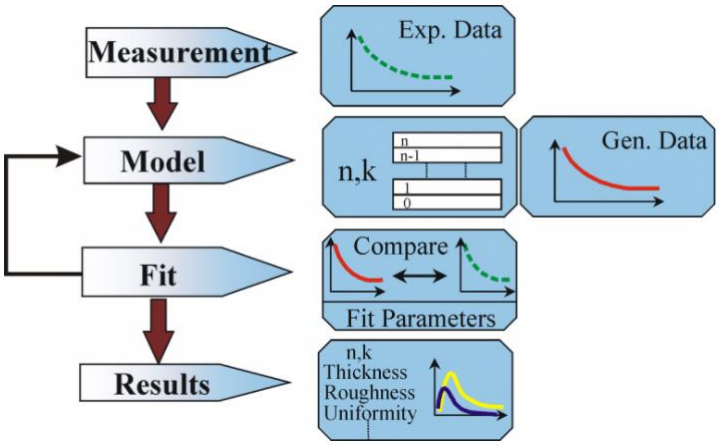

Figure 3-16 Flow chart for ellipsometry data analysis (taken from J.A.Woollam)

Film thickness is determined by interference between light reflecting from the surface and light traveling through the film. Depending on the relative phase of the light re-joining the surface reflected light, interference can be constructive or destructive. The interference involves both amplitude and phase information. The optical constants for a material will vary for different wavelengths and must be described at all wavelengths probed with the ellipsometer.

In this experiment, a J.A.Woollam, M-2000 ellipsometer with xenon lamp source, is used to determine the thickness and refractive index of the dielectric films. The spectral range from 370 nm to 1702 nm (3.35 ev – 0.73 ev) at three different angles of incidence of, 65°, 70° and 75° was measured. This range covers the Brewster angle of the dielectric material region. Calibration was performed to make sure that the sample stage was adjusted such that the reflected light hit the ellipsometer detector precisely. The sample was placed on the ellipsometer sample stage and 49-point measurement patterns were used across each wafer.

3.5 Prism Coupler

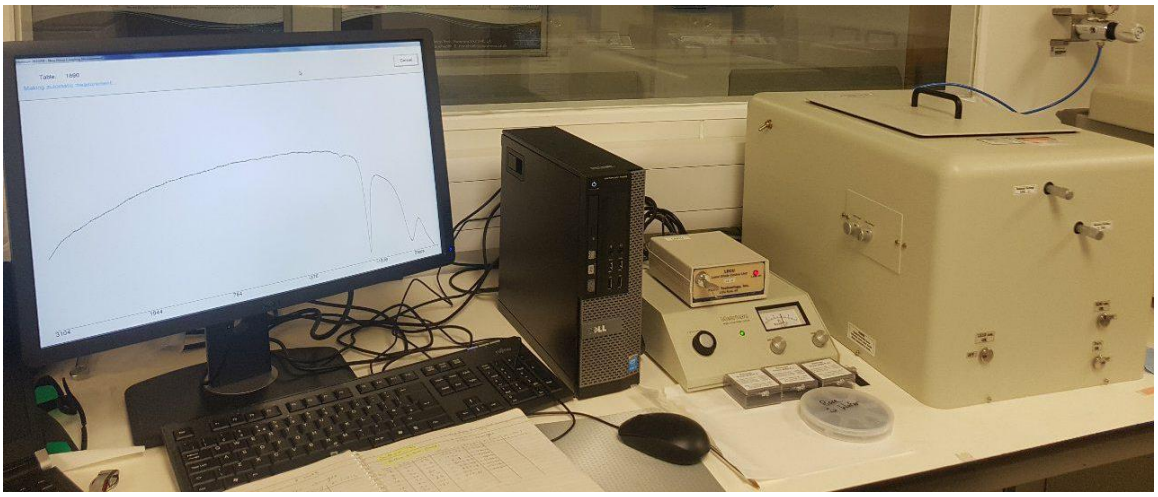

Figure 3-17. A 2010/M prism coupler (Metricon) device

Experiment setup is used in this measurement is a Metricon Prism coupling device which includes a rotatory table and optics module. Metricon model 2010/M prism coupler device (

Figure *3-17*) uses optical wave guiding technique to measure precisely the refractive index/birefringence and thickness of dielectric as well as loss measurements the films. A Metricon Prism Coupler is used to determine the propagation modes inside the films grown on a silicon substrate. Measurement principle for thin film is drawn in Figure 3-18.

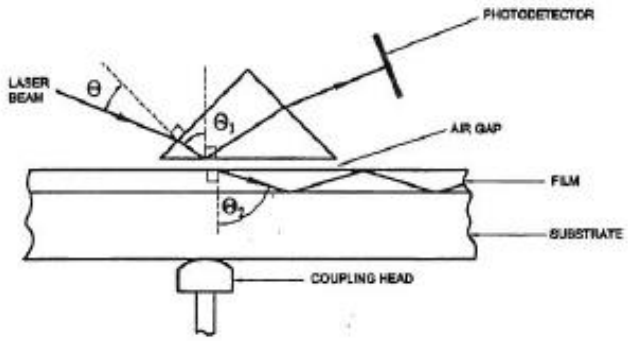

Figure 3-18 Schematic of light interaction with a thin film through a prism coupler (taken from Metricon user manual).

The sample is brought into contact with the base of the prism by a coupling head. There is only small air gap between sample and prism. A laser light strikes the base of prism and the light is completely reflected at the base of prism into the photodetector. At certain values of incident angle (mode angles), photons can transmit across the air gap into the film and enter into the guided optical propagation mode. This process causes a drop, in intensity of light reaching the detector.

The measurement is done with three lasers, 636 nm, 1310 nm and 1550 nm. A few different prisms are using during measurement, low index prism (Metricon Prism # 200-P-1, code: 1000, index range: 1.0- 1.80) and higher index prism (Metricon Prism # 200-P-2, code: 4400, index range: 1.55-2.45).

Prism coupler measures the intensity of reflected light as a function of angle which is converted to propagation constant, β. The propagation modes are displayed as dips in the intensity curve. Prism coupling curves show well-defined sharp dip suggests relatively low loss. The angular location of first mode (dip) indicates the film refractive index and angular difference between the modes determines the thickness of the film. It is also possible to measure both TE and TM modes for each film. Metricon software calculates the refractive index and thickness of the film based on the given effective indices found in propagation modes. Thickness and index of film are calculated when two of the mode angles are detected. Each peak corresponds to a particular effective index and gives an equation which makes a link between the thickness and the refractive index. The equations have two unknown values (refractive index and thickness), and two equations are needed to estimate the two unknown values.

With effective indices of modes, it is possible to calculate the refractive index and thickness for each film. Thickness measurement is dependent on the optical constant and the film thickness measurement affects the optical length of light traveling through the film. Index of the film determines the light waves 'velocity and refracted angle'. Both velocity and refracted angle contributes the delay of between surface reflection and light traveling through the film. Refractive index and wave vector must be known in order to achieve the correct result from an optical measurement. The optical constant varies for different wavelengths and it is determined by ellipsometer at all wavelengths. The material's response at each wavelength can be predicted by table of optical constant however it is not easy to adjust unknown optical constants on a wavelength by wavelength basis. To solve this problem, a dispersion model is introduced

for optical constant as a function of wavelength. The dispersion model is adjusted by optical parameters which allow the optical constant form to match the experimental results. Cauchy dispersion model is often used to describe index of transparent material. The Cauchy relationship is generally described as:

$$n(\lambda) = \mathrm{A} + \frac{B}{\lambda^2} + \frac{C}{\lambda^4}$$

where A, B and C are adjusted parameters to match the refractive index of material and λ is wavelength of material. The total measurement process is completely automated and requires about twenty seconds. The measurement starts with inserting the film in contact with the prism and the laser measurement starts automatically according to the Metricon software. Metricon model 2010/m prism coupler possesses some features such as: It enables to measure refractive index of bulk materials; substrate and it is possible to measure index vs temperature (dn/dt) and waveguide loss.

3.6 Fourier Transform Infrared Spectroscopy (FTIR)

Figure 3-19. A bruker IFS 66/S fourier transform infrared spectrometer (taken from European Virtual Institute for Speciation Analysis)

Fourier Transform-Infrared Spectroscopy (FTIR) is an analytical technique used to identify the characteristic vibrational frequencies of bonds within materials. This technique measures the absorption of infrared radiation by the sample material versus wavelength or wavenumber. The infrared absorption bands identify molecular components and structures.

When a material is irradiated with infrared radiation, absorbed IR radiation usually excites molecules into a higher vibrational state. The wavelength of light absorbed by a particular molecule is a function of the energy difference between the at-rest and excited vibrational states. The wavelengths that are absorbed by the sample are characteristic of its molecular structure.

The FTIR spectrometer uses an interferometer to modulate the wavelength from a broadband infrared source. A detector measures the intensity of transmitted or reflected light as a function of its wavelength. The signal obtained from the detector is an interferogram, which must be analysed with a computer using Fourier transforms to obtain a single-beam infrared spectrum. The FTIR spectra are usually presented as plots of intensity versus wavenumber (in cm^{-1}). Wavenumber is the reciprocal of the wavelength. The intensity can be plotted as the percentage of light transmittance or absorbance at each wavenumber.

In this experiment, a Bruker IFS 66/S Fourier transform infrared spectrometer (Figure 3-19) equipped with a water-cooled global source, a potassium bromide beam splitter and a deuterated triglycine sulphate detector was used to measure the transmittance of the samples (where transmittance is equal to $\frac{I}{I_0}$, is the ratio of the intensity of the transmitted light through the sample and undoped Germanium substrate to I_0, the intensity of the transmitted light through the air). The air spectrum was taken under the same condition as each sample measurement in order to eliminate any background effects. The resolution was 8 cm^{-1} and 1000 scans were coadded for each spectrum. All measurements were performed in ambient air conditions (unpurged conditions). Full spectral range coverage of this equipment is covers from the very far infrared (<5 cm^{-1}) up to the vacuum UV (>55,000 cm^{-1}).

4 INTRODUCTION TO RESULTS

Deposition of silicon oxynitride layers using a range of process parameters has been performed using an SPTS Technologies PECVD tool. Different process parameters have been used in order to tune the refractive index, optimise the optical signal loss, and minimise the extent of hydrogen bonding present within the oxynitride films. The instrument parameters that can be varied are the power, the gas flowrate (to change the composition), the gas ratio of SiH_4 to N_2O to N_2, and the platen temperature. However, in this work, the power and platen temperature and the N_2 flow rate were maintained at a constant level. Only the flow rates of SiH_4 and N_2O were varied in these experiments. Power and temperature parameters had been optimised in previous work by the industry sponsor, BB Photonics, who found the best conditions to be power of 150 W, with a platen temperature 300°C and an N2 flow rate of 2000 sccm.

The reason for this work on modifying the SiH_4 and N_2O flow rates was to understand the effect of varying the SiH_4 / N_2O ratio on the refractive index, deposition rate and optical loss of the oxynitride thin films. In particular, these experiments were performed in order to understand the relationship between the optical loss and the extent of hydrogen bonding content within the films. Hydrogen bonds within the film can absorb photonic energy – which leads to increased optical losses.

Photonic absorption is possible from the following bonds (Si-O; Si-N; N-O; Si-H, N-H and O-H). However, the absorption of the Si-H, N-H and O-H bonds in particular can give rise to more significant optical losses.

Following deposition of the PECVD silicon oxynitride films, extensive film characterisation and analysis has been performed. Film thickness and refractive index measurements on the deposited films was performed using spectroscopic ellipsometry. The film thickness has been correlated to the film deposition rate and film composition (elemental and chemical bonding constituents). The experiments performed include:

• EDX, which analyses the bulk elemental composition of the oxynitride films.

• XPS, which characterises the elemental composition and bonding environment of surface atoms of the oxynitride films (top 10 nm from the surface).

• FTIR, which is used to measure the hydrogen bonding content of the thin films. FTIR was able to detect Si-o, Si-N, N-H, Si-H bonds, present within the oxynitride films.

The refractive index of silicon oxynitride films can vary from 1.46 (pure silicon dioxide) to 2.3 (silicon rich nitride, Si-rich Si-N, which contains a greater number of Si-Si bonds). The RI of silicon oxynitride films can thus be anywhere in between these two extremes. The optimum RI range for the thin films used for the waveguide application in this work is 1.55 to 1.70 for WDM for data communications. In this work, it was attempted to obtain RIs in this desired range. A higher refractive index indicates a higher density material, as light travels more slowly through the higher RI material. Silicon nitride is denser than silicon dioxide and therefore has a higher RI. Materials with an RI range of 1.46 to 1.49 are predominantly silicon dioxide, whilst silicon nitride has an RI range of 2 [40]**.** In the range 1.55 to 1.7, the material is truly an oxynitride.

There are reports of silicon oxynitride films with a refractive index of 1.48 having high optical losses at 1530nm due to Si-H and N-H overtones [40]. These losses can be widely reduced by heat-treatment.

Aside from deposition rate, film thickness and density, RI, optical loss, film composition and hydrogen bonding content, film stress is also an important parameter, as stress effects of how the light propagates through the material and can degrade the electrical properties of devices [41]. Film mechanical stress can be controlled by performing alternative high frequency and low frequency deposition steps**.**

Figure 4-1. Illustration of stressed film and film stress alleviated by sequential deposition of high frequency (HF) and low frequency (LF) layers.

High frequency layers have an associated a tensile stress whilst the addition of low frequency deposited layers can induce a compressive stress, well known in silicon nitride films [42][43] (see Figure 4-1). The higher the power of the low frequency step used, the greater the degree of compressive stress incorporated in the deposited film. The RF frequency mode thus presents

a major influence of residual stress: in low frequency mode a relatively high compressive stress is achieved due to ion bombardment and, as a result, densification of the layer is achieved. Increased low frequency power results in a higher electron density and higher ionisation and dissociation rates, resulting in higher deposition rates and greater incorporation of N bonding in silicon nitride films. The higher volume expansion of the silicon nitride film yields higher compressive stress, which compensates the tensile stress of the whole layer and leads to overall lower tensile stress [43].

By alternating the frequency during the deposition process, the combination of tensile and compressive layers can produce a stress-free film.

However, due to the unavailability of equipment required to measure film stress, together with time constraints, film stress has not been investigated in this work. Film stress can be monitored by measuring the curvature of the substrate before and after deposition of the thin film.

The optical loss is a key performance parameter in optical waveguide structures. The lower the optical loss, the higher the energy efficiency of the waveguide device. The total optical loss for an optical waveguide consists of absorption and scattering losses and should be kept to a minimum. The absorption optical loss is essentially the loss of photonic energy through absorption of photons by the molecular bonds within the dielectric film which is studied in this thesis. Optical waveguides are used for example in fibre optics to transfer a signal over potentially thousands of miles. The desired optical loss would be as close to zero as possible. In reality, there will always be some optical loss.

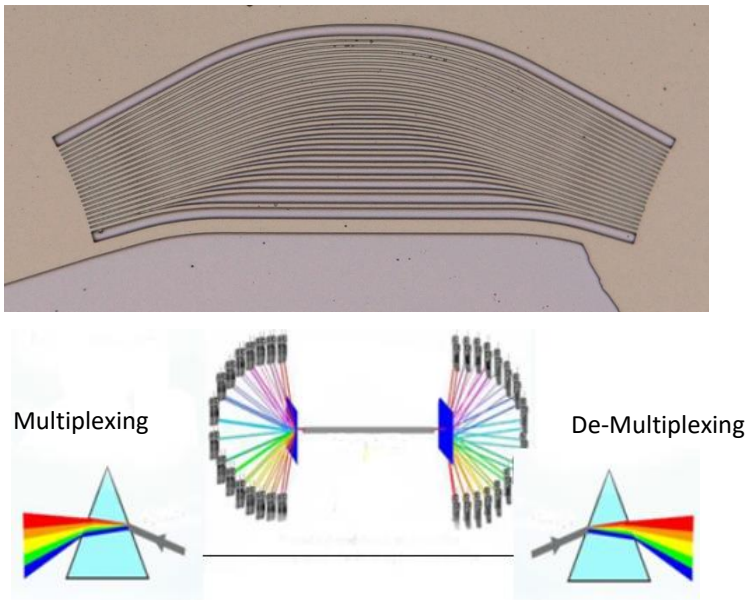

Figure 4-2. Schematic of a WDM system.

In this work, the fabricated waveguide devices are used as wavelength-division multiplexing appliances. A WDM system uses a multiplexer at the transmitter to join several different frequency signals together, and a demultiplexer at the receiver to split them apart Figure 4-2Figure 4-2. WDM systems are popular with telecommunications companies because they allow them to expand the capacity of the network, by using up to 160 different wavelength signals travelling along a single optical fiber, without laying more fiber. In this work, waveguides for the multiplexer and demultiplexer have been developed.

The waveguide device consists of a silicon substrate, a stacked structure of silicon oxynitride layers with varying refractive indices which is sandwiched between two similar low refractive index oxide layers, 5 micrometres in thicknesses (Figure 4-3). The stacked structure can consist of many layers with a silicon or SOI substrate as the first layer. The next layer is a thick buffer layer of SiON with a low RI (1.55). This thick layer provides a suitable layer on which to grow further oxynitride layers. The subsequent stacked SiON layers have varying thicknesses and RI. The red layers represent SiON with a RI of 1.75, which are the waveguide core layers. These are clad either side with lower RI (1.65) SiON layers – represented in the figure as the blue layers. Light is this confined within the red high RI layers. This stacked structure then undergoes further fabrication processes such as patterning, etching and metallisation to produce the final device, as illustrated in Figure 4-3.

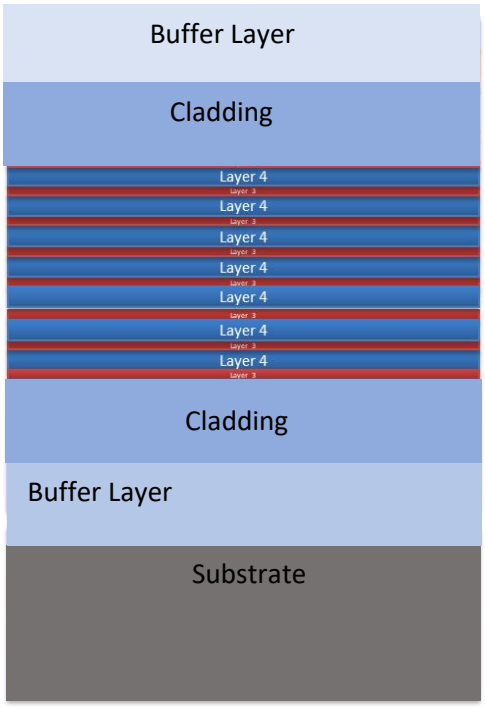

Figure 4-3 Schematic of layered waveguide device (cross section).

The process steps for fabrication of the waveguide device are detailed in Figure 4-4. Following deposition of the SiON waveguide stack, a resist layer is used to pattern a series of WDM waveguide structures (Figure 4-4 a). The next steps use resist patterning and development to vertically isolate the waveguide structures via plasma etching (Figure 4-4 b-e). Following further resist patterning and development steps (Figure 4-4 f-h), the wafer is diced into individual dies (Figure 4-4 i) using a deep silicon RIE (Reactive Ion Etch) process.

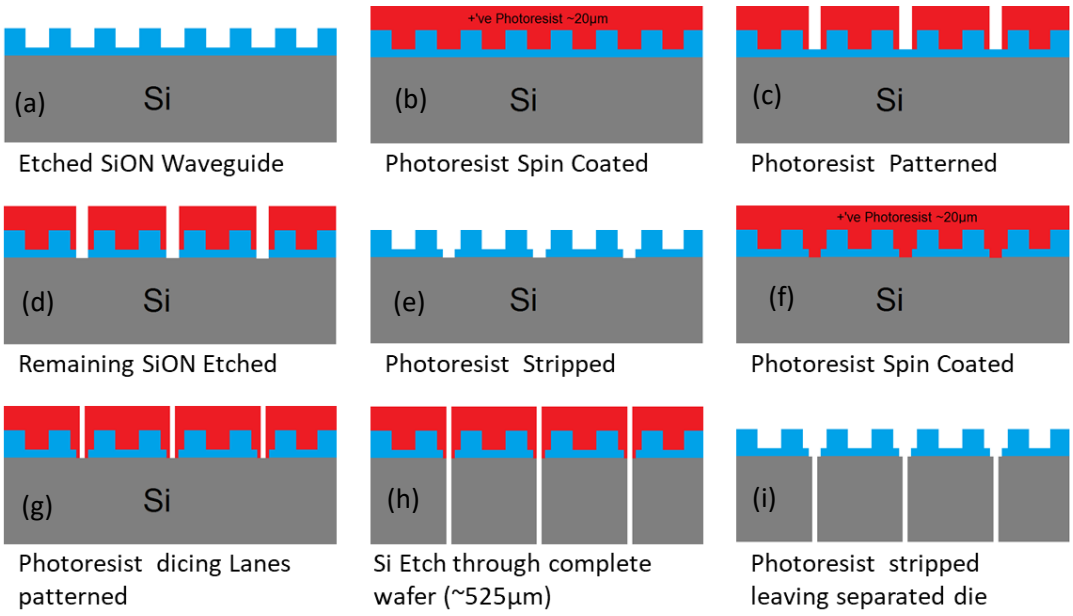

Figure 4-4 Process flow for fabrication of waveguide device.

4.1 PECVD Results

PECVD has been extensively used to deposit different Si-based dielectric layers for optical devices. The optical properties of such layers can easily be adjusted by tuning the deposition parameters. This designed experimental matrix should yield a better understanding of the principle effects of adjusting deposition parameters and in particular, the contribution of the flow rate of two precursor gases, N_2O and SiH_4, on the composition of the deposited SiON layers and their optical properties. In the experiment, other parameters such as N_2 flow rate, pressure, power, temperature of the substrate and the shower head were kept constant.

In this work, silicon oxynitride (SiON) layers were deposited on 4" n-type Si, single side polished (SSP) substrates with 100 mm diameter and 525 μm thickness, using an SPTS PECVD instrument. The platen temperature used was 300°C, with a chamber pressure of 2000 mTorr. The shower head was operated at temperature 250℃ with 150 W power and radio frequency of 13.56 MHz via an automatic matching unit, which matches the impedance of the generator to that of the process chamber to ensure that the maximum power transfers to the plasma.

A matrix of deposited films was prepared by varying the ratio of the two precursor gases, nitrous oxide (N_2O) : silane (SiH_4). Practically, this was achieved by adjusting the flow rate of the N_2O and SiH_4 gases. The (N_2) carrier gas was kept constant at 2700 sccm during deposition of all the films.

The refractive indices of the deposited films were determined using ellipsometry for the spectral range from 370 nm to 1702 nm (3.35 ev – 0.73 ev) at three different angles of incidence of, 65°, 70° and 75° which covers the Brewster angle of the dielectric material region [44][45]. The 49-point measurement patterns were used across each wafer to measure the optical constant uniformity of the deposited films across each whole wafer (Figure 4-5). The final results of the optical constant have been derived by standard deviation at each of these points.

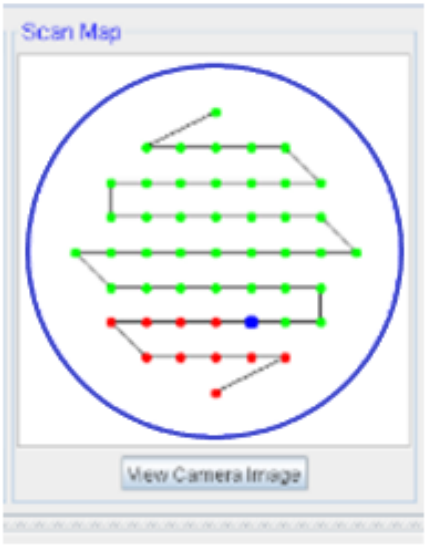

Figure 4-5. Location of the data map points for ellipsometry measurements. The pattern represents data collection from a spread of points across the whole wafer. At each point the RI and film thickness are measured.

In deposition experiments, silane flow rates of 20, 30 and 40 sccm were used. At each of these flow rates, the nitrous oxide gas flow rate was varied from 25 to 130 sccm.

In the second set of experiments, the flow rate of the nitrous oxide was kept constant at 65 sccm, but the flow rate of silane gas was varied from 15 to 135 sccm, using a gas mass flow controller (MFC).

In the last set of depositions, the flow rate of the nitrous oxide was maintained at 130 sccm and the flow rate of the silane gas was varied again from 15 to 135 sccm.

4.1.1 Investigation of silicon oxynitride films with varying nitrous oxide concentration at fixed silane flow 20, 30 and 40 sccm

In order to investigate the effect of varying nitrous oxide gas flow ratios on the properties of the deposited oxynitride films, three set of films were prepared. For each set, the silane gas flow ratio was kept constant at 20 sccm, 30 sccm and 40 sccm respectively (using deposition times of 341, 279 and 460 second respectively - which is the time required to achieve the roughly 1 μm film thickness) and the nitrous oxide was varied from 25 to 135 sccm, using a nitrous gas mass flow controller (MFC). The parameters of these silicon oxynitride films were

fitted using the Tauc-Lorentz dispersion model [46] [47] (a commonly used model to describe the dielectric constant of semiconductors and other UV absorption materials, which has been proven to be useful in modelling these materials). This model provides the best fit to experimental data. Figure 4-6 shows the close fitting of the model (black dashes) with the measured parameters (red and green lines). The uniformity of the thickness and the refractive index of the film with Silane 20 sccm and nitrous oxide 25 sccm across the wafer is illustrated in Figure 4-7-a.

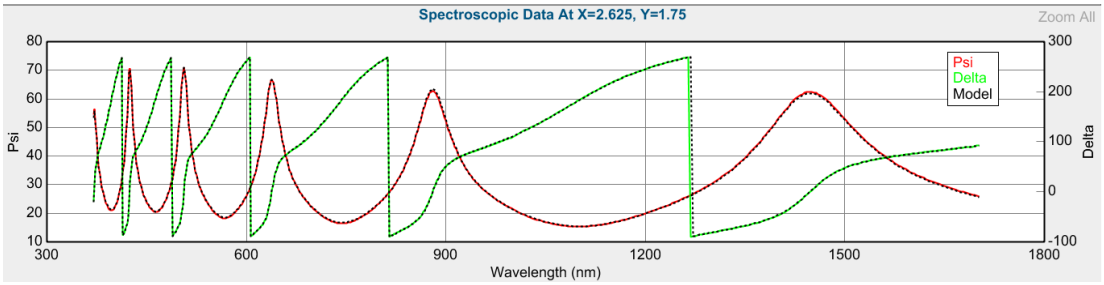

Figure 4-6. The best fitted parameters of silicon oxynitride film with silane 20 sccm and nitrous oxide 25 sccm gas flow ratio which is determined by using the Tauc-Lorentz dispersion model.

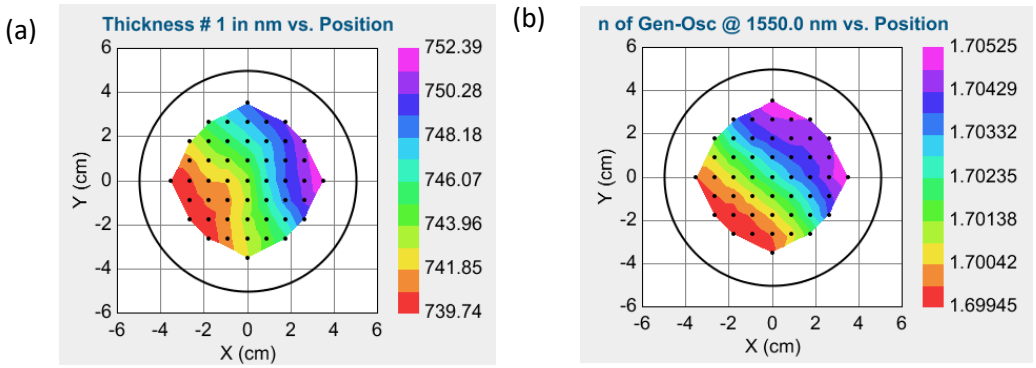

Figure 4-7. Contrast and uniformity of the thickness (a) and refractive index (b) across the film with for the silane flow rate SiH_4=20 sccm and N_2O=25 sccm at wavelength 1550 nm.

Figure 4-7-b shows the uniformity of the RI and the film thickness of the deposited oxynitride, using deposition parameters of silane 20 sccm and nitrous 25 sccm, across a 100mm diameter wafer. The difference between minimum and maximum refractive index across the wafer is only 0.005 which shows a good refractive index uniformity. The thickness uniformity is larger with 19.65 nm difference between two extremes of thickness across this wafer. Even so, this still represents a 3% thickness uniformity range over the whole wafer. From Figure 4-7 it appears as if there is some correlation between the refractive index and thickness variation

across the wafer – with the low RI (1.69945) corresponding to the thinnest film thickness (732.74 nm) and the highest RI (1.70525), which is on the opposite side of the wafer, corresponding to the maximum thickness of the oxynitride film (752.39 nm). The data in Figure 4-7 represents only one single wafer. Other wafers, data from which is detailed in Table 4, show similar variations in refractive index and thickness, indicating that different deposition conditions do not greatly affect film uniformity across the wafer.

Table 4. The refractive index, thickness and the deposition rate of each set of the experiments at silane 20, 30 and 40 represented in this table.

SiH4 (SCCM)	N2O (sccm)	RI (636nm)	RI (1310nm)	RI (1550 nm)	Dep rate (nm/sec)	Thickness (nm)
20	25	1.73781	1.70549	1.69994	2.1886	746.3
20	40	1.62377	1.60258	1.59772	2.3733	809.31
20	50	1.5812	1.56453	1.56297	2.4527	836.37
20	65	1.54819	1.53333	1.53192	2.4992	852.22
20	85	1.5256	1.51168	1.51034	2.5732	877.47
20	100	1.51385	1.50063	1.49935	2.6233	894.53
20	130	1.49843	1.48578	1.48455	2.6992	920.42
SiH4 (SCCM)	N2O (sccm)	RI (636nm)	RI (1310nm)	RI (1550 nm)	Dep rate (nm/sec)	Thickness (nm)
30	25	1.9235	1.8651	1.8583	2.4417	681.24
30	40	1.7990	1.7588	1.7524	2.7395	764.32
30	50	1.7365	1.7031	1.6971	2.8880	805.76
30	65	1.6795	1.6528	1.6475	3.0273	844.23
30	85	1.6157	1.5943	1.5895	3.1729	885.23
30	100	1.5883	1.5692	1.5648	3.2690	912.07
30	130	1.5564	1.5395	1.5354	3.3807	943.22
SiH4 (SCCM)	N2O (sccm)	RI (636nm)	RI (1310nm)	RI (1550 nm)	Dep rate (nm/sec)	Thickness (nm)
40	25	2.0598	1.9824	1.9740	2.5944	1193.41
40	40	1.9256	1.8670	1.8602	2.9405	1352.63
40	50	1.8705	1.8184	1.8118	3.0914	1422.04
40	65	1.7909	1.7495	1.7439	3.3356	1534.36
40	85	1.7318	1.6985	1.6931	3.5192	1618.85
40	100	1.6943	1.6638	1.6583	3.6383	1673.6
40	130	1.6344	1.6109	1.6060	3.8417	1767.2

The refractive index of the three sets of the deposited films at silane flow ratios of 20 sccm, 30 sccm and 40 sccm respectively is illustrated in

.

For films with a silane flow ratio of 20 sccm, by increasing the nitrous oxide flow from 25 sccm to 130 sccm, the refractive index at three different wavelengths decreases and is in the range of 1.73781 to 1.49843 at 636 nm, 1.70549 to 1.48578 at 1310 nm and 1.69994 to 1.48455 at 1550 nm wavelength. These refractive index values are representative of the average across the whole wafer.

For the deposited films at silane flow ratio of 30 sccm, by increasing the nitrous oxide from 25 sccm to 130 sccm, the refractive index decreases from 1.9235 to 1.5564 at 636 nm, 1.8651 to 1.5395 at 1310 nm and 1.8583 to 1.5354 at 1550 nm wavelength.

Finally, for the films deposited with silane flow ratio of 40 sccm, by increasing the nitrous oxide, the refractive index decreases at each of three wavelengths. The refractive index is in the range of 2.0598 to 1.6344 at 636 nm, 1.9824 to 1.6109 at 1310 nm and 1.9740 to 1.6060 at 1550 nm wavelength.

Comparing the three different sets of the experiments shows that increasing the incorporation of the silicon in the films, by increasing the silane flow ratio, leads to an increase the range of the related refractive indices. Therefore, the refractive indices of the films with silane flow ratio of 40 sccm is higher compared to the other silane flow ratios. Also, increasing the level of oxygen incorporation in the film's composition, by increasing the nitrous oxide flow, results in a reduction of the related refractive indexes.

The refractive index changes rapidly with any change in N_2O flow at lower N_2O flow ratios (less than 65 sccm). A small change in this flow, results in a large change in refractive index value. For example, at 1550 nm wavelength and silane flow ratio of 20 sccm, the difference between the refractive index at nitrous oxide 130 sccm and 100 sccm, is 0.0148 whereas this difference for lower nitrous oxide flow ratio of 40 sccm and 25 sccm, is 0.1022 (7 times larger). The slope of the refractive index curve decreases gradually with increasing of the N_2O flow and therefore, the reproducibility of the silicon oxynitride films will be improved at higher nitrous oxide flow ratios. [48]

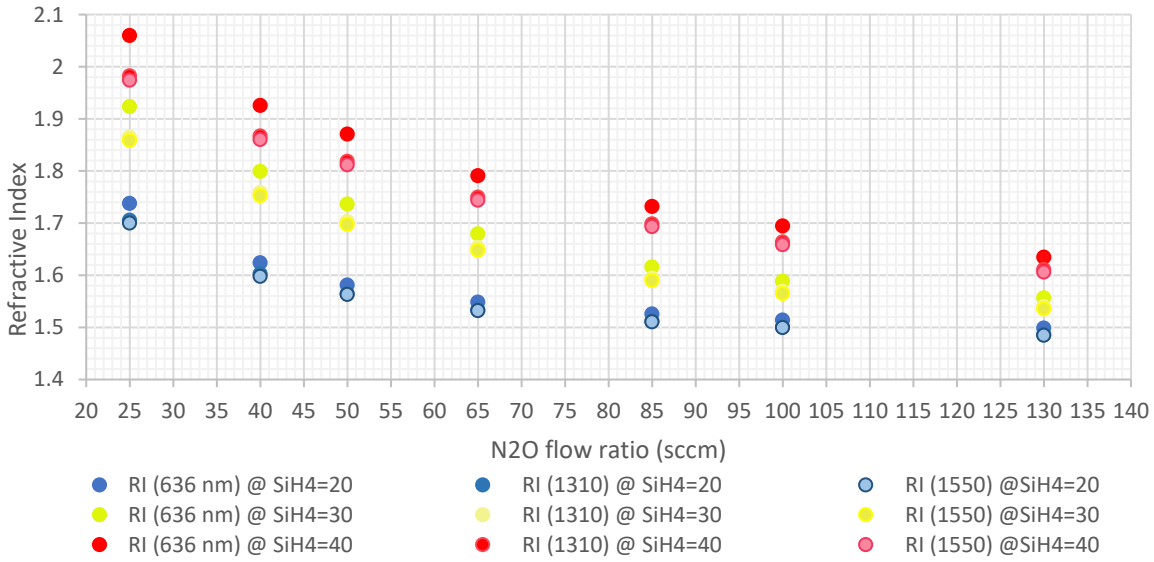

Figure 4-8. The refractive index of three sets of the films with silane flow ratio of 20 sccm, 30 sccm and 40 sccm, at the wavelengths of 636 nm, 1310 nm and 1550 nm has been illustrated.

The deposition rates of each set of the films, are compared in Figure 4-9. The deposition rate increases by increasing the nitrous oxide flow ratio. Also, increasing the silane flow ratio leads to an increase the deposition rate of these films.

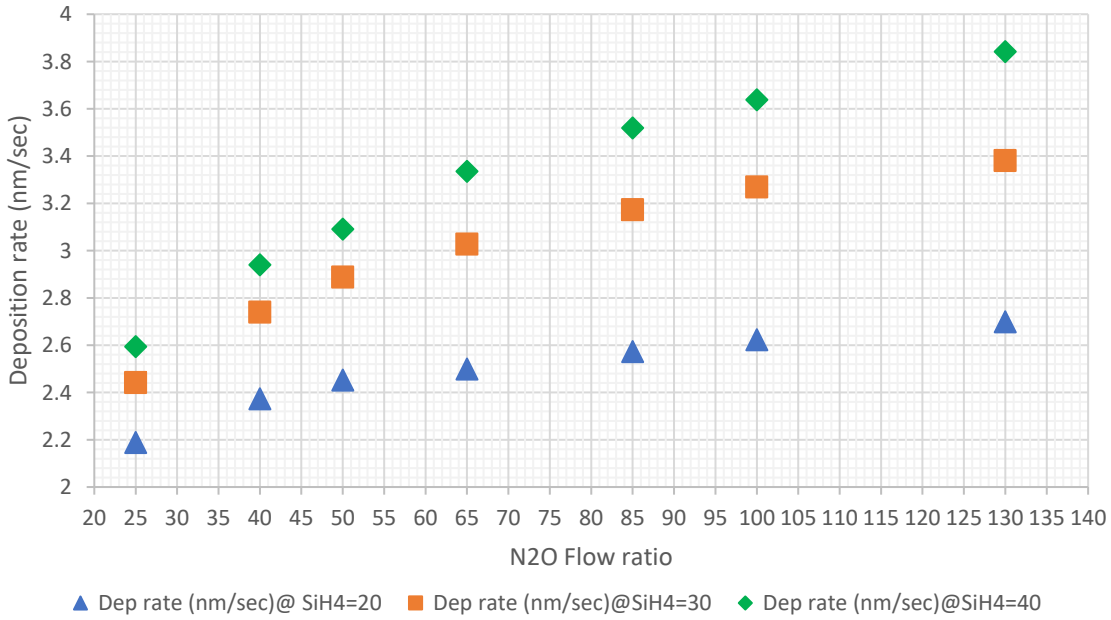

Figure 4-9. The deposition rate at three silane ratios of 20 sccm, 30 sccm and 40 sccm with nitrous oxide flow ratio varied between 25 sccm to 130 sccm.

4.1.2 Investigation of silicon oxynitride films with varying silane concentration at fixed nitrous oxide gas flow 65 sccm

In this set of experiments, the flow rate of nitrous oxide was kept constant at 65 sccm, but the flow rate of silane gas was varied from 15 to 135 sccm, using a gas mass flow controller (MFC).

The ratio of SiH_4 to N_2O flow rates, was varied from 0.231 to 2.077 and the deposition time kept constant at 476 seconds. The pressure (2000 Torr) and power (150 W) were also kept constant for this set of High Frequency (HF) deposition experiments.

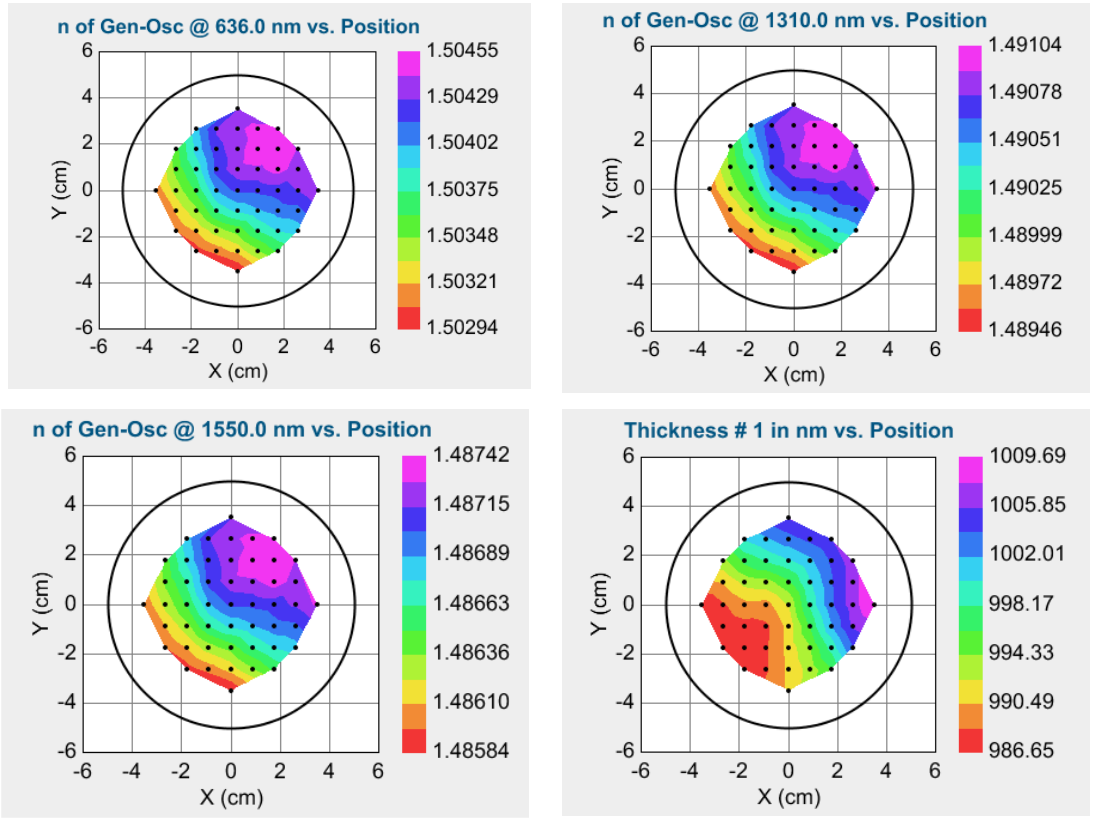

Figure 4-10. Contrast and uniformity of the thickness and refractive index across the film with for the silane flow rate SiH4=15 sccm and N2O=65 sccm at wavelengths 636 nm, 1310 nm,1550 nm.

As can be seen from

Figure *4-10* and (Table 5), the RI varies across the wafer by 0.106% at each of the three wavelengths, whilst the film thickness varies by 23nm or 2.28% across the wafer. This illustrates that the film thickness uniformity is similar to the data in Figure 4-7.

Table 5. Changes in RI and SiON layer thickness across a wafer, measured at three different wavelengths.

	636nm	**1310nm**	**1550nm**	**Thickness**
High	1.50455	1.49104	1.48742	1009.69
Low	1.50294	1.48946	1.48584	986.65
Difference	0.00161	0.00158	0.00158	23.04
Percentage change across wafer	0.107%	0.106%	0.106%	2.282%

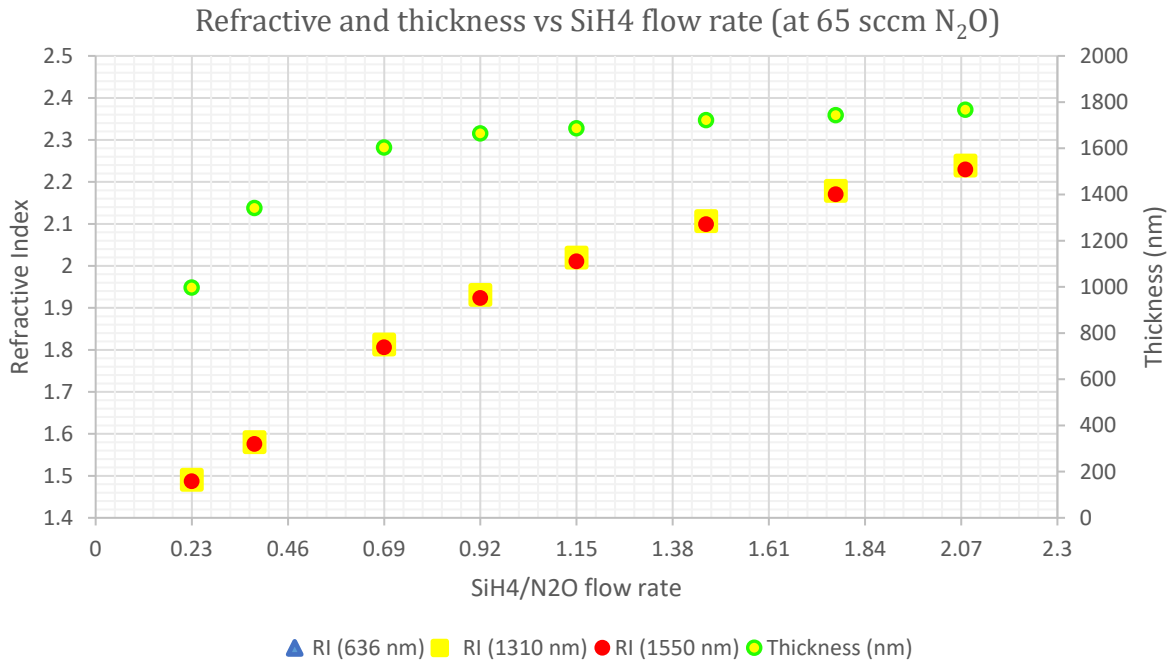

Figure 4-11Change in refractive Index (RI) and thicknesses a function of SiH4 : N2O ratio. Silane flow rate is increased from 15 to 135 sccm

Figure 4-11 shows the dependence of the refractive index as a function of the varying gas N_2O: SiH_4 flow ratio for eight different flow rates of SiH_4 from 15 to 135 sccm. It can be seen that the refractive index for the deposited SiON layers, varies between 1.5039 to 2.3733 at a wavelength of 636 nm, 1.4904 to 2.2389 at a wavelength 1310 nm and 1.4868 to 2.2294 at a wavelength 1550 nm. The difference in refractive index values at each of these three wavelengths can be explained by normal dispersion phenomenon [49], which describes the

refractive index dependence of wavelength where the index increases with increasing optical frequency (i.e. the RI is highest at the shorter wavelength 636nm). The refractive index tends to decrease with increasing wavelength to 1310 and 1550 nm.

As silane gas has a higher dissociation efficiency than nitrous oxide [25], silane radicals dominate the formation of the oxynitride. This is more pronounced when increasing the SiH_4:N_2O flow ratio. This leads to a decrease in the concentration of excited Oxygen atoms and an increasing probability of incorporation of nitrogen and silicon into the films. The relative permittivity (dielectric constant) of the silicon oxide, silicon nitride and silicon is about 3.9, 7.5 and 11.9 respectively [50][51]. The higher the permittivity, the more ability of a material to polarise in response to an applied field. The dielectric constant of a material and its refractive index are closely linked by the equation:

$$\tilde{\varepsilon} = \tilde{n}^2$$

Therefore, by increasing the silane ratio in the films, the composition tends more to the silicon nitride (silicon rich) type material and this consequently results in an increase in the refractive index of the films.

The deposited films with the gas ratios of 0.23 and 0.46, (lower silane content) which are more silicon oxide type films, show a smaller difference of the refractive index between 636 nm wavelength and the two other wavelengths, 1310 and 1550, respectively 0.0135 and 0.0171. By increasing the silane flow rate, which results in increasing the gas ratio to 2.08, the difference between the refractive index at 636 nm and at 1310 nm increases to a higher value of 0.1344, whereas the difference between the RI at 636 nm and 1550 nm was 0.1439. The diversion of the refractive indices at different wavelengths is noticeable in this graph, particularly at higher refractive indices.

The divergence in the RI at high silane : N_2O ratios is related to the higher density of silicon nitride type films (in comparison to lower density silicon oxide type films). In higher density films, the speed of light is slower – and thus the RI changes more with respect to wavelength. The RI is thus more stable and reliable at different wavelengths for silicon oxide films.

Increasing the concentration of reactant species by increasing the gas flow ratio, results in increases of film thicknesses. Film thickness is thus a function of the SiH_4 flow rate. The oxynitride film thickness varied from 996.45 nm to 1766.43 nm for the corresponding flow ratios of 0.23 and 2.08, respectively. From

Figure 4-12, the thickness dependence on the gas flow ratios, shows a significant increase when using SiH_4/N_2O ratios of 0.23 and 0.69 and a more gradual increase in thickness for the deposited films with higher SiH_4/N_2O ratios (*Table 6*).

Table 6. The gas flow ratios, refractive index, thickness and the deposition rate of the fixed nitrous oxide at 65 sccm and varied silane flow experiments, represented in this table.

SiH4 (SCCM)	SiH4/N2O	RI (636 nm)	RI (1310 nm)	RI (1550 nm)	Deposition rate (nm/sec)	Thickness (nm)
15	0.23	1.5039	1.4904	1.4868	2.0934	996.45
25	0.38	1.5991	1.5800	1.5756	2.8171	1340.94
45	0.69	1.8612	1.8128	1.8057	3.3662	1602.33
60	0.92	1.9985	1.9307	1.9230	3.4944	1663.32
75	1.15	2.1040	2.0197	2.0105	3.5421	1686.04
95	1.46	2.2078	2.1064	2.0990	3.6166	1721.51
115	1.77	2.2975	2.1786	2.1700	3.6609	1742.59
135	2.08	2.3733	2.2389	2.2294	3.7109	1766.43

Figure 4-12 illustrates the relation between the deposition rate and the gas flow ratios and their relative refractive indices. The slope of the deposition rate curve increases rapidly for gas ratios of 0.23 and 0.69 and then increases more gradually with silane to nitrous oxide ratios from 0.69 to 2.08.

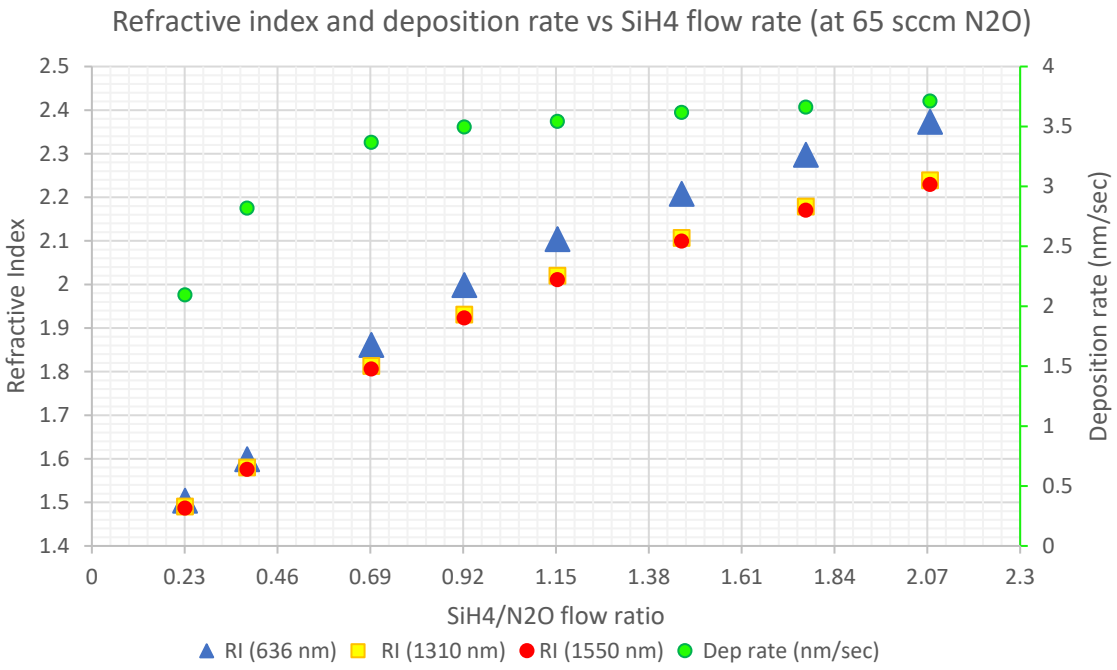

Figure 4-12 shows changing in thickness and deposition rate as a function of the refractive index while SiH_4 varies from 15 to 135 sccm and N2O is constant at 65 sccm.

Figure 4-13 and Figure 4-14 show the spectra of the refractive indices and the extinction coefficient of the deposited films with the silane flows in the range of 15 sccm to 135 sccm. These data were determined by using the best fitted model, Tauc-lorentz dispersion.

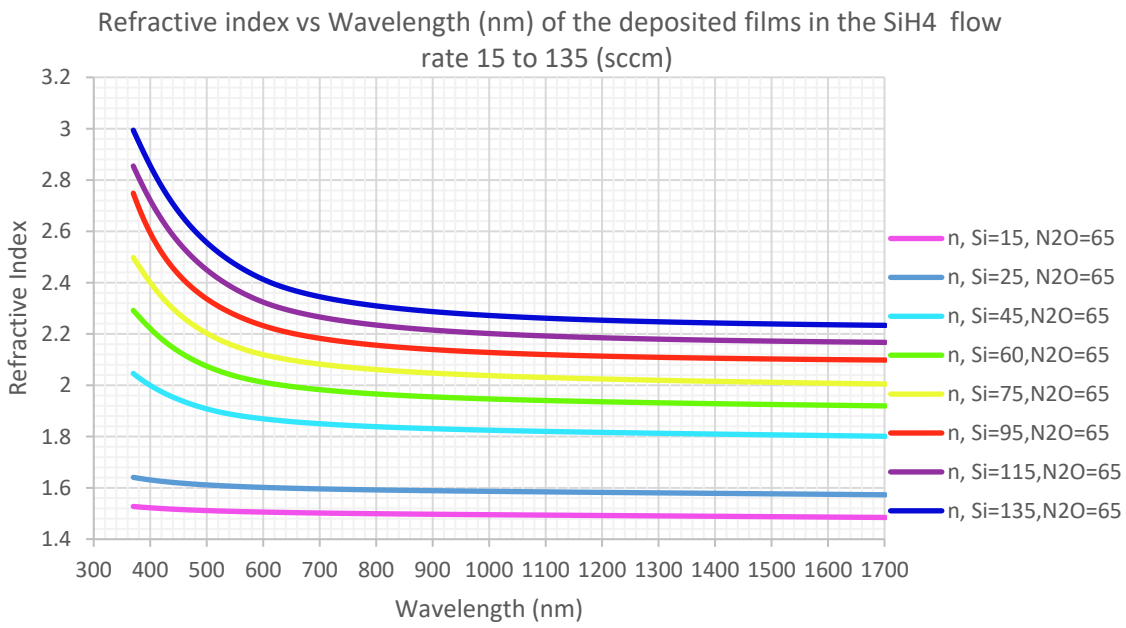

Figure 4-13. Measured RI variation as a function of wavelength and silane flow rate for different films compositions. Larger silicon contents result in larger refractive index.

Figure 4-13 shows the index dispersion curves of all the deposited films. The refractive index increases with increasing the ratio of silane flow to nitrous oxide (SiH_4 / N_2O) from 0.23 to 2.08. The refractive indices vary from 1.5039, 1.4904 and 1.4868 respectively at wavelengths of 636 nm, 1310 nm and 1550 nm (at a SiH_4 / N_2O ratio of 0.23) up to 2.3733, 2.2389 and 2.2294, respectively at a SiH_4 / N_2O ratio of 2.08.

As the gas ratio increases, the RI increases. This is due to a change in the film composition from low silicon content to silicon rich, related to further increasing the SiH_4/N_2O ratio - resulting in a deficiency of both oxygen and nitrogen radicals and the appearance of more Si-Si bonds - which leads to silicon rich oxynitride films. [25][52]

Figure 4-14 indicates that at lower silane flow ratios of 15 sccm and 25sccm, the corresponding extinction coefficient values are extremely low (near zero) and the films appear transparent at wavelengths longer than 370 nm.

At longer wavelengths, the value of the extinction coefficient (as defined on page 3) of the films with higher silane flow rations and silicon content, becomes larger. This results in

absorption by these films in the region between 500 nm to 600 nm. The measured extinction coefficient (k) by Tauc Lorentz model, is near zero at wavelengths beyond 600 nm. The highest optical absorption is for the highest gas flow SiH_4 / N_2O ratio of 2.08, which increases significantly at wavelengths towards 370nm (the lowest wavelength measurable using the ellipsometer).

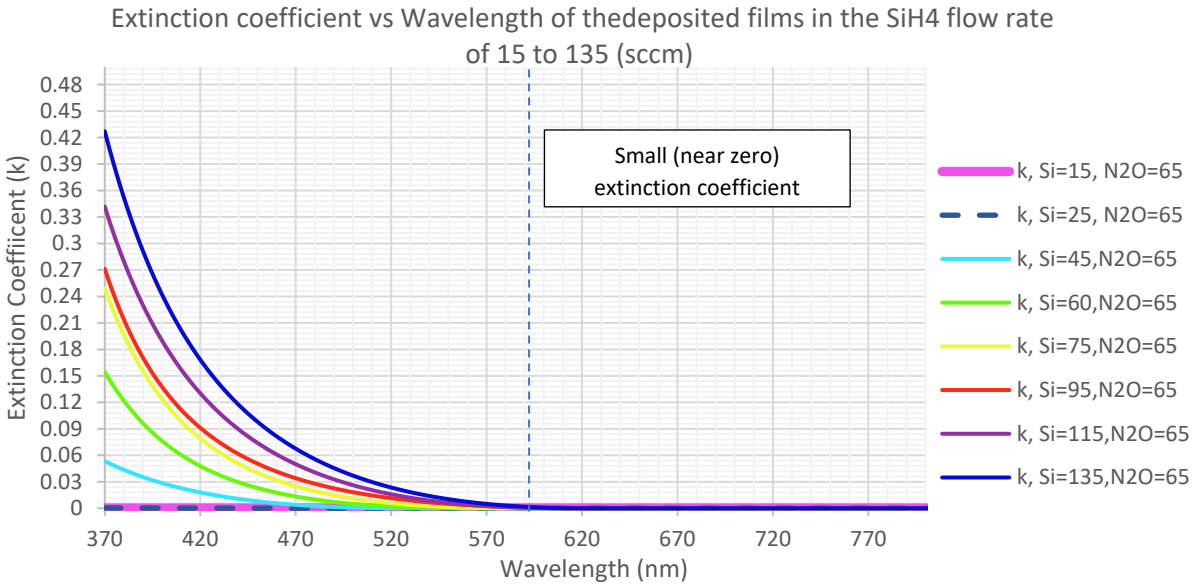

Figure 4-14. Variation of the measured extinction coefficient (imaginary refractive index k) as a function of wavelength for the fabricated compositions with different SiH_4 flow rate from 15 to 135 sccm at a constant 65 sccm N_2O flow. It shows that the measured extinction coefficient is small beyond 600 nm but at shorter wavelengths, by increasing the silicon content in the film, the extinction coefficient becomes larger.

4.1.3 Investigation of silicon oxynitride films with varying silane concentration at fixed nitrous oxide gas flow 130 sccm

The interaction of an incident photon and a material depends on the material's bandgap. Optical transparency of a material at a specific wavelength requires the energy of incident photon to be smaller than the bandgap energy [53] – the material begins to absorb photons with energies similar to the bandgap energy. A larger bandgap implies tightly bound electron, which interacts minimally with an incident photon with energy below its band gap. Materials with larger bandgap therefore possess a smaller refractive index and light experiences a shorter delay when propagating within these mediums. The larger bandgap of silicon oxide (around 9 eV) results in negligible absorption in the 370 to 1700nm experimental range. In contrast, silicon nitride films, with a bandgap of around 5eV start to absorb at wavelengths shorter than 600nm, as these photon energies are approaching resonance with the silicon nitride bandgap.

In this set of depositions, the flow rate of the nitrous oxide was kept at 130 sccm and the flow rate of the silane gas was varied again from 15 to 135 sccm. The ratio of SiH_4 to N_2O flow rates, was varied from 0.231 to 2.077 and the deposition time kept constant at 448 seconds which is the time required to achieve the roughly 1 μm thickness. The pressure (2000 Torr) and power (150 W) were also kept constant for this set of High Frequency (HF) deposition experiments. Table 7 shows the measurement results of this set of the depositions.

Table 7. Measured refractive index, thickness and deposition rate of deposited films with fixed nitrous oxide at 130 sccm and varying silane flow from 15 to 135 sccm.

SiH4 (SCCM	SiH4/N2O	RI (636nm)	RI (1310nm)	RI (1550 nm)	Deposition rate (nm/sec)	Thickness (nm)
15	0.12	1.4735	1.4610	1.4576	2.2660	1015.15
25	0.19	1.5263	1.5110	1.5069	3.0509	1366.8
45	0.35	1.6816	1.6519	1.6481	3.9947	1789.63
60	0.46	1.8028	1.7592	1.7542	4.2334	1896.56
75	0.58	1.8969	1.8398	1.8343	4.3299	1939.79
95	0.73	1.9995	1.9266	1.9204	4.4282	1983.85
115	0.88	2.1078	2.0196	2.0117	4.3881	1965.86
135	1.04	2.1564	2.0586	2.0489	4.4978	2015.03

Figure 4-15 shows the dependence of the refractive index as a function of the varying gas flow ratio between N_2O and SiH_4 for eight different flows of SiH4 from 15 to 135 sccm. It can be seen that the refractive index for the deposited SiON layers, varies between 1.4735 to 2.1564 at a wavelength of 636 nm, 1.4610 to2.0586 at a wavelength 1310 nm and 1.4576 to 2.0489 at a wavelength 1550 nm.

In this figure, the deposited film with the gas ratio of 0.12 is more silicon oxide type and 0.73, 0.88 and 1.04 tend towards more silicon nitride composition films .

Increasing the concentration of reactant species by increasing the gas flow ratio, results in increases of film thicknesses. Thus, film thickness is thus a function of the SiH_4 flow rate. The oxynitride film thickness varied from 1015.15 nm to 2015.03 nm for corresponding flow ratios of 0.12 and 1.04, respectively. From Figure 3, the film thickness dependence on the gas flow ratios, shows a rapid increase when using N_2O / SiH_4 ratios of 0.12 and 0.35 and a more gradual increase in thickness for the deposited films with higher N_2O / SIH_4 ratios.

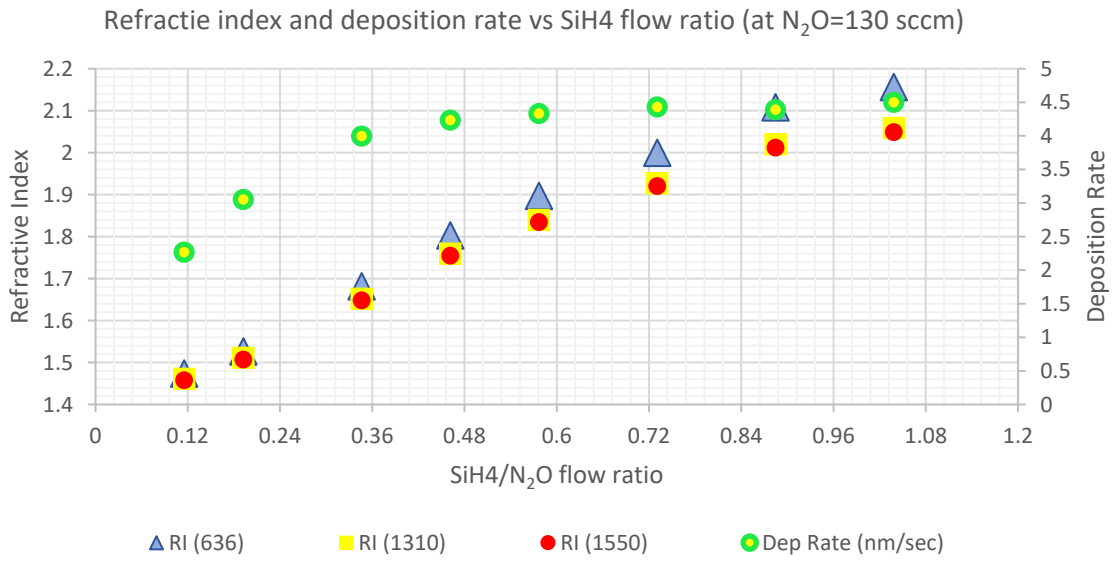

Figure 4-15. Variance in film thickness and deposition rate as a function of the refractive index while SiH_4 varies from 15 to 135 sccm and N_2O is constant at 130 sccm.

The refractive index of the two sets of deposited films at nitrous flow ratios of 65 sccm and 130 sccm were compared and the result is illustrated in Figure 4-16. The results show that the refractive index of the first set of the experiments at N_2O flow rate of 65 sccm, possess a higher refractive index compared to the second set with higher flow rate of nitrous oxide (130 sccm). By increasing the nitrous oxide flow and inserting more oxygen into system, the composition of the deposited film changes and results in reduction in the refractive index values.

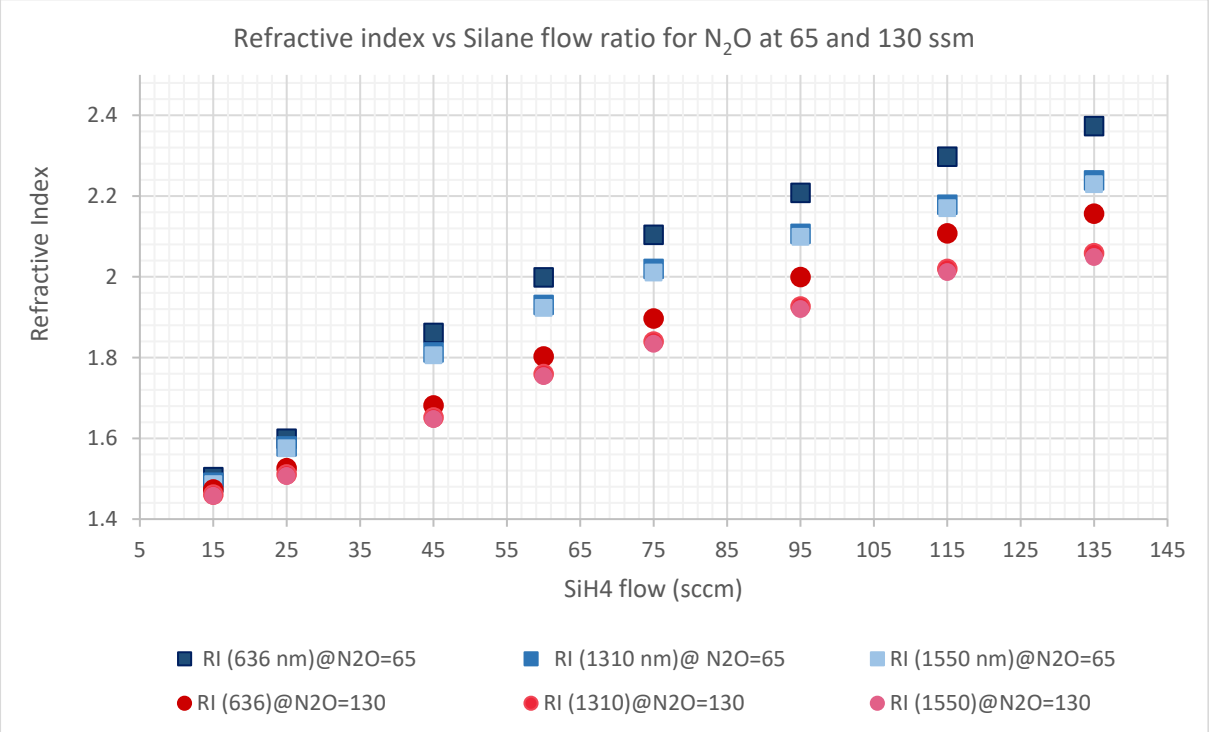

Figure 4-16. The refractive index of the two sets of the experiments with nitrous oxide at 65 sccm and 130 sccm is compared. The higher flow rate of nitrous oxide introduces a higher rate of oxygen in the film compositions and results into the reduction of the refractive index in these films.

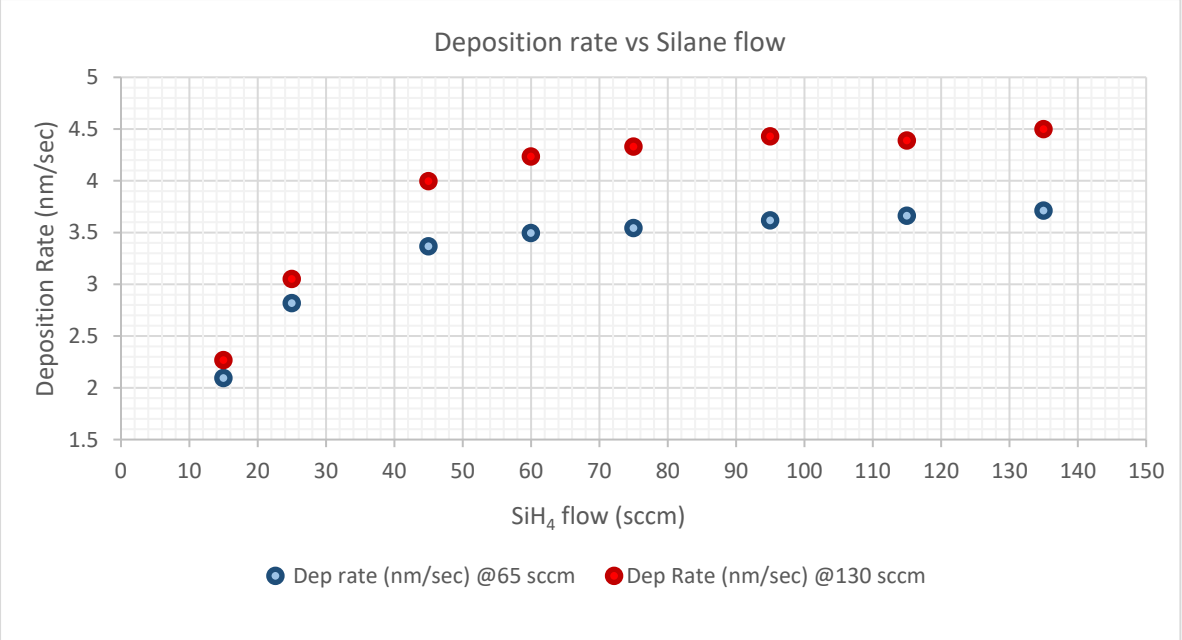

Figure 4-17. Higher rate of nitrous oxide with 130 sccm, increases the deposition rate compare to the lower rate with 65 sccm.

Figure 4-17 illustrates a comparison of the two deposition rates at nitrous oxide 65 sccm and 130 sccm. Increasing the concentration of oxygen by increasing the nitrous oxide flow rate, results in a higher deposition rate. The oxynitride deposition rate varied from 2.2660 to 4.4978 using the nitrous oxide flow rate of 130 sccm and from 2.0934 to 3.7109 for the nitrous oxide with flow rate of 65 sccm.

4.1.4 XPS investigations of silicon oxynitride films with varying silane flow ratio at fixed nitrous oxide 65 sccm and 130 sccm

In order to characterise the chemical composition and stoichiometry of the SiON films, with respect to different deposition conditions, XPS investigations have been performed on PECVD Silicon Oxynitride layers deposited on silicon substrates. XPS spectra can be used to determine the elemental composition of the deposited layers. Using XPS, to obtain the atomic ratios (Si : N : O), the film composition can be correlated to the refractive index of a deposited film and also to the film deposition rate. For example, the elemental ratio for the oxynitride film can be extracted from its XPS spectrum Figure 4-18. This ratio can then be correlated with the film's RI and deposition rate.

In order to avoid contamination and provide "near pristine" surfaces for XPS analysis , a new set of films were deposited using varying silane flows (15 sccm, 25 sccm, 45 sccm, 60 sccm, 75 sccm, 135 sccm) at fixed nitrous oxide 130 sccm flow rate were prepared. Films has approximately 1000 nm film thickness. Some additional films with two extremes of silane flow, 15 sccm and 135 sccm, and nitrous oxide 130 sccm were prepared with different thicknesses of 100 nm, 200 nm, 500nm, 700 nm and 1000 nm thicknesses were also prepared in order to assess the effect of film thickness on the composition of the films.

In figures Figure 4-18 (A) and Figure 4-18 (B) the survey scans of the two extremes silane flow ratios at two N_2O ratios of 130 sccm are illustrated. These figures show that the film composition is primarily silicon, oxygen and nitrogen elements.

Comparing these two graphs in Figure 4-18 shows that the size of the nitrogen 1s peak in counts per second (CPS), increases when using a 75 sccm silane flow ratio in comparison to a 15 sccm ratio.

The C1s peak is always present in air-stored samples due to ambient surface contamination [54][20] (hydrocarbons). This peak significantly reduces after etching (see Figure 4-19), indicating that the hydrocarbon contamination is present on the surface and not in the bulk of the films.

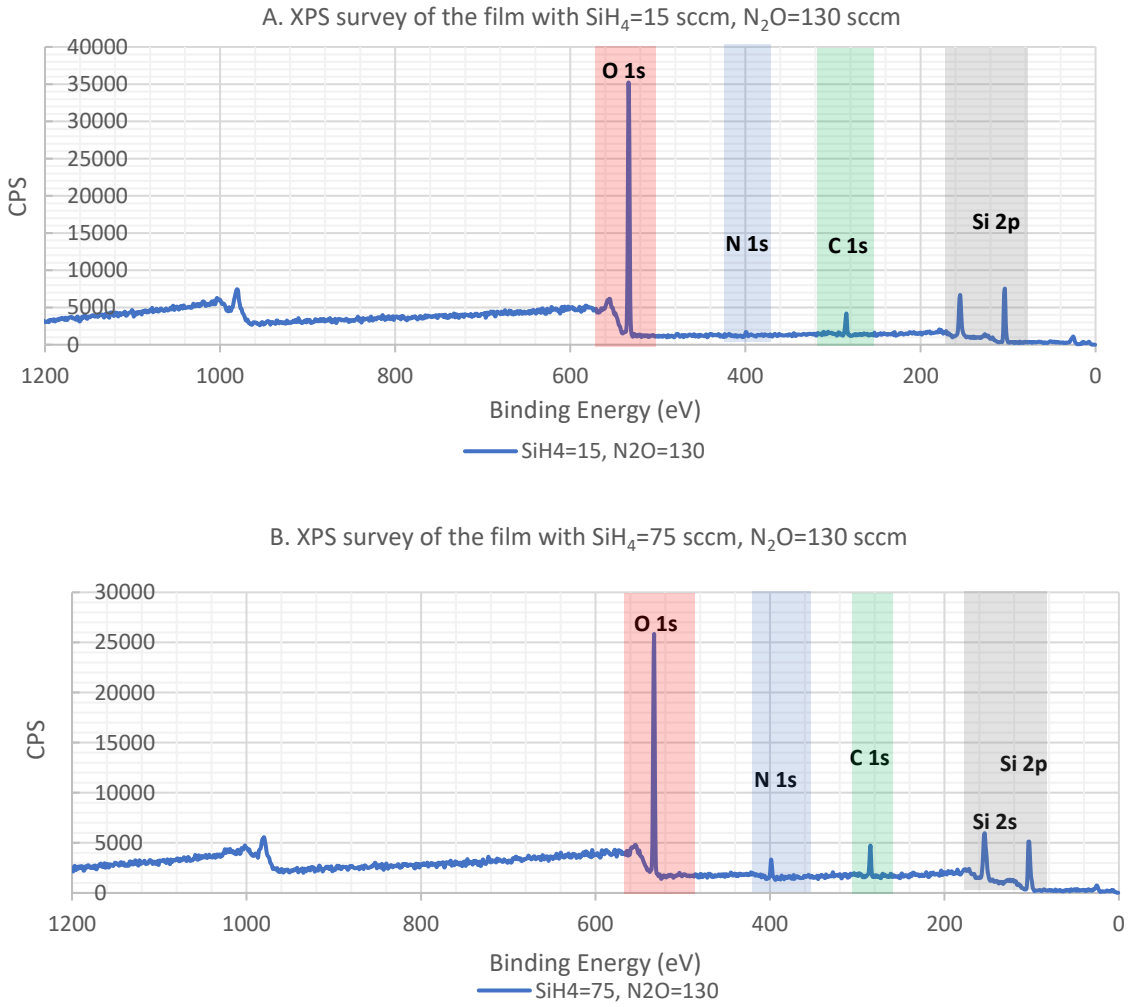

Figure 4-18. XPS full scan spectrum of SiON layer with nitrous oxide of 130 sccm and two different silane flow ratios of A. 15 sccm and B. 75 sccm. (Before etching)

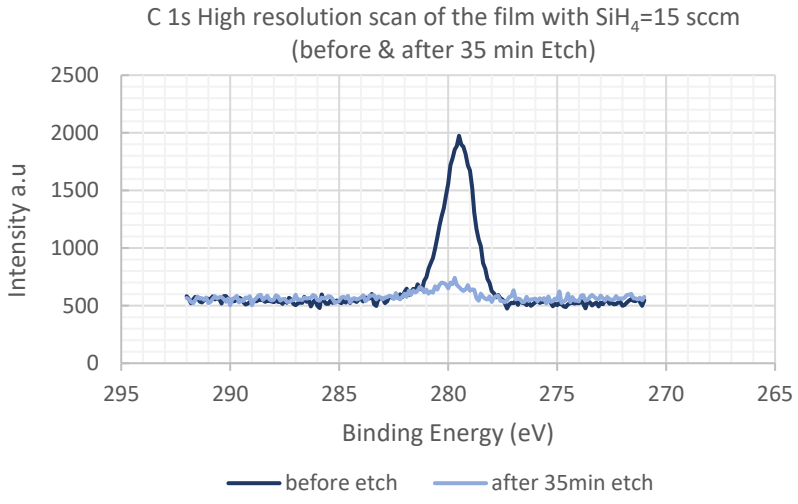

Figure 4-19.. The C 1s high res scan for a film with silane of 15 sccm at before and after 35 minutes etching.

Figure 4-20 shows the high-resolution spectra of the Si 2p peaks for the films with fixed nitrous oxide of 130 sccm and varying silane flows of 15 sccm, 25 sccm, 45 sccm, 60 sccm and 75 sccm respectively. They are calibrated and plotted after the correction of charging effects using a C-C peak binding energy at 285eV.

The binding energy has a correlation with atomic energy levels and hence relates to the electronegativity of the elements. Electronegativity increases from left to right along the periodic table, and decreases on descending a group. Therefore, oxygen has a higher electronegativity of (3.5) compared to the nitrogen (3.0) and silicon (1.8).

The silicon related peaks comes from the 2s and 2p states. In a pure silicon crystal, these two peaks are located at 149 eV and 100 eV respectively. These binding energy positions will be affected when silicon atoms bond to the other elements. Based on which of these elements bond to silicon, the binding energy changes of both the silicon and the bonding element peaks will shift. Decreasing the electronegativity of the bonding elements results in a reduction of the photoelectron energy. These effects can be obesrved in the Si2p high resolution spectra when. According to the literature, [29][34] pure silicon oxide has a Si2p peak with binding energy between 103.3 eV to 104.1 eV [35], whilst pure silicon nitride has a Si 2p binding energy between 101.1 eV to 101.9 eV. Therefore, in this experiment the center of the Si 2p core level (the purple peak) shifted from 104. eV (i.e. a predominantly SiO_2 film) to 103.76 eV(i.e. a mixture of Si_3N_4 , silicon oxynitride and SiO_2 film) corresponding to a silane flow rate of 15 sccm to 75 sccm. Table 8 shows the four Si 2p fitted components (SiO_2, Si_3N_4, Si-Si or Si-H and $SiON/SiO_xN_y$) of the incorporated silicon in the films - obserevd when using different silane flow ratios.

Table 8. Binding energies of the Si 2p, N 1s and O 1s and their average atomic percentages of the films deposited with constant N_2O flow at 130 sccm and varied SiH_4 flow ratios of 15 sccm, 25 sccm, 45 sccm, 60 sccm and 75 sccm.

	Si 2p Components – Binding Energy (eV) ± 0.2			
SiH_4 (sccm)	Si 2p A (SiO_2)	Si 2p B (Si_3N_4)	Si 2p C (Si/Si-H)	Si 2p D (SiON/SiOxNy)
15	104.18	102.18	100.65	103.18
25	104.05	102.05	100.52	103.05
45	103.85	101.85	100.32	102.85
60	103.84	101.84	100.31	102.84
75	103.76	101.76	100.23	102.76

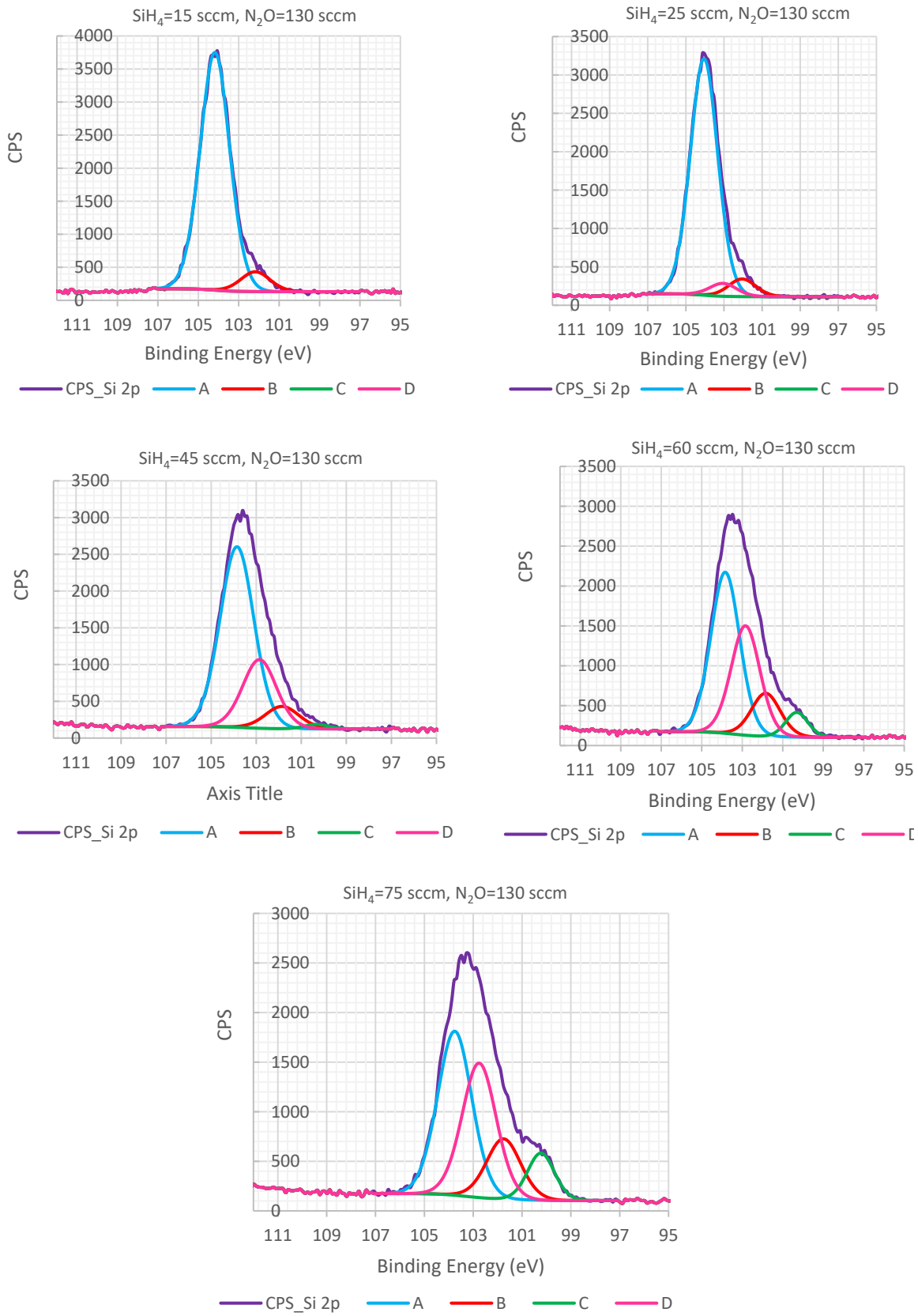

Figure 4-20. Si2p spectra of silicon oxynitride samples subjected to different silane flow ratios of, 15 sccm, 25 sccm, 45 sccm, 60 sccm and 75 sccm.

Figure 4-20 shows the position of the Si 2p peaks components in films deposited using different silane flow ratios. The raw data spectra (purple peaks) are fitted with the aforementioned four components or chemical states: silicon oxide, silicon nitride, silicon -silicon or silicon – hydrogen and some form of silicon-nitrogen-oxygen bonds. These fitted peaks are denoted as A (blue), B (red), C (green) and D (pink) respectively.

In the film with a silane flow of 15 sccm, the blue silicon Si 2p (A) peak, representative of SiO_2, is at a binding energy of 104.18 eV, which is a higher binding energy than the Si_3N_4 red Si 2p peak (B) at 102.18 eV. This is consistent with the more electronegative oxygen atom producing a higher binding energy than for Si-N bonded silicon. The green Si 2p peak (C), shows the Si-Si or Si-H bonds, at around 100.65 eV. These peaks have similar binding energies and are thus difficult to distinguish from XPS data. The pink Si 2p peak (D) at 103.18 eV is suggested to represent some kind of intermediary bonding combination of the silicon, oxygen and nitrogen in the film i.e. O-Si-N.

Figure 4-21 plots the Si 2p peak position at each different silane ratio and illustrates the effect of incorporation of additional Si in the films, as the film constitution changes from predominantly SiO_2, to a more silicon oxynitride-like film. The high-resolution spectra data (purple peaks) of the deposited film with silane flow ratio of 15 sccm has a Si 2p peak centred at 104.06 eV. By increasing silane flow rate to 25 sccm, 45 sccm, 60 sccm and 75 sccm, the peak energies shifted to 104.12 eV, 103.61 eV, 103.48 eV and 103.28 eV respectively (uncertainty of ± 0.2). This figure shows the overall binding energy shifts towards lower binding energies with increasing silane flow ratio.

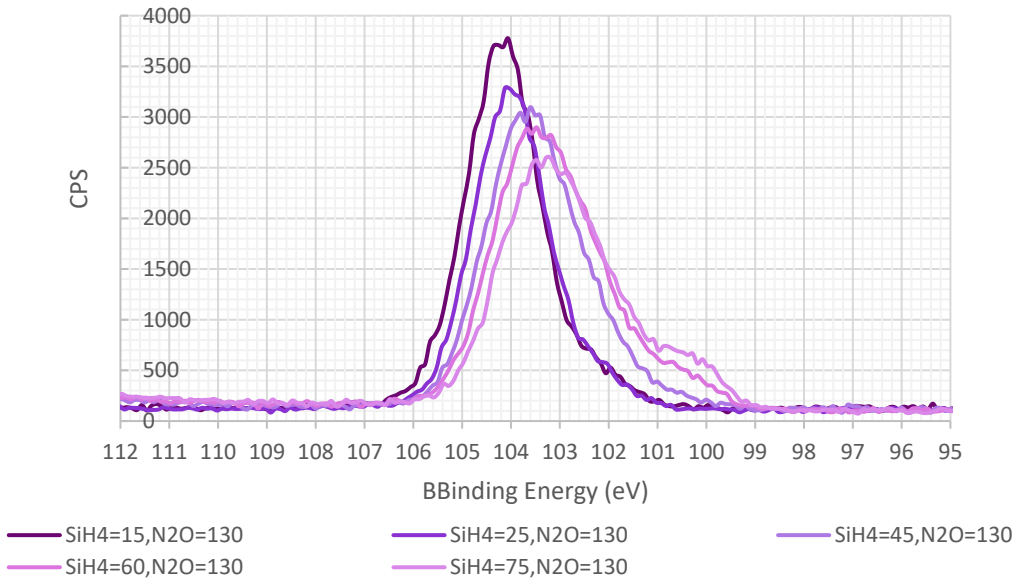

Figure 4-21. Shift in the position of the Si 2p peak in films deposited using different silane flow ratios.

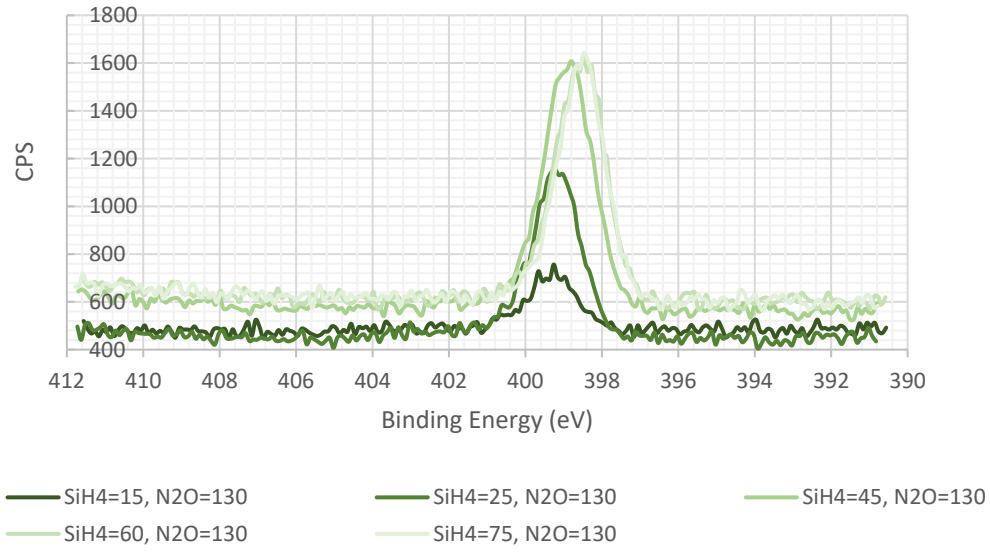

Figure 4-22. High resolution XPS Spectra for N 1s peaks from films deposited using silane flow ratios of 15 sccm to 75 sccm and nitrous oxide flow rate of 130 sccm.

From Figure 4-22 the N 1s peaks related to the silane flow ratios of 15 sccm, 25 sccm, 45 sccm, 60 sccm and 75 sccm, were centred at 399.32 eV, 399.18 eV, 398.88 eV, 398.56 eV and 398.53 eV respectively which were attributed to Si-N bonds. The N 1s peaks shifted by 0.79 eV, which is a similar shift to that see for the Si 2p peak.

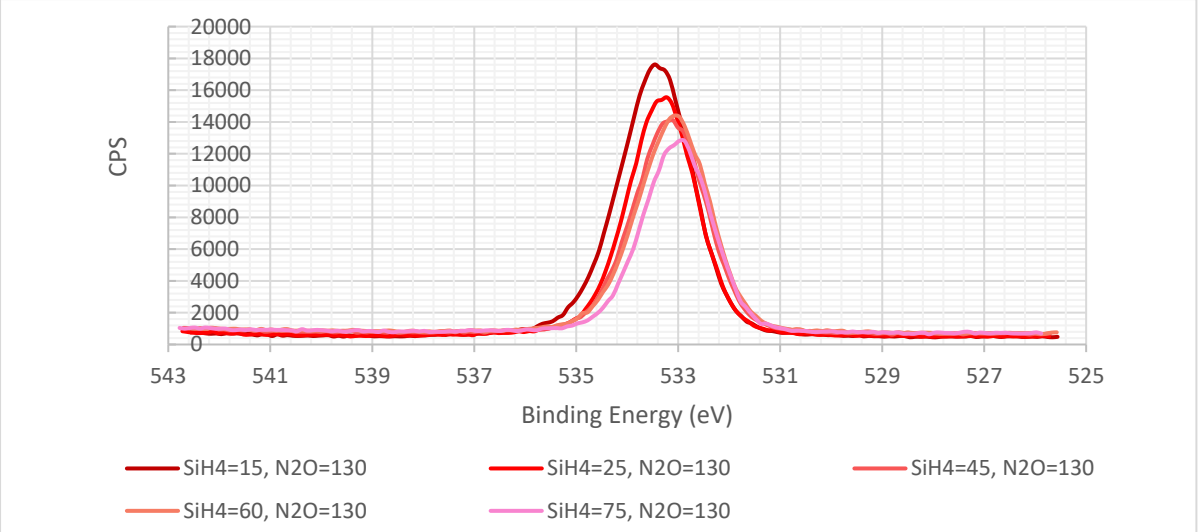

Figure 4-23. High resolution XPS Spectra for O 1s peaks from a film with silane flow ratio of 15 sccm to 75 sccm and nitrous oxide 130 sccm.

The high resolution spectra of the films, corresponding to the O 1s are presented in Figure 4-23. The O 1s peaks were centred at 533.40 eV, 533.31 eV, 533.16 eV, 533.09 eV and 533.02 eV related to the silane flow ratios of 15 sccm 25 sccm, 45 sccm, 60 sccm and 75 sccm respectively. The centre of these peaks shifted by 0.38 eV from the silane 15 sccm to 75 sccm.

Similar data has been recorded for experiments using varying silane flow rates from 15 sccm to 75 sccm but this time, with a fixed N_2O flow rate of 65 sccm.

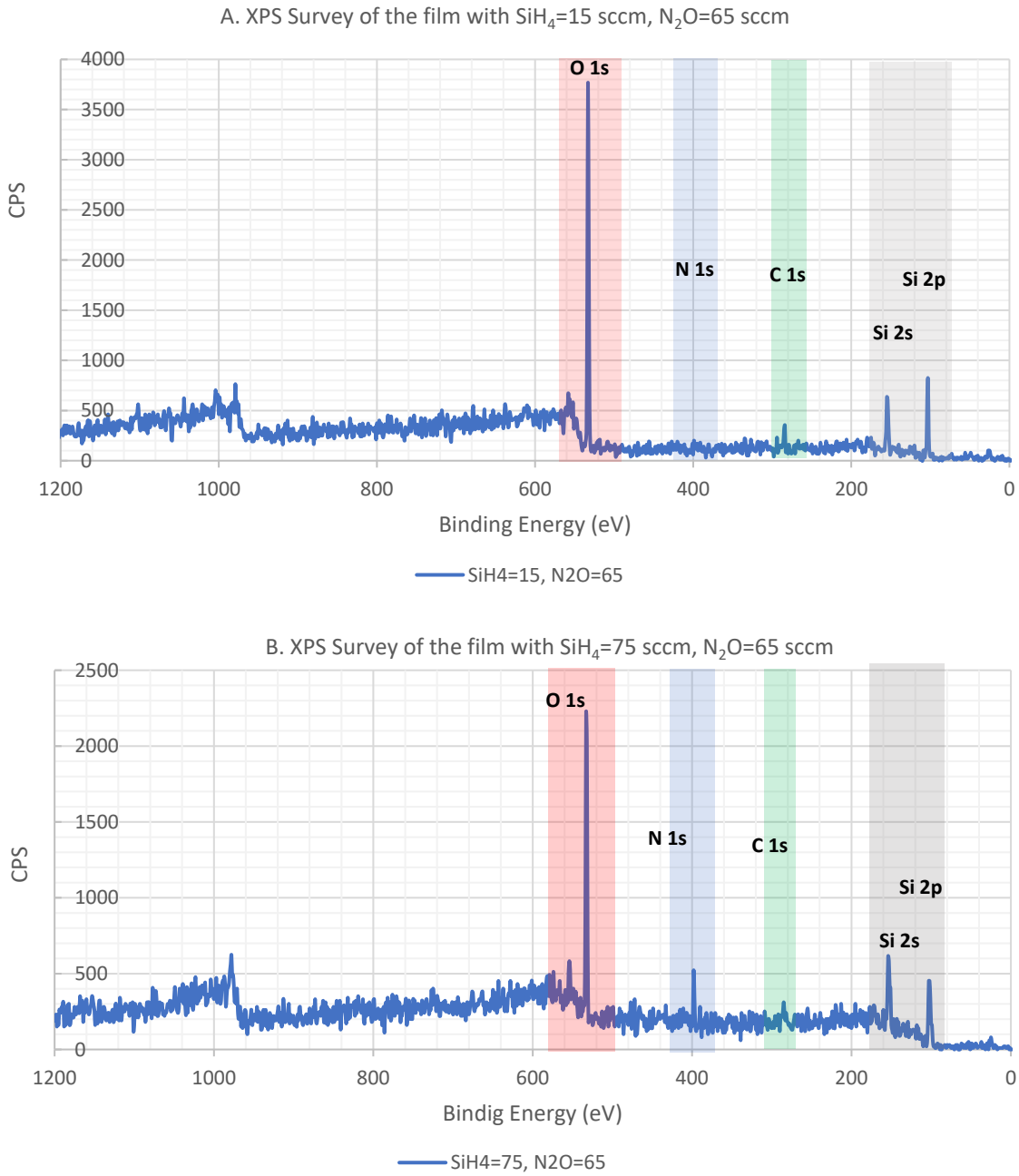

Figure 4-24, XPS full scan spectrum of SiON layer with nitrous oxide of 65 sccm and two different silane flow ratios of A. 15 sccm and B. 75 sccm.

As for the full spectra for the samples prepared using a 130 sccm N_2O flow rate, the N 1s peak is negligible at low silane flow rate (15 sccm), whilst at higher silane ratios, the N 1s peak is clearly visible (see Figure 4-24).

The Si 2p peak changes at each silane flow rate (for the 65 sccm N_2O) are illustrated in Table 9, whilst the corresponding spectral data is shown in Figure 4-25.

Unlike the case where the N_2O flow rate was 130 sccm (Table 8), where there was a clear trend of decreasing binding energy of the Si 2p peak with increasing silane flow rate, when using a N_2O flow rate of 65 sccm no clear trend was observed in terms of the peak binding energies.

Table 9. Binding energies of the Si 2p, N 1s and O 1s and their average atomic percentages of the films deposited with constant N_2O flow at 65 sccm and varied SiH_4 flow ratios of 15 sccm, 25 sccm, 45 sccm, 60 sccm and 75 sccm. (Before etching)

	Si 2p Components - Binding Energy (eV) ± 0.2			
SiH_4 Flow (sccm)	Si 2p A (SiO_2)	Si 2P B (Si_3N_4)	Si 2p C (Si/Si-H)	Si 2p D ($SiON/SiO_xN_y$)
15	103.72	101.72	100.19	102.72
25	103.43	101.43	99.9	102.43
45	103.54	101.54	100.01	102.54
60	103.36	101.36	99.83	102.36
75	103.41	101.41	99.88	102.41

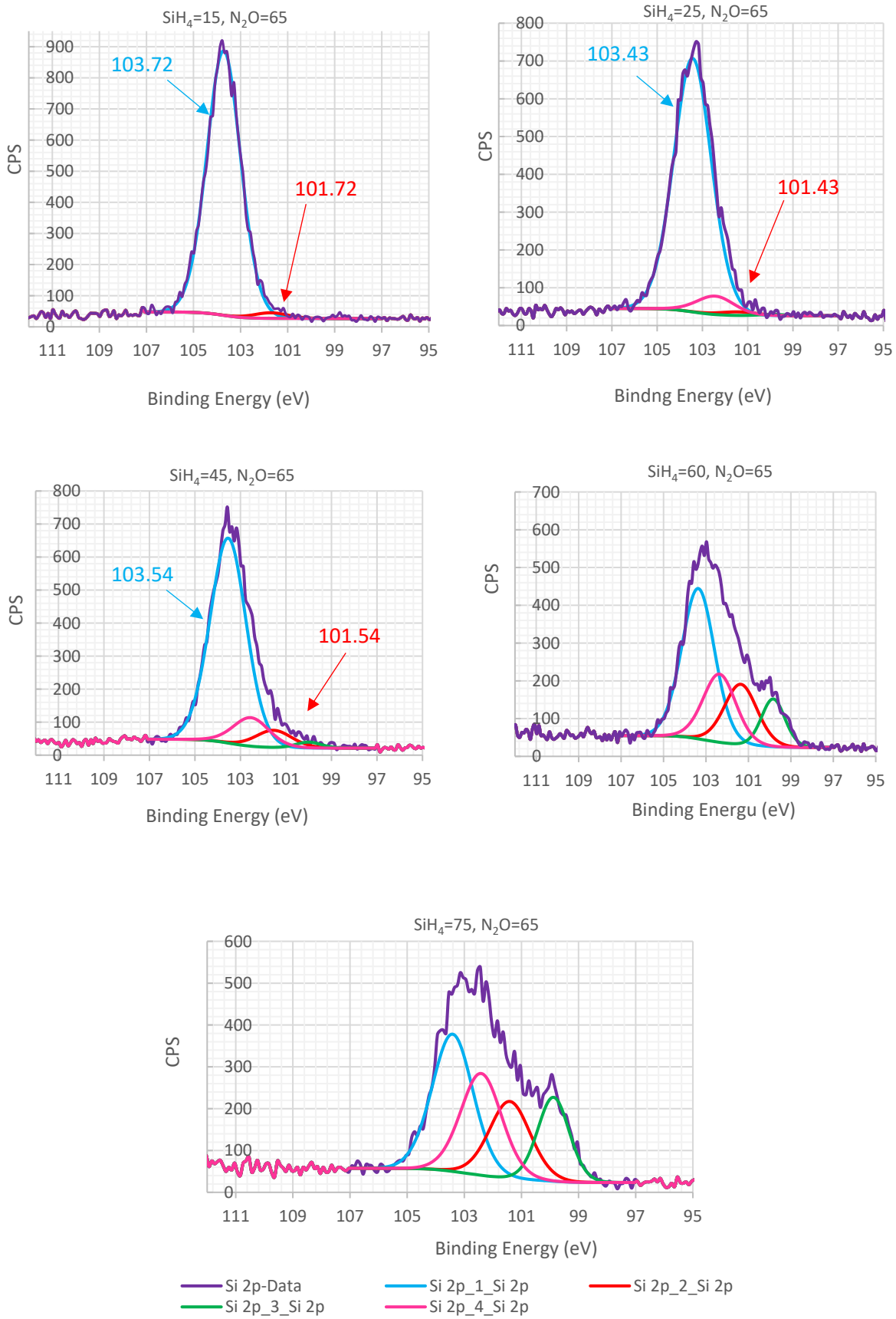

Figure 4-25. Si2p spectra of silicon oxynitride samples subjected to different silane flow ratios of, 15 sccm, 25 sccm, 45 sccm, 60 sccm and 75 sccm.

Figure 4-25 again shows the position of the Si 2p peaks components in films of different silane flow ratios. As for the previously discussed 130 sccm N2O experiments, the blue peak fit represents the silicon 2p peak from the SiO_2 component of the film. Changes in the Si 2p peak with corresponding increases in silane flow rate are related to changes from incorporation of nitrogen and Si into the silicon oxynitride film. The high-resolution data of the deposited films corresponding to Si 2p peak centred at 104.8 eV, is related to the SiO_2. By increasing silane flow rate to 25 sccm, 45 sccm, 60 sccm and 75 sccm, the centres shifted to 104.1 eV, 103.2 eV, 102.8 eV and 102.5 eV respectively. As for the 130 sccm data, increasing the silane flow rate results in the appearance of silicon oxynitride and silicon nitride phases. Interestingly, in the 65 sccm samples at higher silane flow rates (60 and 75 sccm SiH_4), the incorporation of Si-Si or Si-H bonds is significantly increased, compared to the 130 sccm N_2O samples.

Figure 4-26 shows the binding energy shifts to lower energies upon increasing the silane flow ratio. It was also observed that the relative height of the Si 2p peak decreased from 40 CPS to 28 CPS with the increase of the silane flow rate while the peak area increases.

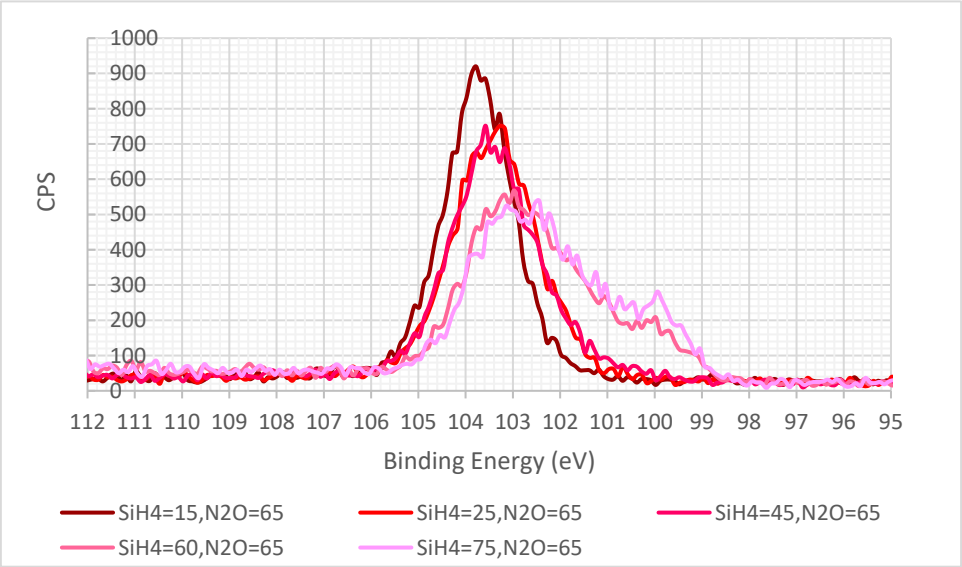

Figure 4-26. Shift in the position of the Si 2p peak in films of different silane flow ratios.

Highlighting the key differences between the films deposited using 65 sccm N_2O compared to those deposited using 130 sccm N_2O, the film compositions are quite similar, but there appears to be slightly higher Si-Si or Si-H bonding ontent in the 65 sccm N_2O films. In fact, there is a more even distribution between SiO_2, Silicon oxynitride, silicon nitride and Si-Si or Si-H

content in this 65 sccm sample compared to the 130 sccm sample – which is mostly SiO_2 and silicon oxynitride (at 75 sccm SiH_4).

This data is of course subject to fitting parameters, where small changes can influence the size of the fitted peaks. The fitted peak data should therefore be viewed in this context.

Considering Figure 4-27 to Figure 4-30, which are scans of the sample surface at three different positions across each sample, it can be seen that the oxygen atomic percentage in Figure 4-27 (silane flow rate of 15 sccm) is nearly double that of silicon. In Figure 4-28, using a higher silane flow rate to 25 sccm, the ratio of oxgen to silicon is decreased and the presence of nitrogen is now clearly detected.

The atomic percentages of the deposited dielectric films in Figure 4-29, where the silane flow rate was increaed to 45 sccm, shows that the Si 2p peak increases further relative to the oxygen atomic percentage ,whilst the nitrogen percentage increases further, relative to lower silane flow rates.

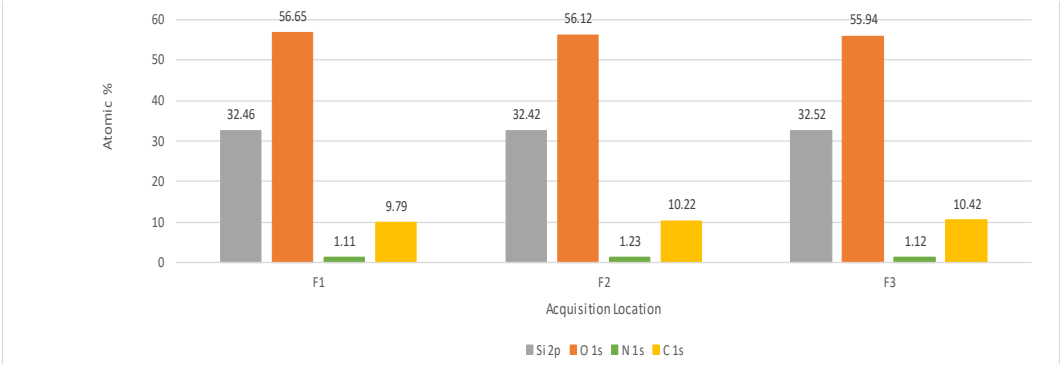

Figure 4-27 XPS data (atomic percentages Si, O, N and C) from three different locations on the sample using SiH_4 15 sccm and N_2O 130sccm. Film thickness is 1 µm.

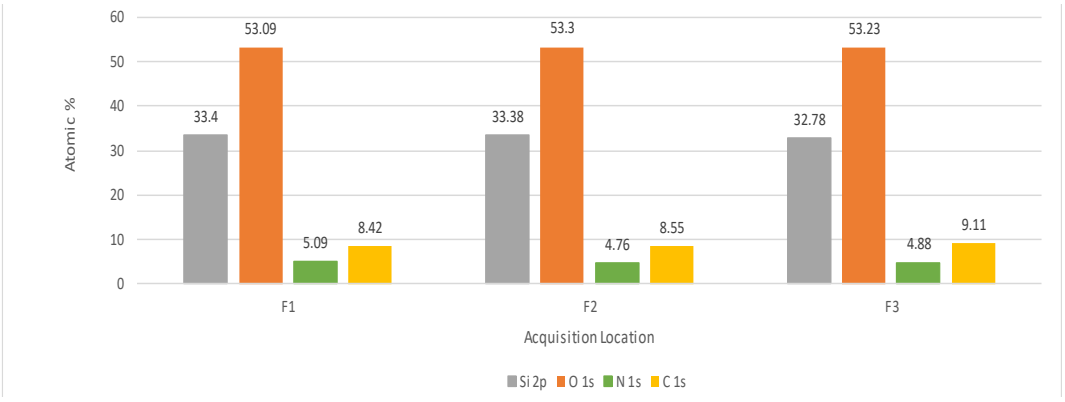

Figure 4-28 XPS data (atomic percentages Si, O, N and C) from three different locations on the sample using SiH_4 25 sccm and N_2O 130sccm. Film thickness is 1 µm.

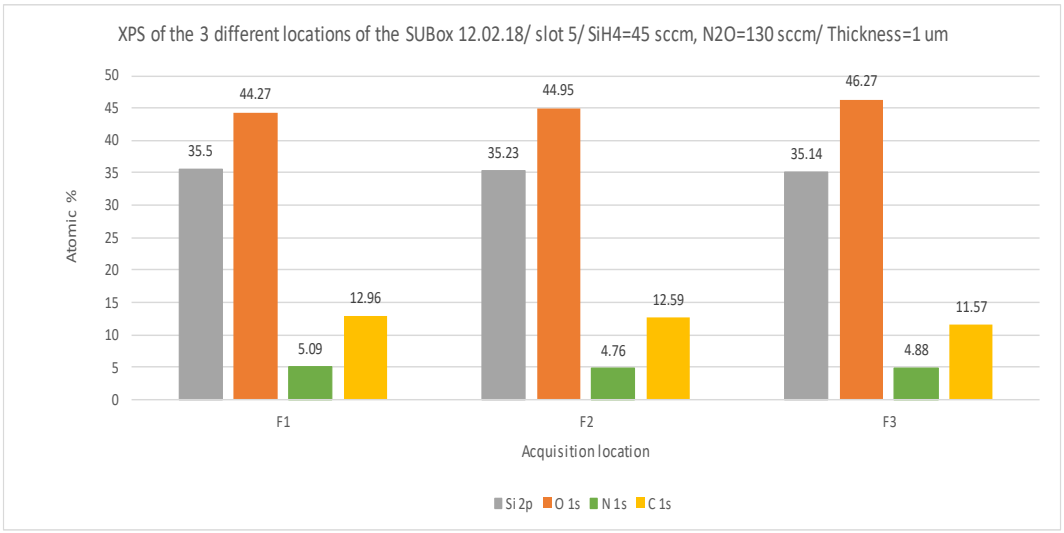

Figure 4-29 Atomic percentages (Si 2p, O1s, N 1s and C 1s) for films deposited using 45 sccm Silane flow rate respectively (before etching). Film thickness is 1 µm.

From Figure 4-30, the average Si : O : N : C ratio of 33 : 57: 1.6: 8.8 was extracted from the XPS data. This average was obtained from three separate scans at different points across the wafer surface. This indicates that the composition of this film, deposited using 15 sccm silane flow rate, is almost exclusively silicon oxide.

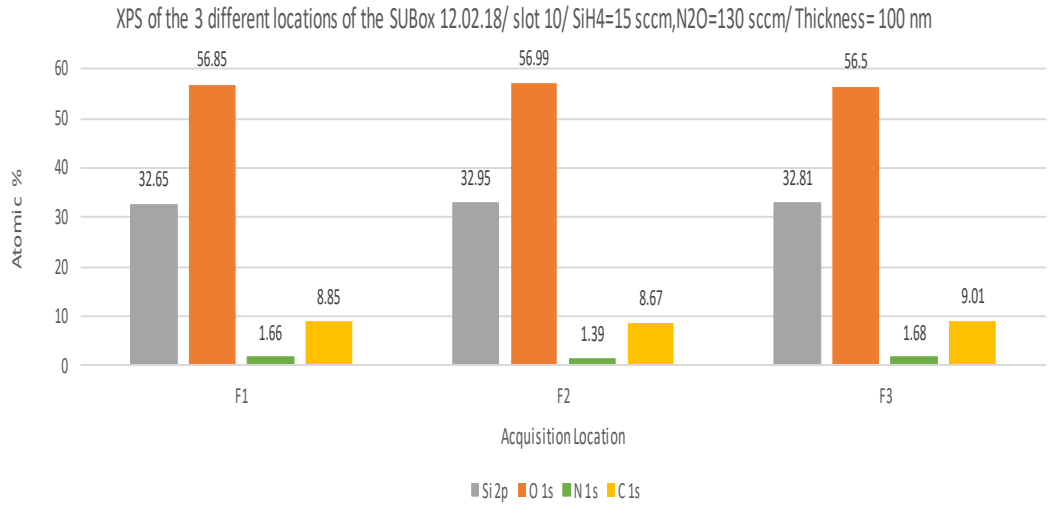

Figure 4-30. Full XPS spectrum of a single 100 nm silicon oxynitride PECVD layer deposited on top of a silicon substrate. The deposition conditions are N2O=130 sccm and SiH4=15 sccm, N2=2000 sccm.

The correlation of the elemental ratio with RI is exemplified by Figure 4-31, where different film thicknesses of 100 nm, 200 nm, 500 nm, 755 nm and 1030 nm with slight differences in elemental composition yield corresponding more marked differences in RI. The most notable difference is for the 100 nm film, where the RI at 1310 nm is higher (1.47) compared to a mean of 1.462 for the other (200 nm, 500 nm, 755 nm and 1030 nm) films.

This RI change from the 100 nm to the 200 nm film correlates with a change in the elemental ratios from O (56.8) : Si (32.8) : N (1.6) : C (8.8) to O (56.1) : Si (32.2) : N (1.4) : C (10.3). These changes are illustrated in Figure 4-31 for the 100 nm, 200 nm, 1030 nm films. The difference in elemental composition between the 200 nm film and the 1030nm film is minor, with similarly minor differences in RI.

Comparing the 100 nm and 200 nm films, both the O and Si ratios decrease in the thicker film, whilst the N content increases. This is expected, as thicker films are more representative of the PECVD deposition conditions and more uniform. The C ratio of the 100 nm film is also higher than in thicker films. Again, this might be expected as the thinner film incorporates more surface hydrocarbons, whereas this is less pronounced in thicker films.

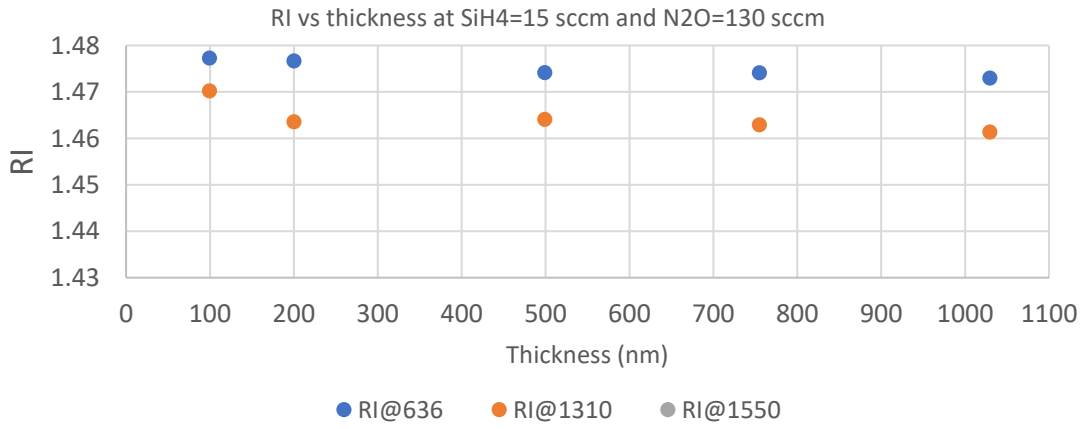

Figure 4-31 Variation in RI (at different wavelengths 636 nm, 1310 nm and 1550 nm) at different silicon oxynitride film thicknesses 100nm, 200nm, 500nm, 750nm and 1030nm.

Despite changes in the elemental composition of O, Si, N and C, the change in RI is believed to be primarily influenced by the change in the nitrogen content (Figure 4-32) [55] [20].

Other than for the 100 nm film, the RI, composition and deposition rate are fairly uniform for thicker films. However, this change is compensated for by a slight increase in silicon and nitrogen contents (see Figure 4-32).

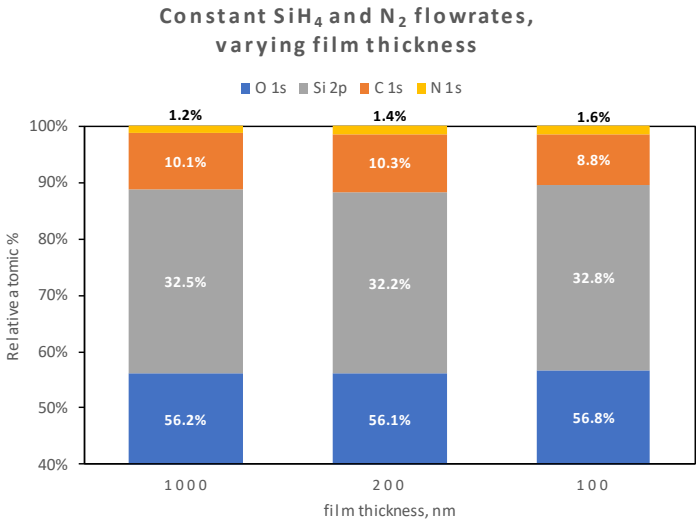

Figure 4-32. O : Si : N and C ratios for different silicon oxynitride 100 nm, 200 nm and 1030 nm films.

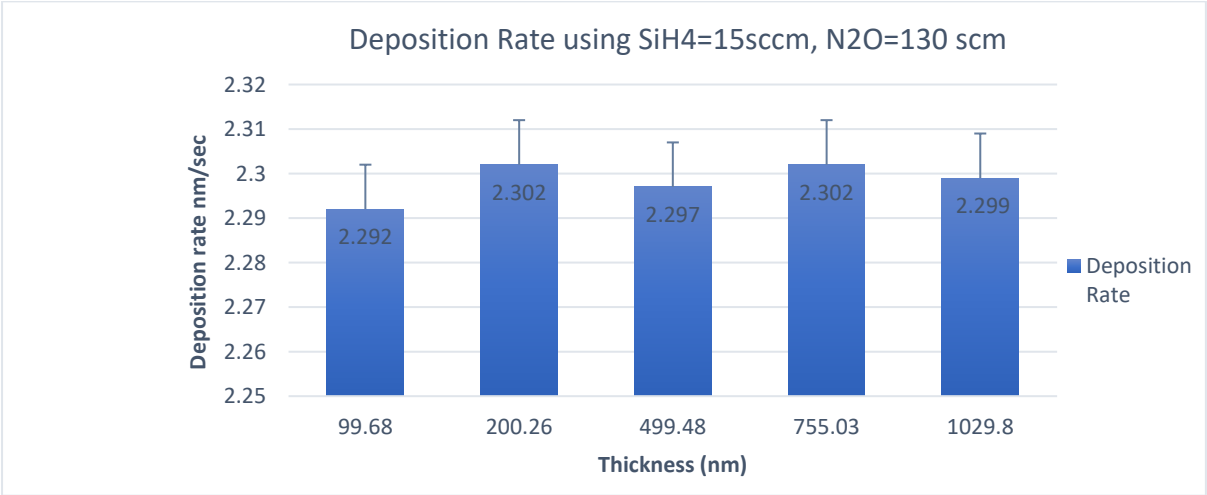

Figure 4-33. Deposition rate for different thickness silicon oxynitride (100 nm, 200 nm, 500 nm,1030 nm) films.

Figure 4-33 shows that the deposition rate, though slightly lower for the 100 nm film, is fairly uniform for the thicker films. This suggests that films of greater than 100 nm thickness are consistent in terms of both their composition and optical properties.

The XPS data discussed so far was taken from the surface of deposited films. These surfaces inherently have a high carbon content – due to hydrocarbon surface contamination. Therefore, experiments have also been performed on samples after depth profile etching (etched using an argon gun). These samples would be expected to have a lower C 1s peak due to the removal of surface contaminants during the etch process.

XPS spectra have also been recorded after depth profiling through the silicon oxynitride films for 35 mins using argon sputtering. Most notable is the decrease in the C 1s peak intensity for depth profiled XPS scans. This is expected, as hydrocarbon surface contamination is more abundant on the surface and is significantly reduced in the depth profiled samples.

Figure 4-34 (A) and (B) illustrate the relative atomic percentage of the O, Si, N and C elements using different silane flow ratios at before and after 35 minutes etching, respectively. This etch duration removes approximately 50 nm of film thickness.

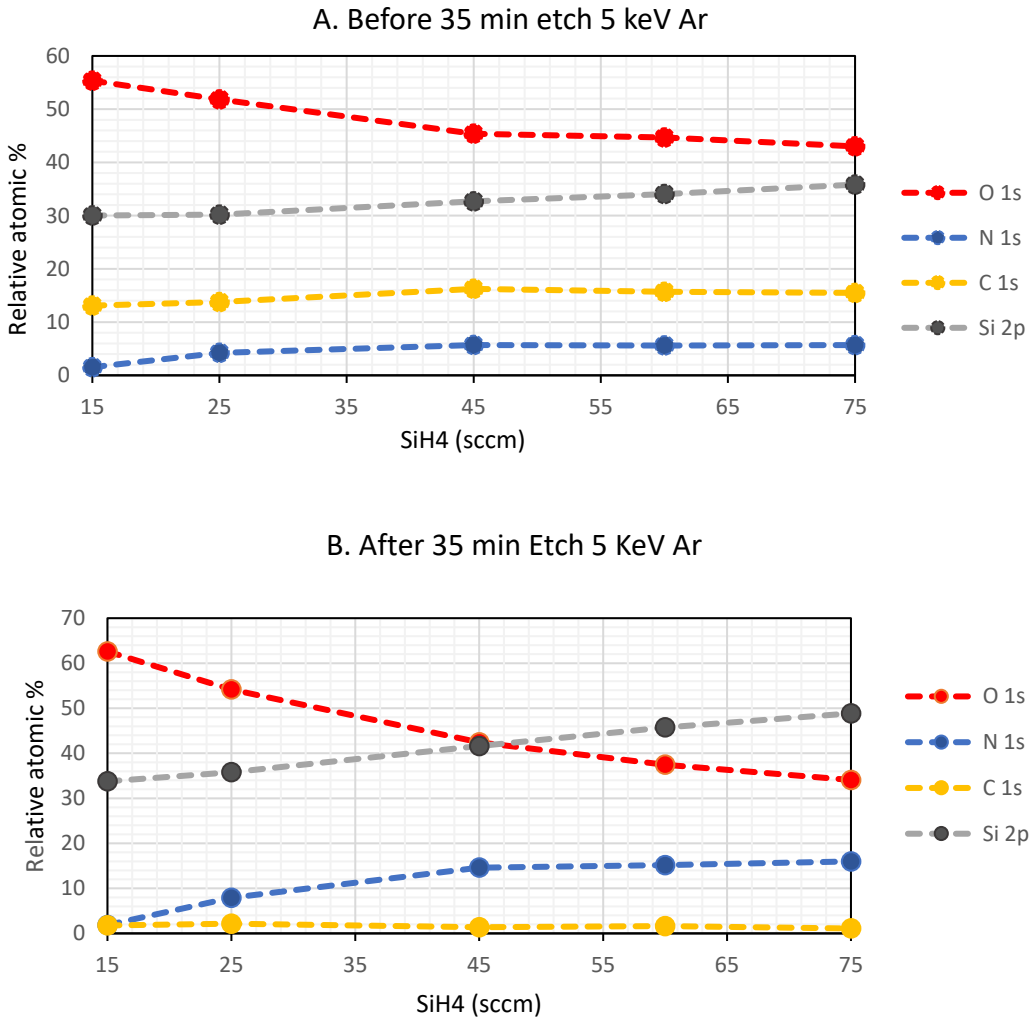

Figure 4-34 (A). before and (B) after 35 minutes etching, XPS comparative data silicon oxynitride films deposited using different silane (SiH_4) ratios. Changes in the Si 2p, C 1s, O 1s and N 1s peak intensities are plotted for each silane ratio in a depth profiled sample.

In these films, the O 1s oxygen atom concentration decreased, and the silicon Si 2p and nitrogen N 1s atom concentrations increased with the silane flow rate. The oxygen atomic concentration was higher than 50%, the silicon concentration was 30% to 50% and the nitrogen atom concentration was lower than 20%.

Figure 4-35 (A) and B shows the elemental ratios of the silicon to nitrogen and oxygen at before and after etching. There is a sudden and large decrease in Si/N from silane 15 sccm to silane 25 sccm in both before and after 35 minutes etching. A slightly increase of the Si/O observed in both before and after etching in the A and B graphs.

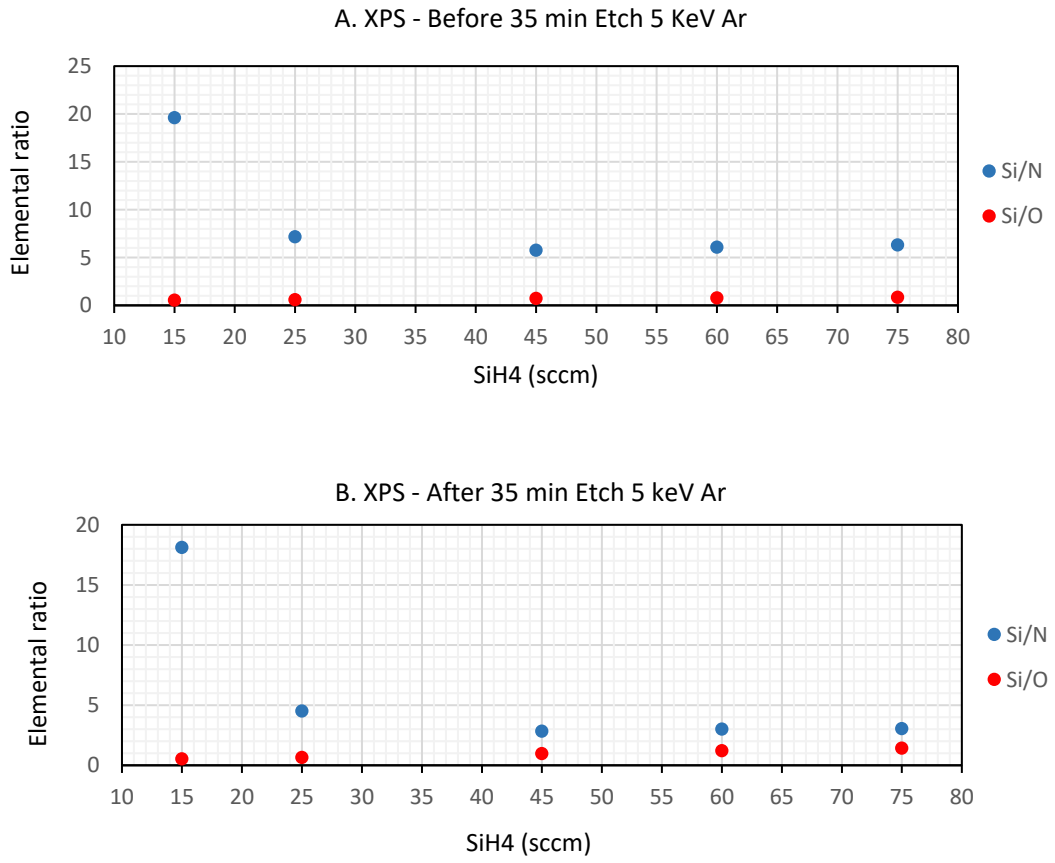

Figure 4-35. The elemental ratios of the Si/N and Si/O in (A) before and in (B) after 35 minutes etching.

At low silane concentrations the N 1s content is low. This is related to silicon bonding preferentially with oxygen. The preference for silicon – oxygen bond formation is related to the lower bond energy of N-O (201 KJ/mol) (or N=O (607 KJ/mol)) to the N=N (945 KJ/mol), the much stronger bond energy for formation of an Si-O bond (800 KJ/mol) relative to

formation of an Si-N bond (437 KJ/mol) and is also influenced by the higher electronegativity of oxygen (X_O =3.44) compared to nitrogen (X_N = 3.04) [56]. Table 10 compares the bond energies for all the relevant bonds of the precursor gases (SiH_4, N_2O and N_2) and the silicon oxynitride products. The N 1s content plateaus at silane concentrations of 45 sccm and over. Changes in the O 1s content are almost inversely proportional to the change in the N 1s peaks. The C 1s peaks are of relatively low intensity and do not vary significantly with silane concentration.

Table 10. Strength of chemical bonds occurring during plasma deposition of SiON.

Chemical bonds	Bond strengths (KJ/mol)
Si – O	800
Si – N	437
Si – Si	325
Si – H	299
N – H	339
O – H	427
O=O	498
N=N	945
N=O	607
N-O	201

As the silane ratio increases, the amount of N incorporated into the silicon oxynitride layer also increases. This is suggested to be related to the increased capacity of silicon for bond formation at the higher silane concentrations. In this situation, there is insufficient oxygen (from the N_2O) to bond to and therefore the excess silicon will form bonds to nitrogen instead. In addition to formation of Si-N bonds, Si-Si and Si-H bonds may also be formed at high silane concentrations. This occurs when the nitrogen concentration plateaus, the oxygen concentration is insufficient, and the silane concentration is still increasing. Hence the likelihood of Si-Si bond formation under these process conditions is increased. This is evidenced by the higher RI when using higher silane concentrations.

4.1.5 Elemental composition of silicon oxynitride films, determined using EDX

Like XPS, EDX can yield information on the elemental composition of the deposited films. A typical EDX spectrum and the data of the silicon oxynitride film is shown in Figure 4-36. The EDX data follows a similar trend to the XPS data, with low nitrogen content at lower silane concentrations, increasing N 1s as the silane content increases to 45 sccm and then plateauing from 45 sccm to 135 sccm. EDX data taken at different accelerating voltages (Figure 4-39) shows a very similar trend, indicating that the film composition at the surface is similar to that in the bulk oxynitride.

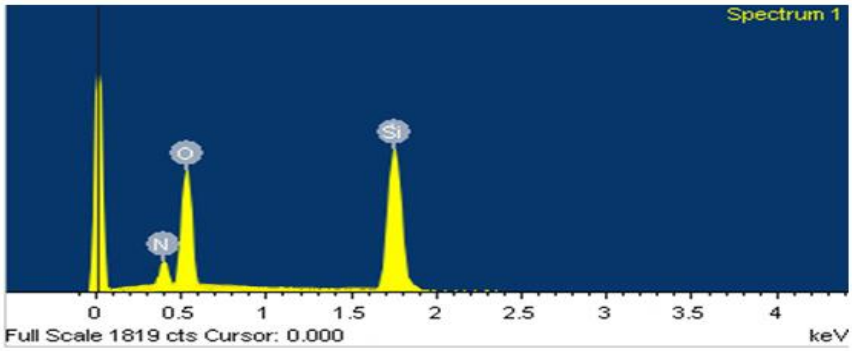

Figure 4-36. The EDX spectrum of the silicon oxynitride and accelerating voltage of 5 keV.

Whilst XPS examines the 10 nm at the surface of the material, EDX can penetrate deeper into the material (depending on the voltage applied). In this work, the applied voltages used were varied from 3 to 20 kV to investigate films of up to 1000 nm.

As the accelerating voltage is increased, the X-rays penetrate deeper into the film. At higher accelerating voltages, the silicon peak increases due to signal being picked up from the silicon substrate – in addition to the oxynitride film itself. According to Moseley's law [57], the energy of the characteristic radiation within a given series of lines varies with atomic number. For silicon, with atomic number of 14, the binding energy of the Kα shell electrons, is about 1.74 keV. Therefore, the incoming beam energy for ionisation must be greater than this corresponding X-ray emission line energy. But at accelerating voltages of 2 kV, silicon did not appear in the EDX spectra, only oxygen, nitrogen and some carbon at low intensities were been detected. The reason for this is that the binding energy of the Kα shell electrons in silicon atoms, is about 1.74 keV, and the incoming beam energy for ionisation must be greater than

the corresponding X-ray emission line energy. Being unable to detect the silicon Kα line at 2 kV suggests that the detector is not providing the exact value of 2 KeV. Figure 4-37 shows that by measuring the energy of a given K, L or M spectra line, the atomic number of the element producing that line can be determined.

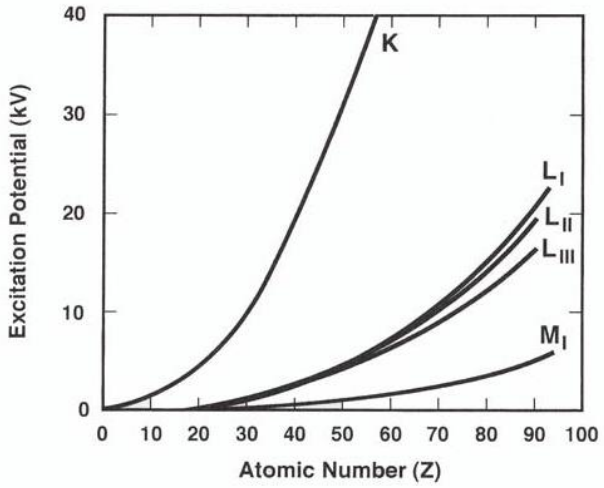

Figure 4-37. Moseley's law which shows the energy of the characteristic radiation within a given series of lines varies monotonically with atomic number. For silicon with atomic number of 14, only the Kα spectra line with 1.74 KeV will be appear. Reproduced from; Energy Dispersive Spectroscopy on the SEM: A Primer, Bob Hafner

For this reason, data at an accelerating voltage of 5kV was selected [58] [59] as a representative voltage to acquire XPS data – as all peaks (Si, O and N) are clearly present using this voltage, and the resulting data predominantly relates to the oxynitride film rather than from a combination of the oxynitride film plus the silicon substrate.

Figure 4-38 shows the variation in elemental composition of silicon oxynitride films as a function of increasing silane concentration (using 5 kV accelerating voltage). It indicates the deceasing oxygen and increasing silicon and nitrogen content in the films.

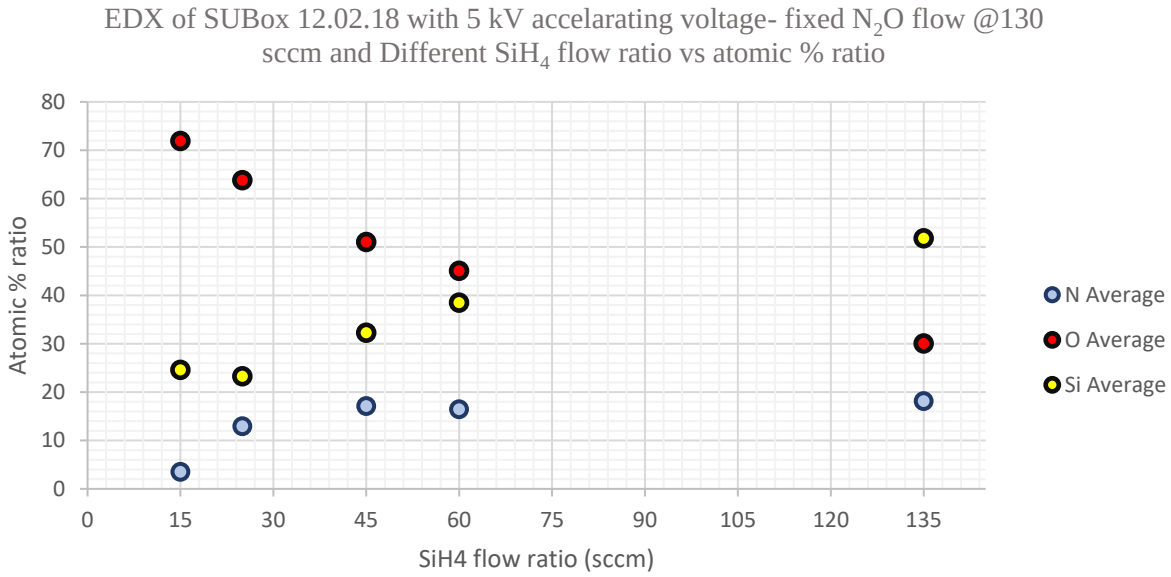

Figure 4-38. Variation in elemental composition of silicon oxynitride films as a function of increasing silane concentration.

Figure 4-39 is based on averaged accelerating voltage from 3 to 20 KV with standard deviation in each film. This graph shows a similar elemental composition to the 5kV data and also shows a similar trend to the XPS results in Figure 4-34 (B) after 35 minutes etching.

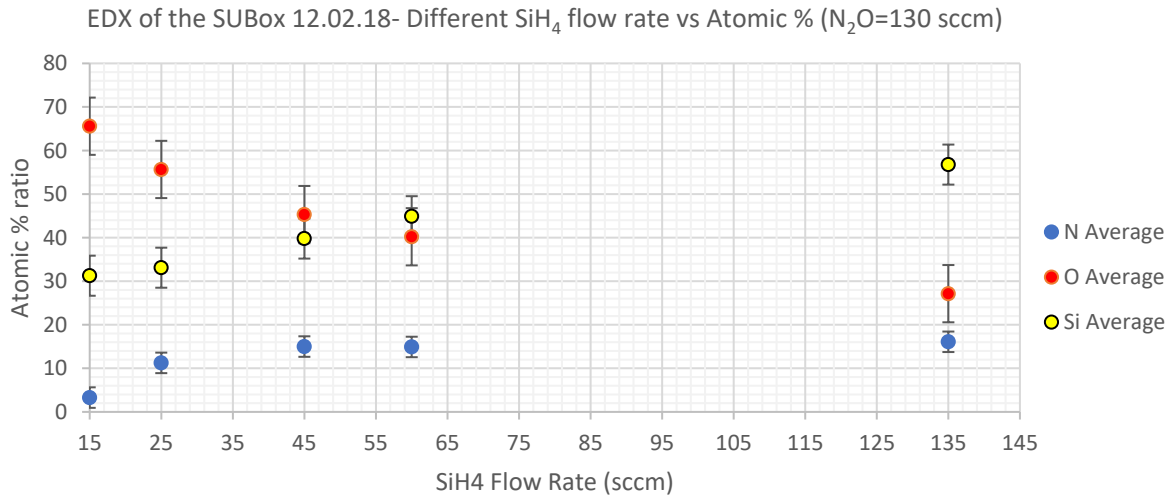

Figure 4-39. Variation in elemental composition of silicon oxynitride films as a function of increasing silane concentration. Data is the average from using the accelerating voltages (3, 5, 7, 10, 15 and 20 kV).

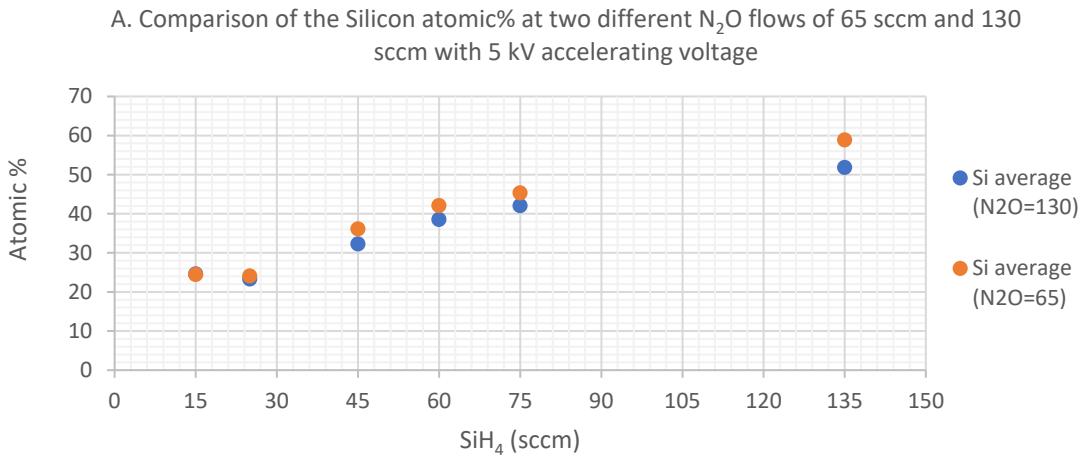

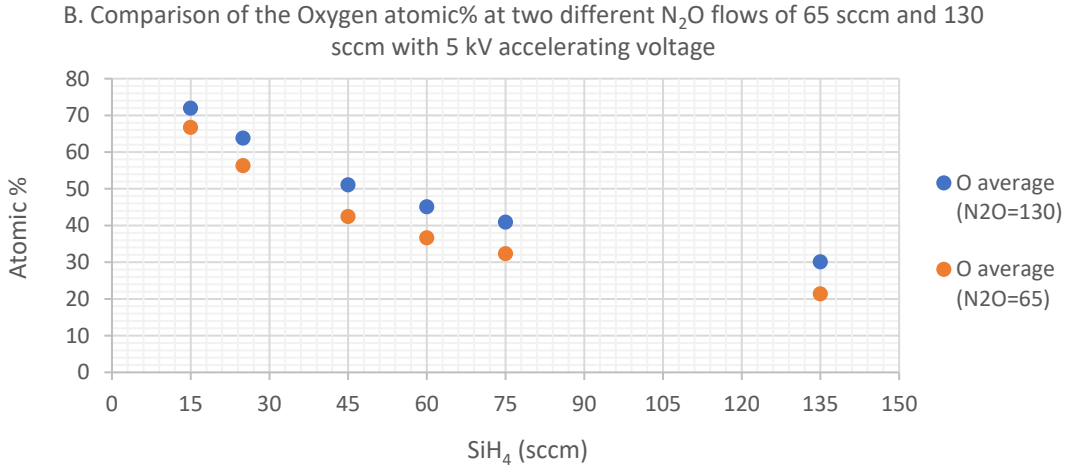

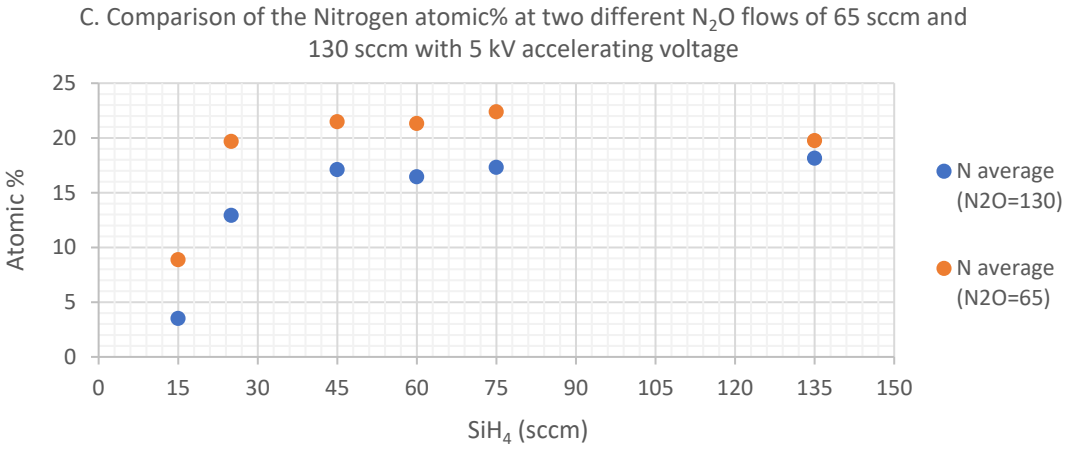

Figure 4-40. A, B and C represent the comparison between the atomic percentage of the Silicon, Oxygen and Nitrogen elements respectively, in the deposited films at two different N_2O flow ratios of 65 sccm and 130 sccm while varying the SiH_4 flow from 15 sccm to 135 sccm at accelerating voltage of 5 KV.

The atomic percentages of the silicon, oxygen and nitrogen elements in the two different deposited films with N_2O flow of 65 sccm and 130 sccm, are compared together in Figure 4-40 (A),(B) and (C) respectively.

In Figure 4-40 (A), the silicon atomic percentage increases from around 20% to 60% with increasing silane flow rate from 15 to 135 sccm. The silicon atomic percentage is lower when using higher N_2O flow ratios. Figure 4-40 (B), compares the oxygen atomic percentage in these two films, where as expected, more oxygen is incorporated in the films deposited using higher N_2O flow ratios. An increase in the nitrogen atomic percentage at the lower N_2O flow ratio of 65 sccm, is observed in Figure 4-40 (C).

The refractive index at wavelength 1550 nm is compared with atomic percentage of the silicon, oxygen and nitrogen elements of the film which have been deposited at N_2O flow ratio of the 65 sccm and varied SiH4 flows from 15 sccm to 75 sccm. The result is illustrated in Figure 4-41 (A), (B) and (C).

In Figure 4-41 (A), the effect of increasing of the silane flow ratio is to increase the silicon atomic percentage in the films and to increase the refractive index.

Figure 4-41 (B), shows the inverse relationship of increasing the silane flow ratio on incorporating of the oxygen element in the silicon oxynitride films, resulting in a decreasing refractive index.

The result of increasing the silane flow ratio on the nitrogen atomic composition and refractive index of the films is presented in Figure 4-41 (C). Incorporating more nitrogen is accompanied by increasing the refractive index of the films.

Similar trends were observed for the silicon oxynitride films deposited using a nitrous oxide flow rate of 130 sccm which is not shown in this thesis.

At high silane ratios the RI is over 2, which suggests a silicon rich oxynitride with a greater density of Si-Si bonds.

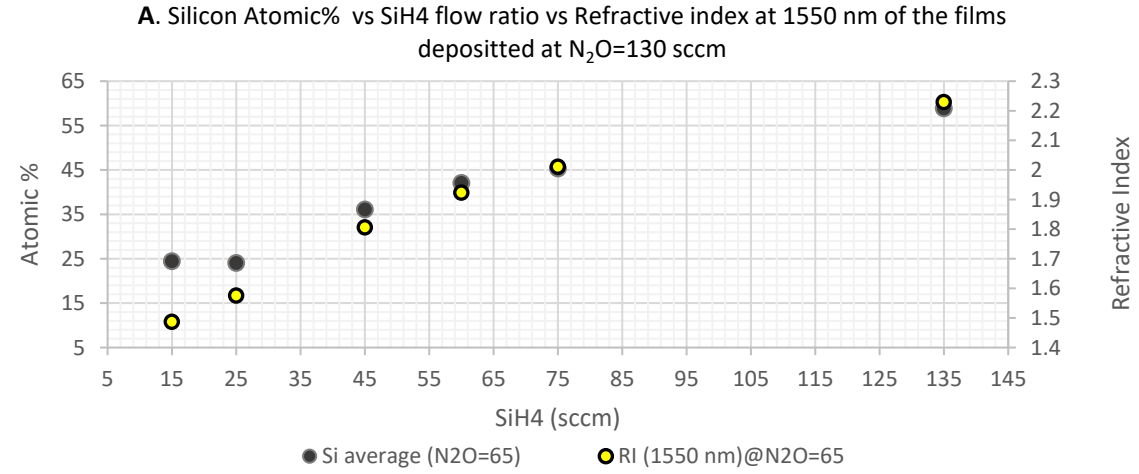

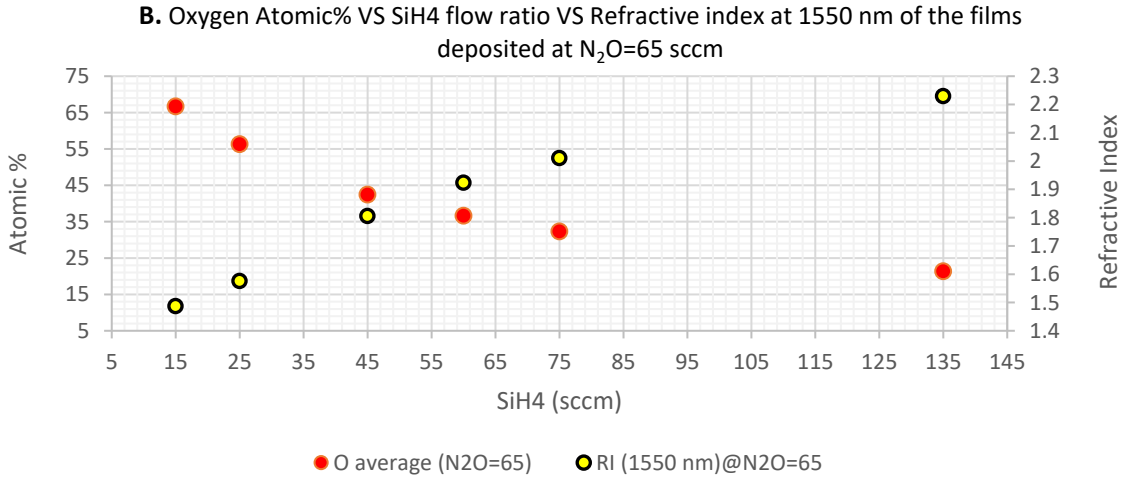

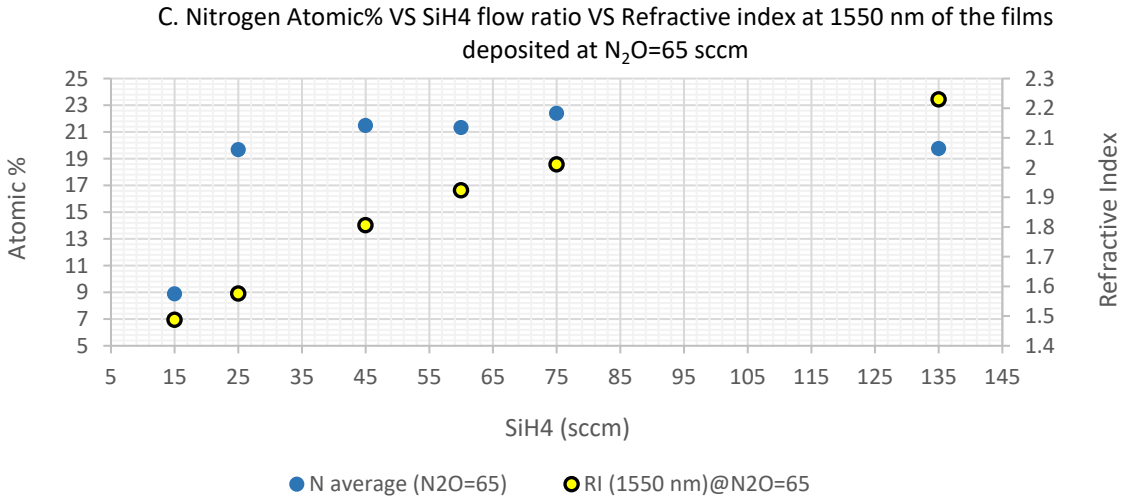

Figure 4-41. A, B and C shows the effects of increasing the silane flow ratio on the incorporating of the three silicon, oxygen and nitrogen elements respectively, in the films and their following effects on the films refractive index.

4.1.6 Fourier-Transform Infrared spectroscopy (FTIR)

In order to analyse the infra-red absorption of thin film silicon oxynitrides, samples were prepared on both silicon and undoped germanium substrates. Germanium was used as a substrate for FTIR spectroscopy, because compared to silicon, it has very few absorption features in its spectrum between 500 and 5000 cm^{-1} (20 - 2 μm) [60]. This enables much clearer identification of absorption bands related to the silicon oxynitride films, compared to spectra from thin films on silicon substrates. Figure 4-42 shows a comparison of the FTIR transmittance spectra of the relatively featureless Germanium substrate contrasted to a Silicon substrate.

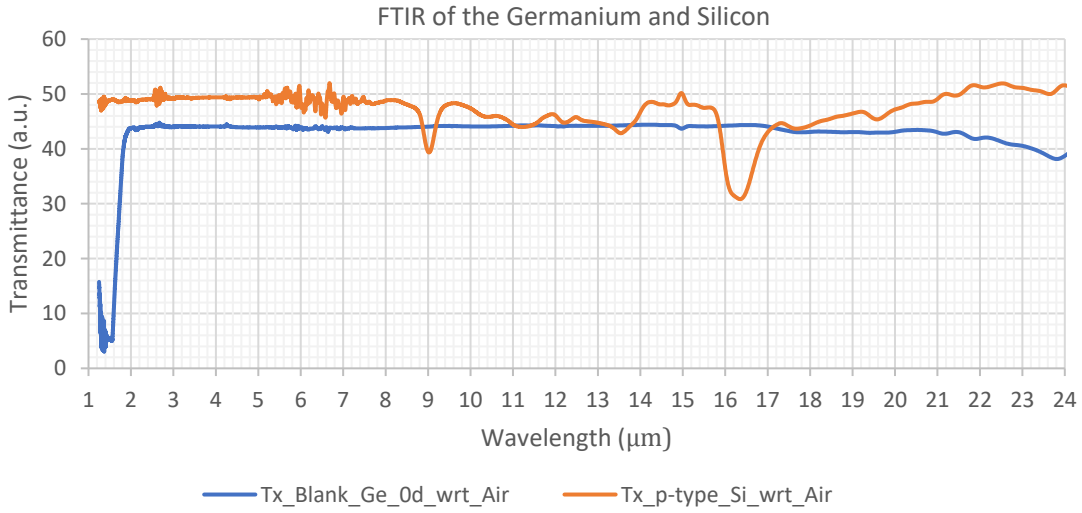

Figure 4-42 Comparison of Germanium and Silicon transmittance FTIR spectra.

During deposition of thin dielectric films, the germanium substrates were placed on a silicon wafer (Figure 4-43 and Figure 4-44). Thus, films were deposited on both Ge and Si substrates at the same time and hence using identical deposition conditions. Thus, film thickness and RI could be compared for films deposited on both the silicon and germanium substrates.

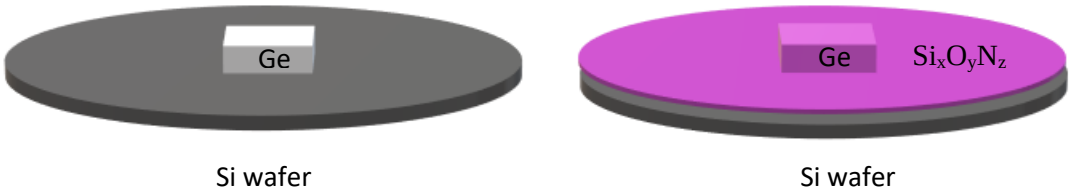

Figure 4-43. Schematic of Ge pieces supported on silicon wafer substrates and subsequent deposition of $Si_xO_yN_z$ film on both the Ge and silicon.

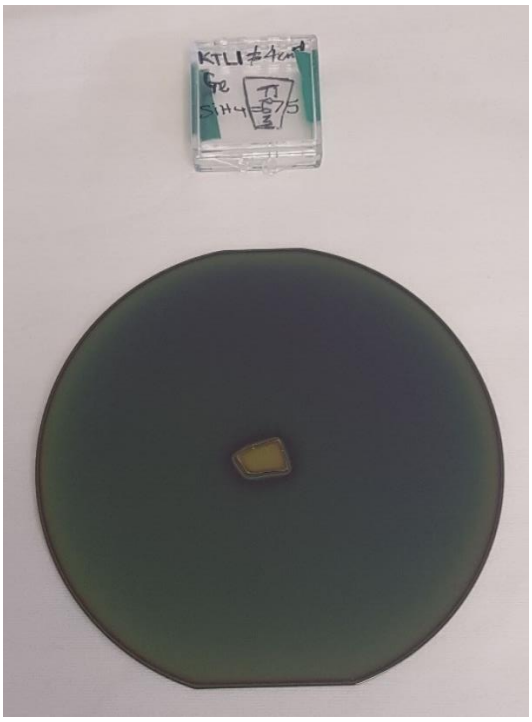

Figure 4-44. A Germanium sample placed on the silicon wafer after depositing a layer of silicon oxynitride film.

Silicon oxynitride films were deposited on top of both the Ge sample and the supporting silicon wafer substrate. Deposition conditions used constant flows of N_2 (2700 sccm) and N_2O (65sccm) in combination with different silane flow rates ranging from 15 sccm to 75 sccm. The RI of the deposited silicon oxynitride layers on the germanium substrates, is plotted in Figure 4-45 as a function of varying flow silane rate. Refractive index was measured at 636 nm, 1310 nm and 1550 nm. The RI at 636 nm is slightly higher than that at 1310 nm and 1550 nm due to normal dispersion which describes the refractive index dependence of wavelength where the index increases with increasing optical frequency and occurs for most transparent media in the

visible spectral regions where the light absorption is less. The refractive index tends to decrease with increasing wavelength to 1310 and 1550 nm.

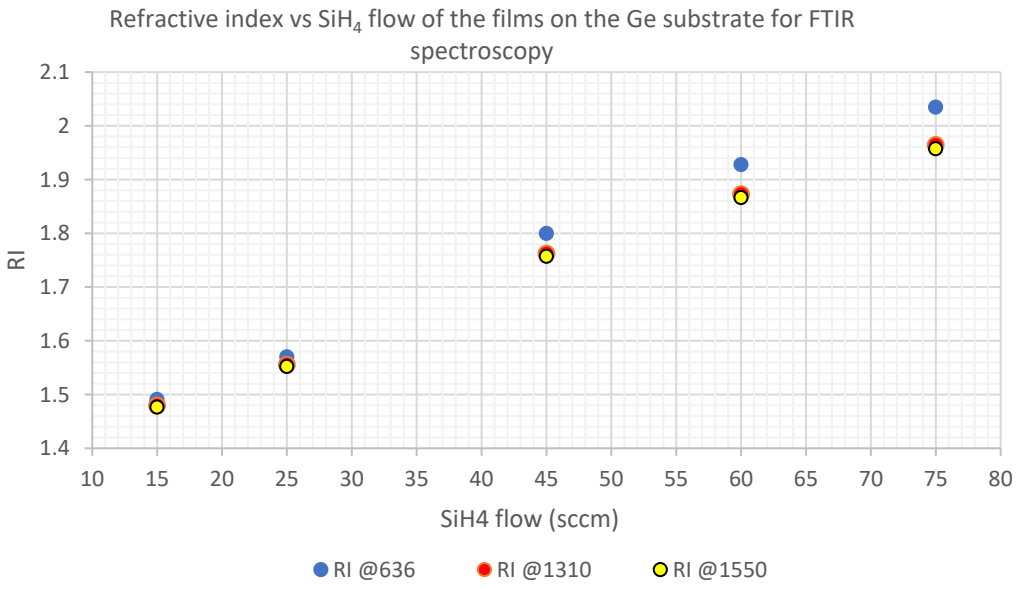

Figure 4-45. RI plotted as a function of silane flow rate, measured at 636 nm, 1310 nm and 1550 nm

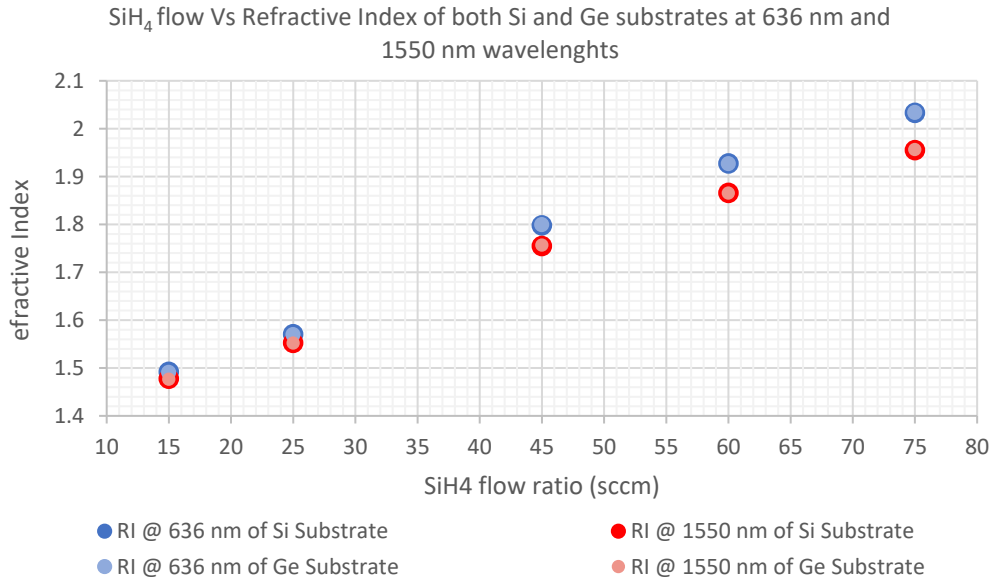

Figure 4-46. RI plotted as a function of silane flow rate, measured at 636 nm, 1310 nm and 1550 nm.

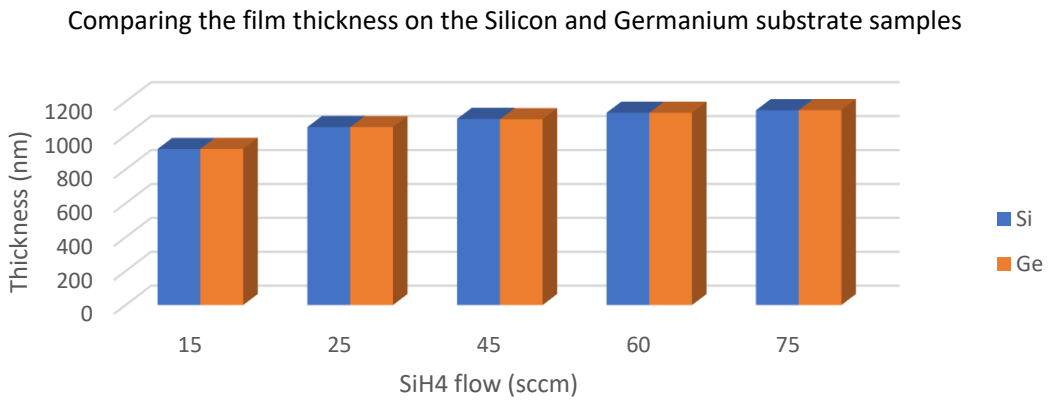

Figure 4-47. Silicon oxynitride film thickness as a function of silane flow rate on Ge and silicon substrates.

The RI varies from 1.5 at low silane flow rates (15 sccm) to 1.95 (1310 nm and 1550) and 2.02 (636 nm) using a silane flow rate of 75 sccm. The composition of the silicon oxynitride film varies with silane flow rate, with higher silane flow rates yielding denser silicon rich oxynitrides – as indicated by XPS and EDX results. The denser films have higher RI due to their greater difference between the speed of light in the denser film relative to the speed of light in air.

The layer refractive indices and thickness of deposited oxynitride films has also been monitored on both the germanium and the silicon substrates (Figure 4-46 and Figure 4-47). The deposited films have very similar refractive indices (at 636, 1310 and 1550 nm wavelength) and thicknesses on both substrates. The film thickness was optimised to deposit films of 1000 nm thickness for this experiment. Further optimisation could be performed to refine the thickness control - especially at lower silane flow rates of 15 sccm, where the film thickness was only around 800nm. Theoretically, the film thickness should have no effect on the RI. However, in practice, the film thickness does have a minor effect on RI, as the composition of the films change slightly between thinner and thicker films. This is related to the deposition conditions where, due to required chamber stabilisation times, deposited thin films have a slightly more variable composition than thicker films.

The similarity of the FTIR data from films deposited on both silicon and germanium substrates, indicates that the deposited films on the different substrates are very similar and that FTIR measurements on both substrates are reliable. The data is also consistent with both XPS and EDX data.

The Ge substrate has few features over the measured spectral range from 2 to 24 μm (5000 to 416.67 cm^{-1}) (see Figure 4-48). Indeed, the features in the spectrum at 4.25 to 15 μm (2352.94 to 666.67 cm^{-1}) are due to atmospheric CO_2 absorption and the features at 2.56 to 2.94 μm (3906.25 to 3401.36 cm^{-1}) and 5.41 to 7.41 μm (1848.43 to 1349.53 cm^{-1}) are related to atmospheric H_2O absorption. These futures are magnified in Figure 4-48 for clarity.

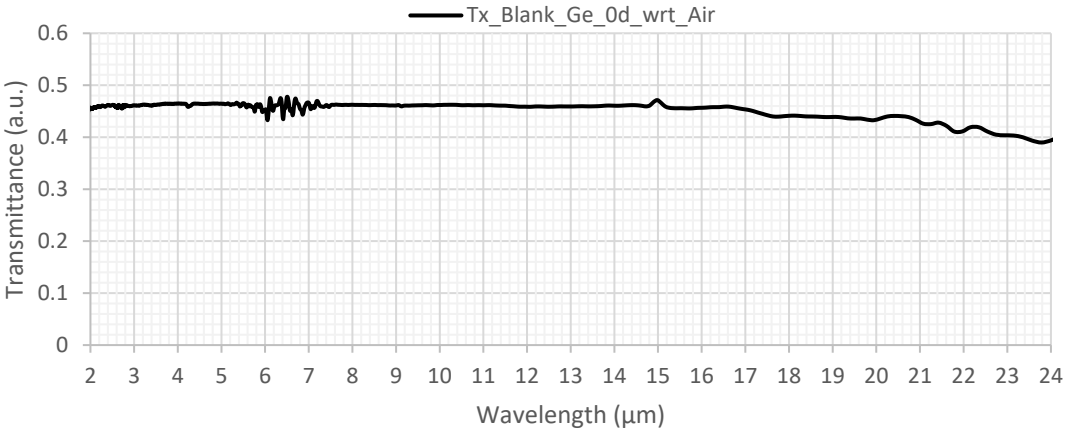

Figure 4-48. Magnified futures in FTIR spectra of an undoped Ge substrate. The futures at 4.25 and 15 μm are due to atmospheric CO_2 absorption and the futures at 2.56 to 2.94 μm and 5.41 to 7.41 are related to atmospheric H_2O absorption.

Figure 4-49 shows the FTIR spectra of silicon oxynitride films deposited on undoped Ge substrates with varying silane flow rates. Spectra overlap, so in Figure 4-50 the spectra have been artificially offset with respect to the y-axis, in order to display the FTIR data more clearly. The FTIR spectrum of the Ge substrate is also shown for reference (black).

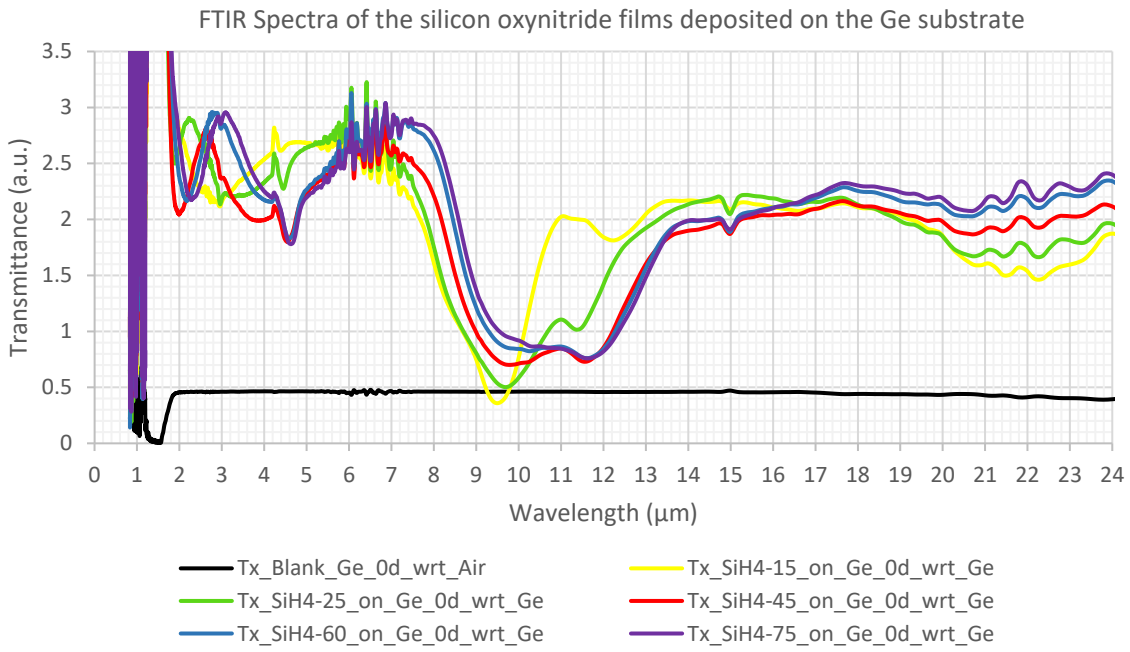

Figure 4-49. Overlap spectra of the silicon oxynitride films deposited at constant N2O flow ratio of 65 sccm and different SiH4 flow ratios of 15 sccm, 25 sccm, 45 sccm, 60 sccm and 75 sccm.

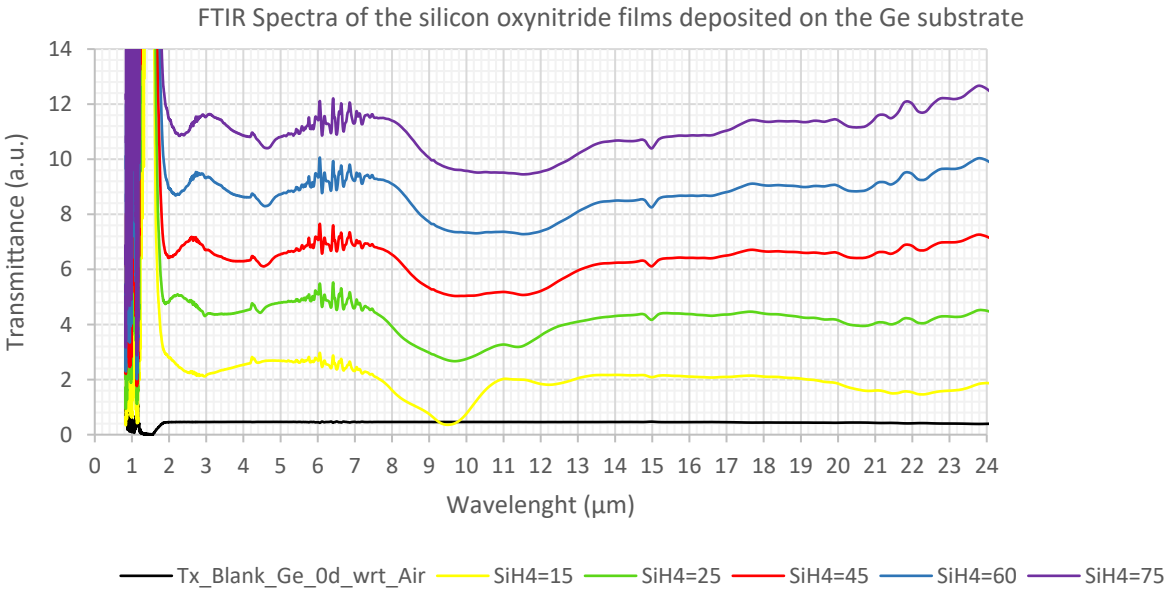

Figure 4-50. The spectra have been shifted in the vertical axis for clarity.

Optical film interference fringes were observed for all silane flow ratios from 15 sccm to 75 sccm on undoped Germanium substrates. This is due to reflection paths that originate from the interfaces between the different media (dielectric / substrate interface) and the relative

amplitude of the different reflection paths is thickness dependent. Spectra shift indicates differing film thicknesses.

The notable absorption peaks present in the FTIR spectra of the silicon oxynitride films are listed in Table 11 in both wavenumbers and wavelength, together with peak assignations.

Table 11. Major absorption peaks in the FTIR spectrum of silicon oxynitride films deposited on Ge substrates.

Absorption peak (cm^{-1})	Absorption peak (μm)	Vibrational absorption mode
450	22.22	related to the Si-N symmetric stretching mode
650 – 700	14.29 - 15.39	possibly related to Si-H bending mode
800 – 850	11.77 - 12.50	Si-N asymmetric stretching
1045-1075	9.30 – 9.57	Si-O-Si stretching
1100 – 1l50	8.696 - 9.09	N-H bending mode
2250	4.44	Si-H stretching mode
3150	3.18	N-H stretching mode

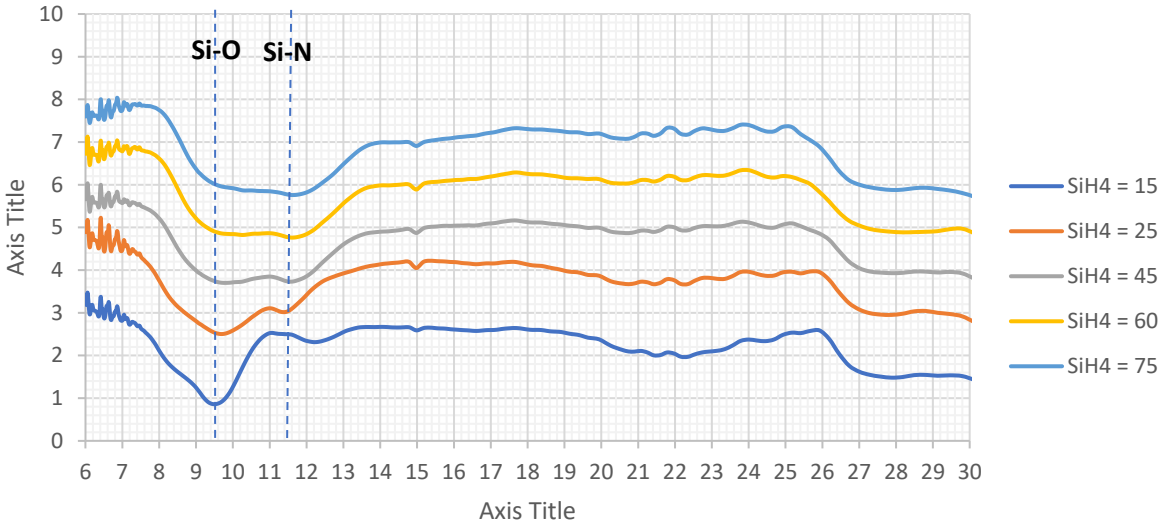

Figure 4-51. The Si-O stretching vibrations modes from 1050 cm^{-1} (9.5 μm) to 1020 cm^{-1} (9.8 μm) related to the silane flow ratio of 15 sccm to 75 sccm. The intensity of these peaks decreases by decreasing the concentration of the oxygen in the films.

In Figure 4-51 the results show that all the deposited films, have a dominant absorption feature which shifted towards smaller wavenumber values (longer wavelengths) from 1050 cm^{-1} (9.5 μm) to 1020 cm^{-1} (9.8 μm) when increasing the silane flow ratio from 15 sccm to 75 sccm respectively. This peak indicates the intensity of the Si-O stretching vibrations in these films which decreases with a decreasing concentration of the oxygen in the films [61][62][63]. So, this peak is largest in the SiH_4 15 sccm films, which are predominantly SiO_2. As the oxygen content of the films decreases, correlating to increased silane flow rates, the absorption peak from Si-O stretching vibrations decreases in intensity.

In Figure 4-51, peaks at about 825.48 cm^{-1} (12.12 μm) to 868 cm^{-1}(11.52 μm) represent the Si-N stretching vibration at silane flow ratios of 15 sccm to 75 sccm respectively. Peaks are shifted to shorter wavelengths on increasing the silane flow ratio. The intensity of this peak increases from its lowest intensity at 15 sccm silane flow rate, up to a maximum intensity at a silane flow ratio of 45 sccm. At higher silane flow rates, there is no further increase in peak in SiN stretching peak intensity [64][65]. This FTIR data correlates to similar trends seem in EDX and XPS data when increasing the silane flow rate i.e. an increase in incorporated nitrogen in the films up to 45 sccm silane flow ration and then no significant change after that point. (see Figure 4-39 and Figure 4-34 (B)).

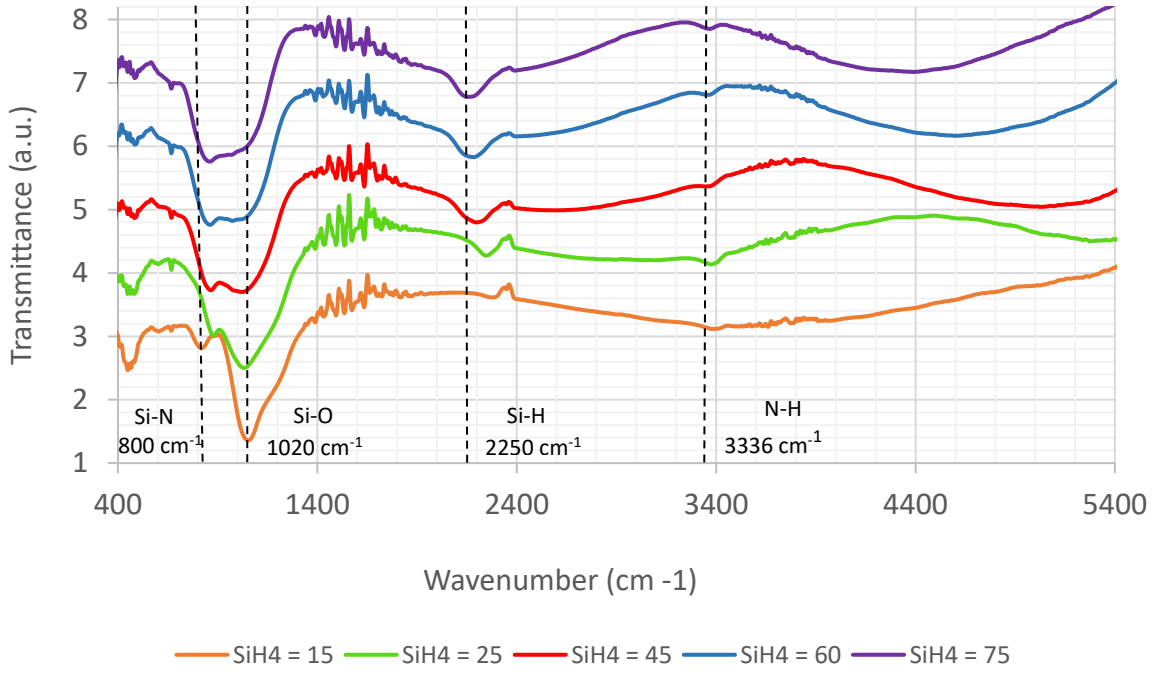

Figure 4-52. FTIR Transmittance spectra showing the N-H stretching vibrations modes from 3336 cm^{-1} (2.99 μm) to related to the silane flow ratio of 15 sccm to 75 sccm.

From Figure 4-52, the peaks at 2.99 μm (3336.67 cm^{-1}) appear in all the films with different silane flows and represent the N-H stretching mode. This peak does not shift with increasing silane flow. The intensity of this peak increases from 15 sccm to 25 sccm and decreases for 45 sccm silane flow ratio and then increases again for 60 sccm and 75 sccm. This suggests a minimum N-H stretching mode at 45 sccm silane flow rate in these measurements. It is possible that the absolute minimum N-H peak intensity could result from a silane flow between 25 sccm and 45 sccm i.e. at around 36 sccm. At silane 25 sccm, there is a larger N-H peak at 3336 cm-1, which is suggested to contribute to the higher optical loss at this silane ratio. At silane rations between 27 sccm and 45 sccm corresponds to lower N-H absorption peaks, which corresponds to minimum optical loss data

Figure 4-53, suggesting that a low N-H peak intensity is an important contributory factor in achieving low optical losses. The optical loss data Figure 6.6.10 shows that for a silane flow rate of 27 sccm, the optical loss is 0.77 whilst for a silane flow rate of 36 sccm, the optical loss is 0.74. This optical loss minima at 36 sccm correlates with a minima in the N-H peak intensity – further emphasising the importance of this particular vibrational absorption mode in relation to optical loss.

The absorption at 4.4 μm (2250 cm^{-1}) is assigned to Si-H stretching vibrations [66][23]. The FTIR results (Figure 4-52) shows that this Si-H peak shifts to shorter wavenumbers with increasing of the silane flow ratio. The peak intensity also increases with increasing silane flow rate, indicating an increase the number of Si-H bonds. Si-H bonds are also related to optical losses, particularly at the communications wavelengths of 1550 nm.

The absorption peaks observed for the N-H stretch (~3300 cm-1) and Si-H stretch (~2250 cm-1) have well known vibrational overtones which affect the telecommunications band at 1550 nm. Quantification of these vibrational bands is thus critical in predicting optical loss [26].

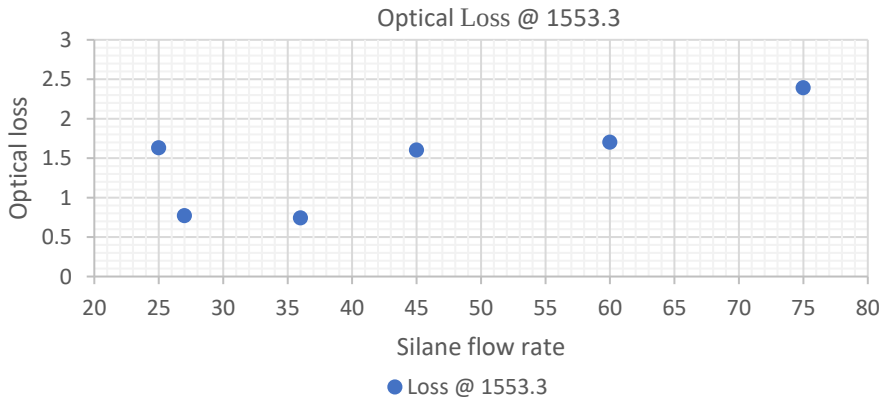

Figure 4-53. Optical loss measurement as a function of silane flow rate.

5 DISCUSSION AND SUMMARY

The science of dielectrics is one of the oldest branches of physics which links to chemistry, materials, and electrical engineering field. [2] The physical and electro-optical properties of these films are related to the chemical composition, morphology and the structure of the materials. These interesting dielectric materials have been used in semiconductor devices and capacitors, particularly oxides and nitrides. However, more recently, silicon oxynitride (SiON), with its excellent optical properties has been investigated and has become increasingly employed in integrated optics such as micro electromechanical systems (MEMS), optical waveguide devices, gate dielectric materials, sensors for optical telecommunication and sensing device applications.

Silicon oxynitride combines the distinct beneficial properties of silicon oxide and silicon nitride in one film - for all the aforementioned applications. Silicon oxide has a large band-gap (near 9 eV) [67][68] so it is an excellent insulator, it has a low refractive index value (1.46) [68], it can be deposited in very pure form and its interface with silicon exhibits excellent electrical properties when thermally grown. On the other hand, silicon oxynitride has smaller band-gap than SiO_2, which can be tailored (between 5eV and 9eV) by controlling the oxygen and nitrogen content, so its refractive index can be adjusted to the desired value. This RI property is very important in the design of integrated optical wave-guides and anti-reflective stacks. [68]

Silicon oxynitride can thus be deposited with a wide range of refractive indexes from silicon oxide to silicon nitride by tuning the material composition which results in great flexibility in design of the optical waveguide devices. Transparency of the silicon oxynitride films in a broad range of wavelength is another useful property of this material in integrated optics. [69]

This thesis has reported the development and in-depth characterisation of silicon oxynitride thin films for optical waveguide applications.

The purpose of the thesis was to deposit a range of dielectric silicon oxynitride films with a different gas flow ratios, in order to establish the effect of each process parameter on the chemical, physical and optical properties (hydrogen and silicon content, film thickness, RI, optical loss) of the films.

In terms of the deposition process parameters, the nitrous oxide (N_2O) and silane (SiH_4) gas flow rate were varied to adjust the proportion of N:O in the final film composition while all other parameters such as N_2 flow rate, pressure, temperature, radio frequency power, and plasma power for generating the initial ionized carrier gas remain constant. N_2 is responsible for supplying the nitrogen (N) atoms for the reaction. Decreasing the N_2 flow rate leads to a 'Si-rich' silicon oxynitride layer.

By understanding which parameters produce low optical loss films, an understanding of the mechanisms for optical loss can be elucidated. This knowledge could be used to further optimise film quality and enable more intelligent design of the films for specific applications.

In this work, the key objective was to deposit low propagation loss silicon oxynitride films for use in optical waveguides.

When the N_2O/SiH_4 flow ratio increases, the excited oxygen atom density increases too. As a result, the formation of Si–O becomes favoured because of the, lower bond energy of N-O (201 KJ/mol) (or N=O (607 KJ/mol)) bond in N_2O compare to the N=N (945 KJ/mol) bond in N_2 gas molecules, the much stronger bond energy for formation of an Si-O bond (800 KJ/mol) relative to formation of an Si-N bond (437 KJ/mol) and is also influenced by the higher electronegativity of oxygen (X_O =3.44) compared to nitrogen (X_N = 3.04) [56], leading to a layer composition close to SiO_2 material.

The gas flow ratio (N_2O/SiH_4) correlates negatively with the refractive index and positively with the deposition rate. This relation can be explained by Lorentz-lorenz equation [70], which relates the refractive index of a substance to its density,

$$\frac{n^2-1}{n^2+1} = \frac{4\pi}{3} A \frac{\rho}{M} \alpha$$

Where, n is the film refractive index, A is the Avogadro number, ρ is the density, M is the molecular mass and α is the volume polarizability.

Increasing the N_2O/SiH_4 ratio leads to increase the number of the oxygen reactants and formation of the SiO2 type film with lower structure density (ρ) of (2.15 $g.cm^{-3}$) [71] [72][73]and lower polarizability (α) of (3.09 $\times 10^{-24}$) compare to the Si_3N_4 type film with higher density of (2.97 $g.cm^{-3}$) [72][74] and higher polarizability of (3.13×10^{-24}) which results to formation of the lower refractive index SiO_2 type materials.

When the N_2O/SiH_4 flow ratio decreases, the incorporation of nitrogen and silicon in the form of Si–H, Si–N, N–H and Si–Si becomes more probable, leading, as expected, to an increasing refractive index. The increase of the deposition rate with increasing N_2O/SiH_4 flow ratio is expected, as we suppose that our deposition conditions give rise to a complete dissociation of the silane and that the process is limited by the nitrous oxide concentration [25].

Optical loss is due to incorporating of the hydrogen contents which have precursor deposition sources in the silicon oxynitride films. The vibrational overtones of the Si-H and N-H bonds cause absorption losses in the 1500 nm wavelength region.

Optical loss has been associated with the hydrogen content of oxynitride films [25] [48]. The vibrational overtones of the Si-H and N-H bonds cause absorption losses in the 1500-nm wavelength region. Incorporation of hydrogen bonds is due to incorporating of the hydrogen contents which have precursor deposition sources in the silicon oxynitride films which can only be removed by annealing at high temperature. Unfortunately, this treatment can cause undesired changes in the material as well, e.g.: refractive index change, shrinkage, interface diffusion, and in the worst-case cracks in the layer, due to thermal stresses. Studies have been carried out recently with the goal of decreasing the hydrogen content in the as-deposited SiON layers and lowering the annealing temperature [69].

In terms of deposition methods, one of the reported problems of growing silicon based dielectric materials via CVD is the greater incorporation of hydrogen in the form of the N-H bonds into the film matrix. [61]. The main advantages of LPCVD are the excellent uniformity of thickness and purity, simple handling, high reliability, homogeneity of deposited layers and high reproducibility [68]. Disadvantages include lower deposition rates and high temperatures, usually above 600°C, needed for process [75]. Other issues with using LPCVD include the difficulty in depositing a thick film due to high stress problems. Therefore, SiN films deposited by PECVD at low temperature with low stress and without post-annealing are more attractive.

Comparing to other CVD processes, one of the main advantages of PECVD is that the process can be operated at low temperature (between 100˚C and 400˚C) while the deposition rate is comparable to other CVD process.

The deposition rate of PECVD layers with low refractive indexes is typically in the range from 30 to 50 nm/min, enabling the economical deposition of even thick waveguides (0.5–

10m) [76]. PECVD is also a thin-film deposition technique that allows for tunable control over the chemical composition of a thin film.

For deposition of optical waveguide films, the most extensively applied technologies are plasma-enhanced chemical vapor deposition (PECVD) and low-pressure chemical vapor deposition (LPCVD).

Since the LPCVD dielectric films have to be deposited at very high temperature (over 800 °C) at prolonged process time, many issues can arise including excessive solid state diffusion, junction leakage and metal silicide agglomeration [77]. The Plasma Enhanced Chemical Vapor Deposition (PECVD) silicon nitride process is usually chosen either to reduce the thermal budgets or to avoid undesirable thermal effects.

A key advantage of LPCVD films is their low hydrogen content. In contrast, lower temperature PECVD processes (300-500°C) usually have a higher hydrogen content. The difference in hydrogen content is related to the higher LPCVD deposition temperature which provides enough energy to disrupt the N-H bonds within the film and hence reduces the hydrogen content of the films.

Due to the hydrogen bonds in the oxynitride films, which constitute Si-H and N-H bonds, oxynitride waveguides can suffer from high propagation loss – a similar phenomenon to that seen in silicon nitride films.

In the generation of thin silicon oxynitride and phosphorous-containing silicon oxynitrides, silane (SiH_4), nitrous oxide (N_2O), ammonia (NH_3), and nitrogen (N_2) can be used as reactant gases. To reduce hydrogen content, an ammonia free process may be used. There are some advantage and disadvantage of using NH_3 free processes in silicon oxynitride films. The advantages are including of low hydrogen content, low deposition temperature (high temperatures are needed to provide the kinetic energy required to eliminate the hydrogen impurities incorporated into the films)[78] whilst the disadvantages are; lower deposition rate (7-20 nm/min), slightly worse uniformity, slightly worse repeatability.[7]

Hydrogen in the films is covalently bound to Si and N and both the N-H bonds and Si-H bonds absorb in the spectral region used for telecommunications i.e. around 1550 nm. The N-H bonds in particular act as absorption centres with absorption loss in the region of 1510-1565 nm. Since the hydrogen comes from the deposition reactants, the density of hydrogen can be reduced by changing the deposition precursors.

In this work, the PECVD ammonia free precursors have been used in order to minimise the hydrogen content of the deposited dielectric films, using an N_2 precursor instead of NH_3.

In comparison to ammonia-based process, the ammonia free process significantly reduces the hydrogen content of the oxynitride films. This in turn reduces the optical loss at 1550nm [69].

The pressure, temperature, radio frequency power, and plasma power for generating the initial ionized carrier gas can be adjusted to ensure optimum reaction efficiency.

Critical process parameters have been investigated in this work, including the silane and nitrous oxide flow rates and ratios.

It has been observed that increasing the silane ratio firstly increases the nitrogen content of the films, leading to silicon oxynitrides with a more nitride-like content. Secondly, at higher silane ratios, the films incorporate a greater amount of silicon, present as Si-H bonds in the silicon-oxynitride films. As the SiH_4 : N_2O ratio increases, there are increases in the number of Si-N, Si-Si, Si-H and N-H bonds, whilst there is a corresponding reduction in the number of Si-O bonds. The silicon nitride films thus have higher hydrogen content and therefore exhibit greater optical losses. The reduction in Si-O content and increase Si-H bonding has been verified in this work, using FTIR. The N-H bonding shows more varied changes in response to changing silane ratios.

The conclusion of this work is that higher silane ratios yield greater hydrogen content in the oxynitride films and thus greater optical losses.

The RI values desirable in optical waveguide devices are 1.55, 1.6 and 1.7. These RI values can be obtained with SiH_4 flow rates of 23, 36 and 45 sccm respectively, in combination with a N_2O flow rate of 65 sccm. The lowest optical loss observed in this work corresponded to 36 sccm silane / 65 sccm N_2O.

Lower silane flow rates (15 sccm) yielded films which were predominantly silicon oxide – like in nature, and this had a RI below 1.55. These films are not ideal, in terms of the RI, and are instead used as buffer layers.

The silane flow rate of 25 sccm yielded films with an RI approximately 1.57 but also with a relatively high N-H bond content. The high N-H content leads to higher optical losses.

The 36 and 45 sccm silane flow rates both yielded lower N-H bond content (from FTIR data). The optical losses for these films were the lowest observed and thus the suggestion of a correlation between optical loss and N-H content is strongly supported.

6 CONCLUSION

Silicon oxynitride films have been investigated in relation to photonic waveguide devices for optical communications applications.

Silicon oxynitride films have intermediate properties (RI, bandgap, deposition rate, elemental composition) between silicon oxide and silicon nitride films).

The higher RI values of oxynitride films, relative to silicon dioxide or silicon oxynitride with lower RI, are desirable for waveguide devices – which use a high RI silicon oxynitride core and a lower RI silicon oxynitride or silicon oxide buffer layer. It is beneficial to use an oxynitride layer in place of an oxide layer as using both oxynitride processes in the PECVD chamber greatly reduces process times.

This is related to an etch-back chamber preparation process being required if oxide deposition is used. In contrast, if PECVD oxynitrides are used for both the core and the buffer layers, no etch back process is required.

The elimination of the etch-back process significantly reduces process run-times, and this increases production rates.

In this work, a matrix of oxynitride films have been produced using a range of process gas ratios. The critical gas ratios relate to the silane (SiH_4) and nitrous oxide (N_2O) concentrations (flow rates). Silane flow rate has been varied to produce almost oxide like films (using low silane flow rates – 15 sccm), to silicon rich nitride films (using 135 sccm silane flow rate). These films have been investigated in terms of their elemental composition (XPS and EDX) and bonding content (FTIR). Parameters including film thickness, deposition rate and uniformity have also been investigated. These parameters showed little influence on either the stoichiometry of the films or the RI.

The key factors determining RI are oxygen, nitrogen and silicon content. Higher oxygen content yielded lower RI films, whilst higher nitrogen content (more nitride-like films) had higher RI. The highest RI values were observed for films deposited with the highest silane flow rates, which had the highest Si-H silicon rich bonding content.

The films have also been monitored using FTIR to determine the Si-H, N-H, Si-O and SiN bonding content. The oxygen content was varied by using different flow rates of N2O (65 and

130 sccm). A flow rate of 65 sccm also provides good stability, reliability and reproducibility of films. Flow rates below 65 sccm can cause a high degree of fluctuation in the RI.

Lower silane flow rates (15 sccm) in combination with high N2O flow rates yielded films which were predominantly silicon oxide – like in nature. The higher oxygen content (using higher N2O flow rate) gave low RI values below 1.55 which makes them ideal as buffer layers.

Higher silane ratios increased the Si-H and N-H content, which consequently increased optical losses.

The 25 sccm flow rate yielded films with an RI approximately 1.57 but also with a relatively high N-H bond content. The high N-H content leads to higher optical losses.

The 36 and 45 sccm silane flow rates both yielded lower N-H bond content (from FTIR data). The optical losses for these films were the lowest observed and thus the suggestion of a correlation between optical loss and N-H content is strongly supported [79].

7 REFERENCES

[1] D. T. H. Tan, K. J. A. Ooi, and D. K. T. Ng, 'Nonlinear optics on silicon-rich nitride—a high nonlinear figure of merit CMOS platform [Invited]', *Photonics Res.*, vol. 6, no. 5, p. B50, May 2018.

[2] D. A. P. Bulla and N. I. Morimoto, 'Deposition of thick TEOS PECVD silicon oxide layers for integrated optical waveguide applications', *Thin Solid Films*, vol. 334, no. 1–2, pp. 60–64, 1998.

[3] R. A. Soref and J. P. Lorenzo, 'All-Silicon Active and Passive Guided-Wave Components for λ = 1.3 and 1.6 μm', *IEEE J. Quantum Electron.*, vol. 22, no. 6, pp. 873–879, 1986.

[4] J. P. Lorenzo and R. A. Soref, '1.3 μm electro-optic silicon switch', *Appl. Phys. Lett.*, vol. 51, no. 1, pp. 6–8, 1987.

[5] D. J. Albares and R. A. Soref, 'Silicon-On-Sapphire Waveguides', 1987, p. 24.

[6] B. N. Kurdi and D. G. Hall, 'Optical waveguides in oxygen-implanted buried-oxide silicon-on-insulator structures', *Opt. Lett.*, vol. 13, no. 2, p. 175, Feb. 1988.

[7] A. F. Gavela, D. G. García, J. C. Ramirez, and L. M. Lechuga, 'Last advances in silicon-based optical biosensors', *Sensors (Switzerland)*, vol. 16, no. 3, 2016.

[8] J. Ballato *et al.*, 'Advancements in semiconductor core optical fiber', *Opt. Fiber Technol.*, vol. 16, no. 6, pp. 399–408, 2010.

[9] L. Lagonigro *et al.*, 'Low loss silicon fibers for photonics applications', *Appl. Phys. Lett.*, vol. 96, no. 4, pp. 6–9, 2010.

[10] K. K. Lee, D. R. Lim, H. C. Luan, A. Agarwal, J. Foresi, and L. C. Kimerling, 'Effect of size and roughness on light transmission in a Si/SiO2waveguide: Experiments and model', *Appl. Phys. Lett.*, vol. 77, no. 11, pp. 1617–1619, Sep. 2000.

[11] G. P. Agrawal, *Fiber-Optic Communication Systems: Fourth Edition*. 2011.

[12] M. Drahansky *et al.*, 'We are IntechOpen , the world ' s leading publisher of Open Access books Built by scientists , for scientists TOP 1 %', *Intech*, vol. i, no. tourism, p. 13, 2016.

[13] B. Brown, D. Hess, V. Desai, and M. J. Deen, 'Dielectric Science and Technology', 2006.

[14] R. Larker, 'Reaction Sintering and Properties of Silicon Oxynitride Densified by Hot Isostatic Pressing', *J. Am. Ceram. Soc.*, 1992.

[15] M. Ohashi, H. Tabata, and S. Kanzaki, 'High-temperature flexural strength of hot-pressed silicon oxynitride ceramics', *J. Mater. Sci. Lett.*, 1988.

[16] M. Ohashi, S. Kanzaki, and H. Tabata, 'Processing, Mechanical Properties, and Oxidation Behavior of Silicon Oxynitride Ceramics', *J. Am. Ceram. Soc.*, 1991.

[17] P. Rocabois, C. Chatillon, and C. Bernard, ‘Thermodynamics of the Si-O-N System: II, stability of Si2N2O(s) by high-temperature mass spectrometric vaporization’, *J. Am. Ceram. Soc.*, 1996.

[18] Y. Iwase, Y. Horie, Y. Daiko, S. Honda, and Y. Iwamoto, ‘Synthesis of a novel polyethoxysilsesquiazane and thermal conversion into ternary silicon oxynitride ceramics with enhanced thermal stability’, *Materials (Basel).*, vol. 10, no. 12, 2017.

[19] M. Ohashi, S. Kanzaki, and H. Tabata, ‘Effect of additives on some properties of silicon oxynitride ceramics’, *J. Mater. Sci.*, 1991.

[20] Z. Gan, C. Wang, and Z. Chen, ‘Material Structure and Mechanical Properties of Silicon Nitride and Silicon Oxynitride Thin Films Deposited by Plasma Enhanced Chemical Vapor Deposition’, *Surfaces*, vol. 1, no. 1, pp. 59–72, 2018.

[21] H. T. Philipp, K. N. Andersen, W. Svendsen, and H. Ou, ‘Amorphous silicon rich silicon nitride optical waveguides for high density integrated optics’, *Electron. Lett.*, 2004.

[22] S. C. Mao *et al.*, ‘Low propagation loss SiN optical waveguide prepared by optimal low-hydrogen module’, *Opt. Express*, 2008.

[23] F. Ay and A. Aydinli, ‘Comparative investigation of hydrogen bonding in silicon based PECVD grown dielectrics for optical waveguides’, *Opt. Mater. (Amst).*, vol. 26, no. 1, pp. 33–46, 2004.

[24] A. Gondarenko, J. S. Levy, and M. Lipson, ‘High confinement micron-scale silicon nitride high Q ring resonator’, *Opt. Express*, vol. 17, no. 14, p. 11366, 2009.

[25] M. G. Hussein, K. Wörhoff, G. Sengo, and A. Driessen, ‘Optimization of plasma-enhanced chemical vapor deposition silicon oxynitride layers for integrated optics applications’, 2006.

[26] M. G. Hussein, K. Wörhoff, G. Sengo, and A. Driessen, ‘Reduction of hydrogen-induced optical losses of plasma-enhanced chemical vapor deposition silicon oxynitride by phosphorus doping and heat treatment’, *J. Appl. Phys.*, vol. 101, no. 2, 2007.

[27] D. A. P. Bulla, B. V. Borges, M. A. Romero, N. I. Morimoto, L. G. Neto, and A. L. Cortes, ‘Design and fabrication of SiO/sub 2//Si/sub 3/N/sub 4/ CVD optical waveguides’, no. February, pp. 454–457, 2003.

[28] M. R. Amirzada, A. Tatzel, V. Viereck, and H. Hillmer, ‘Surface roughness analysis of SiO2 for PECVD, PVD and IBD on different substrates’, *Appl. Nanosci.*, vol. 6, no. 2, pp. 215–222, 2016.

[29] V. Bhatt and S. Chandra, ‘Silicon dioxide films by RF sputtering for microelectronic and MEMS applications’, *J. Micromechanics Microengineering*, vol. 17, no. 5, pp. 1066–1077, May 2007.

[30] S. S. Ho, S. Rajgopal, and M. Mehregany, ‘Thick PECVD silicon dioxide films for MEMS devices’, *Sensors Actuators, A Phys.*, vol. 240, pp. 1–9, Apr. 2016.

[31] J. Chen, Y. Zheng, C. Xue, C. Zhang, and Y. Chen, ‘ Filtering effect of SiO 2 optical waveguide ring resonator applied to optoelectronic oscillator ’, *Opt. Express*, vol. 26, no. 10, p. 12638, May

2018.

[32] D. M. Brown, P. V. Gray, F. K. Heumann, H. R. Philipp, and E. A. Taft, ‘Properties of SixOyNx Films on Si’, *J. Electrochem. Soc.*, vol. 115, no. 3, pp. 311–317, 1968.

[33] G. Sombrio, P. L. Franzen, R. L. Maltez, L. G. Matos, M. B. Pereira, and H. Boudinov, ‘Photoluminescence from SiNxOy films deposited by reactive sputtering’, *J. Phys. D. Appl. Phys.*, vol. 46, no. 23, Jun. 2013.

[34] J. Dong, P. Du, and X. Zhang, ‘Characterization of the Young’s modulus and residual stresses for a sputtered silicon oxynitride film using micro-structures’, *Thin Solid Films*, vol. 545, pp. 414–418, Oct. 2013.

[35] J. Won Lim *et al.*, ‘Transparent high-performance SiO x N y /SiO x barrier films for organic photovoltaic cells with high durability’, *Nano Energy*, vol. 33, pp. 12–20, Mar. 2017.

[36] A. Soman and A. Antony, ‘Broad range refractive index engineering of SixNy and SiOxNy thin films and exploring their potential applications in crystalline silicon solar cells’, *Mater. Chem. Phys.*, vol. 197, pp. 181–191, 2017.

[37] N. Massa, ‘Telecommunication’, pp. 293–347.

[38] T. M. Okon and J. R. Biard, ‘The First Practical LED’, pp. 1–14, 2015.

[39] D. Jäger and A. Stöhr, ‘Microwave Photonics – From Concepts to Applications’, *Architecture*, no. December, pp. 1–4, 2005.

[40] K. Worhoff and A. Driessen, ‘Silicon Oxynitride : A Versatile Material for Integrated Optics Applications A Versatile Material for Integrated Optics Applications’, no. August, 2002.

[41] K. D. Mackenzie, D. J. Johnson, M. W. DeVre, R. J. Westerman, and B. H. Reelfs, ‘Stress control of Si-based PECVD dielectrics’, *Proc. - Electrochem. Soc.*, vol. PV 2005-01, no. January 2005, pp. 148–159, 2005.

[42] K. D. Mackenzie, D. J. Johnson, M. W. Devre, R. J. Westerman, and B. H. Reelfs, ‘STRESS CONTROL OF Si-BASED PECVD DIELECTRICS Wafer Bow (mm) Film Thickness (μm)’, *207th Electrochem. Soc. Meet.*, no. May, pp. 148–159, 2005.

[43] C. Iliescu *et al.*, ‘Residual stress in thin films PECVD depositions: A review’, *J. Optoelectron. Adv. Mater.*, vol. 13, no. 4, pp. 387–394, 2011.

[44] J. Steinlechner *et al.*, ‘Optical absorption of silicon nitride membranes at 1064 nm and at 1550 nm’, *Phys. Rev. D*, vol. 96, no. 2, 2017.

[45] Y. Chen and G. Jin, ‘Refractive index and thickness analysis of natural silicon dioxide film growing on silicon with variable-angle spectroscopic ellipsometry’, *Spectrosc. (Santa Monica)*, vol. 21, no. 10, pp. 26–31, 2006.

[46] G. E. Jellison and F. A. Modine, ‘Erratum: Parameterization of the optical functions of amorphous materials in the interband region [Appl. Phys. Lett. (1996) 69 (371) (10.1063/1.118064))’, *Applied Physics Letters*. 1996.

[47] P. Petrik, ‘Parameterization of the dielectric function of semiconductor nanocrystals’, *Phys. B Condens. Matter*, vol. 453, pp. 2–7, 2014.

[48] K. Wörhoff, L. T. H. Hilderink, A. Driessen, and P. V. Lambeck, ‘Selicon oxynitride. A versatile material for integrated optic applications’, *J. Electrochem. Soc.*, vol. 149, no. 8, 2002.

[49] H. Abramczyk, ‘Dispersion phenomena in optical fibers’, *Doktorsavhandlingar vid Chalmers Tek. Hogsk.*, no. 2499, pp. 1–91, 2006.

[50] T. General and N. Si, ‘The General Properties of Si, Ge, SiGe, SiO 2 and Si 3 N 4’, no. June, pp. 5–9, 2002.

[51] P. R. Gray and R. G. Meyer, ‘Analysis and Design of Analog Integrated Circuits’, *Eur. J. Eng. Educ.*, 1993.

[52] M. I. Alayo, I. Pereyra, W. L. Scopel, and M. C. A. Fantini, ‘On the nitrogen and oxygen incorporation in plasma-enhanced chemical vapor deposition (PECVD) SiOxNy films’, *Thin Solid Films*, 2002.

[53] K. Debnath, T. D. Bucio, A. Al-Attili, A. Z. Khokhar, S. Saito, and F. Y. Gardes, ‘Photonic crystal waveguides on silicon rich nitride platform’, *Opt. Express*, vol. 25, no. 4, p. 3214, 2017.

[54] S. M. Castanho, R. Moreno, and J. L. G. Fierro, ‘Influence of process conditions on the surface oxidation of silicon nitride green compacts’, *J. Mater. Sci.*, vol. 32, no. 1, pp. 157–162, 1997.

[55] E. Atanassova and D. Spassov, ‘X-ray photoelectron spectroscopy of thermal thin Ta 2 O 5 films on Si’, *Appl. Surf. Sci.*, vol. 135, no. 1–4, pp. 71–82, 1998.

[56] L. Šimurka *et al.*, ‘Effect of deposition conditions on physical properties of sputtered silicon oxynitride thin films on float glass’, *Int. J. Appl. Glas. Sci.*, 2018.

[57] B. Hafner, ‘Energy Dispersive Spectroscopy on the SEM ’:

[58] S. Meziani, A. Moussi, L. Mahiou, and R. Outemzabet, ‘Compositional analysis of silicon oxide/silicon nitride thin films’, *Mater. Sci. Pol.*, vol. 34, no. 2, pp. 315–321, 2016.

[59] T. U. Eindhoven and D. Version, *Silicon dangling bonds measurement.pdf*, no. 2006. 2019.

[60] I. Glasses, ‘Materials for infrared optics’, pp. 2–7.

[61] F. Ay and A. Aydinli, ‘Comparative investigation of hydrogen bonding in silicon based PECVD grown dielectrics for optical waveguides’, 2004.

[62] R. K. Bhan and R. Ashokan, ‘Fourier transform infrared study of thermally grown SiO2 in the presence of 1,1,1, trichloroethane’, *J. Appl. Phys.*, vol. 71, no. 5, pp. 2387–2391, 1992.

[63] D. V. Tsu, G. Lucovsky, and B. N. Davidson, ‘Effects of the nearest neighbors and the alloy matrix on SiH stretching vibrations in the amorphous SiOr:H (0<r<2) alloy system’, *Phys. Rev. B*, vol. 40, no. 3, pp. 1795–1805, 1989.

[64] A. Fejfar, J. Zemek, and M. Trchová, ‘Hydrogen and nitrogen bonding in silicon nitride layers deposited by laser reactive ablation: Infrared and x-ray photoelectron study’, *Appl. Phys. Lett.*, vol. 67, p. 3269, 1995.

[65] D. Schalch, A. Scharmann, and R. Wolfrat, ‘IR transmittance studies of hydrogen-free and hydrogenated silicon nitride and silicon oxynitride films deposited by reactive sputtering’, *Thin Solid Films*, vol. 155, no. 2, pp. 301–308, Dec. 1987.

[66] M. S. Kang, T. H. Chung, and Y. Kim, ‘Plasma enhanced chemical vapor deposition of nitrogen-incorporated silicon oxide films using TMOS/N2O gas’, *Thin Solid Films*, vol. 506–507, pp. 45–49, 2006.

[67] S. S. Nekrashevich and V. A. Gritsenko, ‘Electronic structure of silicon dioxide (a review)’, *Phys. Solid State*, vol. 56, no. 2, pp. 207–222, 2014.

[68] D. Davazoglou, ‘Optical absorption threshold of low pressure chemically vapor deposited silicon oxynitride films from SiCl 2 H 2 – NH 3 – N 2 O mixtures’, vol. 437, no. 03, pp. 266–271, 2003.

[69] K. Wörhoff, E. Klein, G. Hussein, and A. Driessen, ‘Silicon Oxynitride based photonics’, pp. 2–5.

[70] H. Kragh, ‘The Lorenz-Lorentz Formula: Origin and Early History’, *Substantia*, vol. 2, no. 2, pp. 7–18, 2018.

[71] A. Bender, T. Gerber, H. Albrecht, and B. Himmel, ‘X-ray reflectivity study of r.f.-sputtered thin SiO2 films’, *Thin Solid Films*, 1993.

[72] T. Hänninen, *Silicon Nitride Based Coatings Grown by Reactive Magnetron Sputtering*, no. 1901. 2018.

[73] H. I. Lee *et al.*, ‘Degradation by water vapor of hydrogenated amorphous silicon oxynitride films grown at low temperature’, *Sci. Rep.*, vol. 7, no. 1, pp. 1–8, 2017.

[74] T. Serikawa and A. Okamoto, ‘Properties of Magnetron-Sputtered Silicon Nitride Films’, *J. Electrochem. Soc.*, 1984.

[75] R. Curley, T. Mccormack, and M. Phipps, ‘Low-pressure CVD and Plasma- Enhanced CVD’, no. Cvd, pp. 1–5, 2012.

[76] W. Kerstin, P. V Lambeck, A. Driessen, and S. Member, ‘Design , Tolerance Analysis , and Fabrication of Silicon Oxynitride Based Planar Optical Waveguides for Communication Devices’, no. October 2012, 1999.

[77] N. Sharma, M. Hooda, and S. K. Sharma, ‘Synthesis and Characterization of LPCVD Polysilicon and Silicon Nitride Thin Films for MEMS Applications’, *J. Mater.*, vol. 2014, pp. 1–8, 2014.

[78] T. Domínguez Bucio *et al.*, ‘Material and optical properties of low-temperature NH3-free PECVD SiNx layers for photonic applications’, *J. Phys. D. Appl. Phys.*, vol. 50, no. 2, p. 25106, 2017.

[79] A. Dogan, ‘The Reliability of the Silicon Nitride Dielectric in Capacitive MEMS Switches’, no. August, p. 173, 2005.